1-1-2003

Use of carbon fiber reinforced polymers for the repair of impact damaged prestressed concrete bridges

Brian Jon Kempers
Iowa State University

Use of carbon fiber reinforced polymers for the repair of impact damaged prestressed concrete bridges

by

Brian Jon Kempers

A thesis submitted to the graduate faculty

In partial fulfillment of the requirements for the degree of

MASTER OF SCIENCE

Major: Civil Engineering (Structural Engineering)

Program of Study Committee:
F. W. Klaiber, Co-major Professor
T. J. Wipf, Co-major Professor
L. W. Zachary

Iowa State University

Ames, Iowa

2003

Graduate College

Iowa State University

This is to certify that the master's thesis of

Brian Jon Kempers

has met the thesis requirements of Iowa State University

Signatures have been redacted for privacy

TABLE OF CONTENTS

LIST OF FIGURES

LIST OF TABLES

ABSTRACT

As a result of frequent vehicular collisions to prestressed concrete (P/C) bridge structures around the state of Iowa, a project was begun to investigate the capabilities of carbon fiber reinforced polymers (CFRP) as a method to repair and/or strengthen damaged bridges. A literature review was performed during the course of the project to identify other research related to carbon fiber repair/strengthening. There was a significant amount of literature involving reinforced concrete (RC), but very little concerning the use of CFRP to repair P/C bridges.

A full-sized P/C beam was tested in the laboratory. Impact damage was simulated by removing a section of the bottom flange as well as cutting two prestressing strands, and the beams were repaired using a standard mortar and CFRP. The beam was subjected to cyclic loading simulating traffic before being statically tested to failure. The load testing showed that the CFRP increased the cracking load and restored a portion of lost flexural strength.

Three bridges, southbound I-65 near Altoona, Iowa; westbound IA-34 near Osceola, Iowa; and westbound I-80 near De Soto, Iowa were damaged by impact of overheight vehicles. They were load tested in their damaged condition and then repaired using CFRP. The Altoona bridge was retested to observe the differences in strains and deflections, and some of the results showed minor improvement from the damaged to the repaired tests for certain heavier load cases.

A design/application guide was developed based on the Osceola Bridge work for design using CFRP and to provide documentation for repair. This includes a working design software template as well as a design example of a previously designed repair.

1. INTRODUCTION

1.1. Background

The overall state of bridges in North America has slowly been deteriorating, since over 50% of the bridges in the United States were built before 1940 (1). Many of these bridges were originally designed for smaller vehicles. Of the approximately 300,000 bridges built before 1940, up to 42% are considered structurally deficient (2). These deficiencies are caused by several factors including increased loading, increased traffic volume, change in use, degradation, and design or construction problems (3). Another cause of structural deficiency is vehicular impact damage, and Shanafelt and Horn (4) found that approximately 160 prestressed concrete (P/C) bridges are damaged due to vehicular impact per year. Some of these bridges need minimal repair, however others may require extensive repair that could even involve the replacement of damaged girders.

In the past, several methods have been employed to repair and/or strengthen these old or damaged bridges. Three of these methods include external post tensioning cables, internal splicing of strands, and a steel jacket mechanically fastened to the damaged beam. All three methods can be successful in restoring some strength to the beams, but they are all time consuming repairs with significant material, labor, and traffic control costs.

More recently, carbon fiber has been employed as a structural repair method similar to the steel jacket. Carbon Fiber Reinforced Polymers (CFRP) have a high strength to weight ratio and are more pliable than steel resulting in an easier application. Over the last ten years, CFRP has been tested and documented on several reinforced concrete (R/C) members. Only recently has there been research on repairing damaged P/C beams and bridges with CFRP; whether CFRP can make up for the loss of prestressing is the real question.

1.2. Objective and Scope

The objective of this research was to determine the effectiveness of CFRP as a repair method for P/C members. A literature review, a full-scale laboratory beam test, and two field tests on actually damaged bridges were completed to obtain pertinent information and data. Some comparisons were also drawn from previous laboratory tests.

A literature review examining current and previous work in related areas of research was completed. Also included was a case study of certain bridge repairs obtained from the Iowa Department of Transportation. The review looked at previous tests mostly involving reinforced concrete or older repair procedures.

A full scale Iowa DOT LXA-38 beam was brought into the laboratory where a composite 4 ft by 8 in. deck was added. The beam was instrumented, damaged, and repaired with CFRP. The damage was similar to vehicular damage that occurs in the field, and the repair was similar to a field repair, which relies on a patch material. Longitudinal CFRP was added to restore some flexural strength, and a CFRP transverse wrap was installed to help contain the patch and to increase the bond strength. Finally the beam was cyclically loaded for 2.2 million cycles and then loaded to failure in an ultimate static load test. The test setup is in Chapter 3, while the test procedure and results are presented in Chapters 4 and 5, respectively.

Three impact damaged P/C bridges were also investigated. Bridges near Altoona, Osceola, and De Soto, Iowa that had been struck by overheight vehicles were subsequently strengthened and repaired using CFRP sheets and plates. The full-size beam specimens, bridge schematics, and test setups are discussed in Chapter 3. The installation of the patch and CFRP is presented in Chapter 4, and the results of the bridge tests are presented and summarized in Chapter 5.

Chapter 6 consists of a brief summary of the research followed by the conclusions. Chapter 7 provides suggestions for further research. CFRP design techniques are presented in Appendix B along with photographic documentation of the application process.

2. LITERATURE REVIEW

A literature review was conducted of topics similar in nature to the project at hand. Several sources of reference material were utilized for this review including the Iowa Department of Transportation, the Internet, and the Parks Library on the Iowa State University campus.

2.1. Conventional Repair Methods

Conventional repair methods for impact-damaged beams depend on the type and severity of the beam damage. The three current standard methods are again external cables, internal splices, and steel jackets. The external post tensioning cable method consists of running post-tensioning tendons along the length of the underside of the beam and through jacks that are fastened near the ends of the beam. The tendons are then stretched and released for the post-tensioning effect, but this method of repair leaves the new tendons exposed to the environment and invites corrosion damage to occur.

The internal splice method involves splicing the ruptured tendons and restoring the original prestressing forces to them. After the tendons are restored to their old strength, a load is placed upon the bridge and the concrete is then repaired. When the concrete cures, the load is taken off the bridge. This method requires specialized chucks and a lot of time but can be used to repair several ruptured tendons.

The final method, the steel jacket repair, is used most often in this area. A welded steel jacket is attached to the bottom flange of the damaged girder after the concrete patchwork has been completed. Bolts are fastened through the concrete to initially adhere the steel to the concrete; however, the steel jacket does not provide any prestressing forces. Epoxy is injected into the interface between the two materials to complete the adhesion. One main function of this repair is to contain the patched area and prevent any patch fallout. The steel jacket repair is the most common type of bridge repair in the Midwest.

2.2. Carbon Fiber as a Repair Method

In the last 10 years, advances in carbon fiber technology have been tremendous. Carbon fiber is being used for reinforcement rods, external repair sheets, and even entire bridge structures. Its light weight, high strength to weight ratio, and non-corrosive

properties have turned it into one of the preferred methods for repairing existing structures that have sustained impact damage, environmental damage, or are under-designed due to some change in use. A continued reduction in cost of CFRP composites, has also contributed to their popularity (5).

2.2.1. Case study

Some repair data was collected from the Iowa DOT involving different bridge repairs that had been performed. From this data, some comparisons were drawn between the steel jacket and CFRP repair costs. The data came from five bridges repaired in Iowa in recent years, four using the steel jacket and one using CFRP. Most of the bridges were from the Central Iowa area, but one was from the western side of the state, and these bridges all incurred damage due to vehicular impact and were in need of various repairs. Some of the bridge data used to draw comparisons are shown in Table 2.1, which includes bridge locations, dimensions, beams, damage amount, and the extent of the repair work.

Table 2.1. Bridge locations and damage amounts.

Bridge	No. of beams repaired	Length of repair	Location	Extent of Repair Needed	Degree of Traffic Control
Polk 3498 (Steel)	1	30 ft	Euclid over I-235	1*	Moderate
Polk 2095 (Steel)	2	29 ft	Beaver Road over I 80/35	2*	Extreme
Woodbury 597 (Steel)	1	15.7 ft	Local K25 over I-29	3*	Total Shutdown of K25
Warren 599 (Steel)	1	13.5 ft	Iowa 92 over I-35	4*	Little
Polk 3400 (CFRP)	6 total, 1 extensive	6 ft, and 80 ft	US-65 over US-6	5*	Little

*See repair description below.

1. This bridge required repair of two relatively large areas of concrete on the damaged beam. Steel plate assemblies were attached to the upper and bottom portion of the beam. It was then sealed using an epoxy gel and injected with an epoxy resin. The welded area was painted with zinc paint. The steel jacket continues higher up the web for bridge #1 and #4 than it does for bridge #2.

2. This bridge needed repair of two relatively large areas of concrete on the beam. Steel plate assemblies were attached to the upper and lower portion of the beams. It was sealed using an epoxy gel and injected with an epoxy resin. The welded area was painted with zinc paint.
3. This bridge had incurred more damage than the others and required the repair of one beam and total replacement of another. This makes it hard to compare with the other repair jobs.
4. This repair was approximately the same as repair #1.
5. The concrete on this bridge was repaired using shallow repair and/or regular repair techniques. FRP plates were installed under the heavily damaged areas on one beam. CFRP was wrapped around damaged areas (8-15 ft.), and then down the entire length of the heavily damaged beam.

Bids were taken separately for the five jobs. The costs and bids varied widely from company to company and bridge to bridge. Table 2.2 shows a summary of the bids with the winning bids in bold type.

Table 2.2. Bids for different bridge repairs.

Bridge	Bidding Company	Cost of Traffic Control	Mobilization	Beam Repair
Polk 3498 (Steel)	Shaw	***$5,200***	***$2,000***	***$24,952***
	Cramer	$5,700	$5,500	$23,252
	Jensen	$7,700	$5,000	$28,717
	Herberger	$7,700	$5,000	$36,101
Polk 2095 (Steel)	Cramer	***$17,061***	***$2,400***	***$5,500***
	Jensen	$17,477	$2,000	$15,000
Woodbury 597 (Steel)	Elk Horn	***$30,535***	***$12,000***	***$23,440***
	Christensen	$54,701	$15,000	$39,312
Warren 599 (Steel)	Shaw	***$2,920***	***$3,500***	***$12,050***
	Jensen	$4,720	$2,500	$16,900
	Cramer	$2,920	$5,000	$14,375
	Herberger	$4,220	$4,000	$23,400
Polk 3400 (CFRP)	Cramer	***$3,150***	***$5,500***	***$34,000***
	Shaw	$5,550	$3,500	$35,000
	BRB	$4,000	$5,000	$61,000

Drawing direct comparisons from the steel jacket vs. the CFRP wrap is difficult because in the field most beams are not exactly alike, and if they are, the damage on one beam is going to be different from the damage on an identical beam. The length of the beams, the amount of damage, the damage location on the beam, the damage location over the roadway, the need for extensive traffic control, and the amount of time to do the repair, are all factors in figuring which method is the better.

The first impression of the tables indicates that the CFRP method looks to be more expensive than the steel jacket method. This is a result of possibly three things: the length of the beam wrapped with CFRP was 75 feet, the wrapped beam also had its flexural strength enhanced by carbon fiber plates, and the CFRP process is very new.

The cost to repair a 30 ft beam for the Polk 3498 bridge was $24,952, which included $15,312 for structural steel. This is approximately $826 per lineal foot. The Polk 3400 bridge repair cost $34,000. With 80 feet being wrapped and ignoring the cost of the other five beams, the cost of this repair was $425 per lineal foot. This does not include the fact that the bridge repaired with CFRP was also flexurally strengthened.

Unlike the bridges repaired with the steel jacket, the Polk 3400 bridge was flexurally enhanced with carbon fiber plates. The plates used for this job were 4 in. Sika S1012 plates, which cost $44 per lineal foot. Four plates were placed side by side along the bottom with a length of 75 feet for a total of 300 lineal feet. This means that the plates alone cost $13,000. Subtract that from the $34,000 total, and the price is $262.50 per lineal foot for the CFRP wrap, which is less than 1/3 of the cost of the steel jacket repair.

As more companies continue to use the CFRP the cost should decrease as the competition increases. Hopefully more repairs can be documented to increase the data bank of bridge repair costs. This will make it easier to see the advantages of CFRP.

2.3. Reinforced Concrete

Numerous studies have been done involving CFRP strengthening of RC beams. Several have looked at shear and flexural enhancements for static as well as fatigue loading. Of the studies looked at, some involved strengthening using CFRP, and others looked at repair using CFRP.

2.3.1. Static Performance

Shahawy and Beitelman (6) looked at static performance of T-beams strengthened with CFRP. They statically tested ten T-beams, nineteen feet long, with differing wrap patterns varying from fully wrapped to partially wrapped stems. The partially wrapped stems only had CFRP on the bottom of the stem and not on the sides, and the CFRP layers varied from 0 to 4 sheets. Two-point loading was used for the tests. From their static tests, ultimate flexural strength was shown to increase from 19% to 70% with a rate of increase beginning to diminish past two layers. They determined that concrete crushing was occurring before the full strength of more CFRP layers could be realized.

It was also concluded that perhaps partial wrapping was not the best way to wrap the beams. When a CFRP layer was only placed on the bottom of the stem, horizontal cracks developed along the level of the reinforcing steel causing delamination of the concrete. The fully wrapped beams were found to be more ductile than the partially wrapped beams, which seems odd and does not seem to follow what most other researchers are saying.

Copozucca and Cerri (7) looked at the behavior of RC beam models strengthened after cracking with CFRP. After running single point bending tests on different beams with one and two layers of CFRP, they concluded that models with more layers of CFRP will have more strength but less ductility then those with fewer or no layers of CFRP. This could lead to undesirable brittle failures. With only one layer of CFRP, a good level of ductility was shown from their Moment-Curvature plots.

2.3.1.1. Shear

Chaallal et al. (8) performed tests looking into shear strengthening with CFRP fabric. They tested fourteen 20 ft long RC T-girders with various stirrup spacings a total of twenty-eight times to determine the effect of CFRP shear reinforcement. They drew several conclusions from their tests. The failure mode for the unwrapped beams was determined to be concrete crushing. For the wrapped beams the failure mode was usually fabric delamination near the support because of sliding along the line of the shear crack. The concrete in the wrapped beams appeared to have undergone significant deformations past its ultimate capacity due to the wrap confinement.

The researchers stated that for wrapped beams the maximum shear force generally increased with the number of layers of CFRP, but the shear forces were not a function of the number of layers. The optimum number of layers depended on the steel reinforcement; the shear reinforcement also increased the ductility of the members. They also claim that a certain combination of CFRP layers and steel stirrups exists that would create a maximum increase in ductility. Norris et al. (9) concluded that certain combination of fibers and orientations could provide a ductile yielding response similar to steel plate retrofits that is more satisfactory for concrete design. Chaallal et al. (10) gives a design procedure for shear strengthening using CFRP fabrics including an example problem.

Tann et al. (11) presented a design approach for externally bonded shear using FRP composites as well as a major literature review of previous research. This literature review documented growths in shear design technology and included names such as Sharif et al.(12), Chajes et al.(13), Sato et al.(14), Triantaffilou (15), and Swamy et al. (16). The review spanned the years from 1993-2000.

2.3.2. Fatigue Performance

Shahawy and Beitelman (6) also looked at fatigue performance of strengthened T-beams. Six beams, nineteen feet long, were cyclically loaded for up to 3,215,000 cycles. There was one control beam, two beams had 2 layers of CFRP with the stem fully wrapped and two beams had 3 layers of CFRP with the stem fully wrapped. A sixth beam was damaged in fatigue for 150,000 cycles before 2 layers of CFRP were added to its stem.

The damaged beam that had been rehabilitated showed improved fatigue life similar to the undamaged beams that were wrapped before they were loaded. This led to the conclusion that severely cracked beams in the field could be successfully repaired with CFRP. From the tests it was also concluded that the stiffness of all of the wrapped beams was greater than the unwrapped control beam. Finally the testers concluded that full wrapping of beams with CFRP is an effective method of rehabilitating and strengthening fatigue critical structures.

Barnes and Mays (17) conducted some fatigue tests on reinforced concrete beams with CFRP plates attached. Five identical beams were tested in fatigue, two original and 3 strengthened beams. Three different aspects of loading were addressed. These aspects

included the following: apply the same loads to plated and unplated beams, apply loads that would give the same stress range in the rebar to each, or apply the same percentage of ultimate load capacity to both beams. All three of these aspects were addressed in this single test.

The final results of this experiment showed that a plated beam had significantly longer fatigue life than an unplated beam with the same loading. A plated beam also has a longer fatigue life than an unplated beam when the rebar is loaded to identical stress ranges. Finally it was noted that an unplated beam had a longer fatigue life than a plated beam when each was loaded to the same percentage of the predicted ultimate strength.

2.3.3. Field Testing

Stallings et al. (18) tested a bridge in Alabama that had been damaged and repaired with CFRP. The bridge was a 4 girder, 7 span bridge with 34 ft spans. The bridge had not been impacted but needed to be strengthened due to additional load requirements, since it had developed flexural cracks near the midpoint of several spans. The plans called for FRP strengthening of one span with CFRP plates along the bottom of the flanges for flexural strengthening and GFRP along the sides of the flanges to prevent flexural cracks from opening further. The intent of the design was to increase the bending moment 20% so the needed CFRP was calculated based on this requirement.

The girders were repaired according to the recommendations provided by the manufacturer. These recommendations included grinding and sandblasting the concrete, creating a smooth surface on the plates and correctly mixing and applying the epoxy as well as using rollers to create a better bond. Static and dynamic load tests were done before and after the repair using ALDOT trucks, with decreases in reinforcement stresses for the static tests ranging from 4% to 12%. Decreases in mid-span deflection for the static tests ranged from 2% to 12%. For the dynamic tests, reinforcement stresses decreased from 4% to 9%, and mid-span deflection decreased from 7% to 12%.

The testers concluded that application of the CFRP was a simple, straightforward process with little or no need for special equipment or tools. They also found that deflections and reinforcement stresses in the girders strengthened with GFRP on the sides were noticeably less than for the girder without the GFRP. This led them to conclude that cheaper

GFRP plates may be added to the sides of girders to increase stiffness while the more expensive CFRP plates could be added to the bottom flanges to increase load capacity.

Masoud and Soudki (19) investigated the serviceability of corroded RC beams that had been strengthened with CFRP sheets. They tested 8 strengthened beams that had been corroded with a chloride solution, and they concluded that the CFRP was capable of restoring strength lost due to corrosion. Their results also showed that longitudinal crack widths were reduced about 20% from unstrengthened to strengthened beams, and mid-span deflection was also reduced an average of 33% for strengthened beams.

Watson (20) reported on several aspects of CFRP uses including column wraps, corrosion inhibition, and beam strengthening, including laboratory and field beams. One investigation included a bridge in South Carolina that had been significantly damaged by vehicular impact. The state had to choose the best possible repair option. It was determined that the replacement of the beam would have cost upwards of $250,000. Finally a CFRP strengthening option was designed and approved that only took 3 weeks, saved the state over $150,000, as well as minimized traffic disruption.

Many other people have conducted tests on RC bridges strengthened with either CFRP and/or GFRP. Some of the more recent include Nanni et al. (21), Brena et al. (22), Kachlakev (23), and Keble et al. (24). There are also up to hundreds more not mentioned.

2.4. Prestressed Concrete

There have been relatively few papers published concerning CFRP and prestressed concrete. Klaiber et al. (25) tested a P/C beam with 3 of the 12 strands cut to simulate impact damage. The beam was repaired using a corrosion inhibitor followed by a mortar patch. The beam was fitted with CFRP plates for flexural strengthening. A GFRP wrap was also put on at the end of the plates to prevent debonding and near the middle to prevent patch fallout and restrain peeling as a result of flexural cracks in the maximum moment region. Following an ultimate load test, it was concluded that the CFRP and GFRP contributed to a gain of 17% from the unstrengthened to the strengthened beam. They concluded that the repair was effective in restoring stiffness and providing strength increases in the damaged beams.

Russo et al. (26) investigated the effects of overheight vehicle damage to prestressed concrete I-beam bridges. The testing involved two bridges, one (westbound lanes) that had

two beams damaged by an overheight vehicle and a second (eastbound lanes) nearly identical bridge that was used as a basis for the load testing. Laboratory beam tests and analytical modeling were included in the investigation as well. Service tests, which consisted of forty-three static load configurations, were performed on the undamaged (EB), damaged (WB), and repaired (WB) bridges to observe any differences in load distribution. The repair consisted of beam replacement. The two damaged beams were then taken to a laboratory where further tests were performed. One of the damaged beams was repaired using CFRP while the other was used as a basis for the experiment.

The results of the testing showed that the damaged bridge behaved differently from the undamaged and repaired bridges. The redistribution of loads away from the damaged beams was evident in the damaged bridge, while the undamaged and repaired bridges behaved almost identically. The analytical modeling showed that the moments in the damaged beams for critical load locations were significantly less than the moments expected from AASHTO equations, showing plenty of extra strength. The laboratory beam tests showed that the damaged beam had sufficient strength to have remained in service. The beam that was strengthened with CFRP attained a capacity 12% greater than the basis beam.

2.5. Beam Design Using CFRP

Norris et al. (9) presented design guidelines for RC beams strengthened in flexure and shear with FRP plates or fabrics based on the Canadian Concrete Standard. Their presentation of flexural design includes the flow chart shown in Figure 2.1 devised for ease in designing. A design example problem was also included to show the steps for designing a beam with CFRP.

The MBrace company (27) that produces many of the CFRP materials used as well as other products also has created some design specifications for its CFRP products. Their design approach includes investigating several possible failure modes and limit states. Like Norris et al. (9) they obtain an initial area of FRP and modify it based on a comprehensive analysis of the strength, ductility, and serviceability of the member. This requires an iterative design so the company also provides a simple computer program for ease in design.

Kelley et al. (28) wrote an article meant to emphasize and discuss key issues related to the methodology for the design of concrete structures using CFRP. The issues were based

on guidelines being considered by ACI Committee 440 F. Some of the issues that Kelley et al. wanted to address were minimum required pre-strengthened strength criterion, limits on strength enhancement, appropriate φ factors, and the condition of the concrete substrate.

For the first issue dealing with the pre-strengthened strength of the members, the authors mentioned the potential for failure due to uncontrollable events, with the number one risk being damage due to fire. The high temperatures involved in a fire would cause the adhesive to flow plastically, which would cause a loss in load transfer to the FRP. Thus it was contended that the unstrengthened structure be capable of resisting service loads without the steel reinforcement yielding. It was also recommended that the ultimate strength of the unstrengthened system exceed the service loads by a safety factor of 1.2. This safety factor was to account for 4 things, unintended load, understrength of material, unintended construction influences, and unintended environmental influences.

The second issue discussed dealt with the lack of ductility of the CFRP. CFRP is not a ductile material as it exhibits nearly linear stress-strain behavior to failure in tension, but R/C members strengthened with CFRP can exhibit ductile behavior. In this article, this phenomenon was referred to as pseudo-ductile behavior. In order to get the desired pseudo-ductile behavior, the amount of CFRP must be limited. If a member were strengthened with so much CFRP that the reinforcing steel fractures when only a fraction of the CFRP strength is used, the member would have little ductility and no warning of impending failure. The designer must understand the behavior of the member prior to and after strengthening. The main emphasis of the ductility section was that the ratio of CFRP to steel reinforcement be one that is favorable to promote ductile behavior near the ultimate loads.

The final area of major discussion involved φ factors. The claim was that there needs to be some standardized test data to develop φ factors that mean anything. Assigning specific values to individual φ factors is an ambiguous task without the proper comprehensive study. With all of the variables currently involved such as different manufacturers, different material and performance properties, and different installation procedures, it is difficult to assign one factor to all models. The proposed equation for φFRP was the following:

$$\varphi_{FRP} = \varphi_{MAT} * \varphi_{PROC} * [(\varphi_{CURE} + \varphi_{LOC})/2] * \varphi_{DEGR}.$$

φ_{MAT} accounts for the deviation and level of uncertainty of the material properties;

φ_{PROC} accounts for variation due to processing methods;

φ_{CURE} accounts for variation in properties due to degree of cure achieved;

φ_{LOC} accounts for uncertainty due to the location of processing;

φ_{DEGR} accounts for material property changes due to environmental effects.

The values of all of these factors would range between 0.3 and 1.0. With a continuing influx of data, these factors should be refined over time and standardized.

Pouliot et al. (29) developed design charts to improve the designability aspect of CFRP for design and repairs. These charts were meant to ease the calculation process which in turn increases the speed of the decision making process during preliminary design. The procedure developed for producing the design charts was also discussed at great length. A design example was included as well.

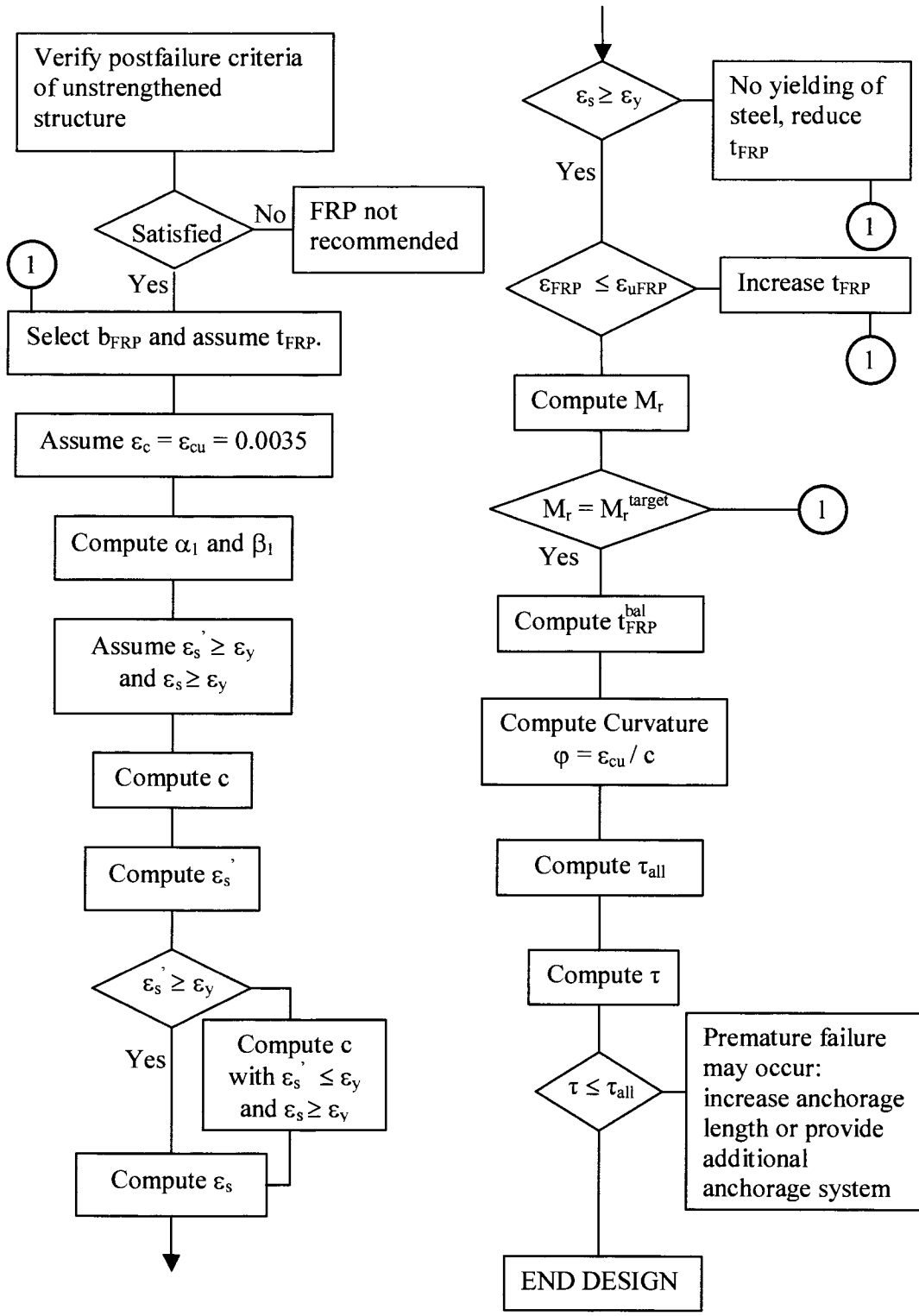

Figure 2.1. Flexural design flow chart.

3. TESTING PROGRAM

There were four tests involved in the testing program including one laboratory beam and three field bridges. The tests included service tests, fatigue tests, and ultimate load tests. The test set-ups and procedures of all the tests are described herein.

3.1. Prestressed Beam

The prestressed concrete beam analyzed in the laboratory segment of this project was an Iowa DOT LXA-38 beam. Humboldt Concrete Products of Humboldt, Iowa, provided the beam. The beam measured 39 ft – 4 in. long from end to end, and it weighed approximately 29,000 lbs. Figure 3.1 shows a cross sectional view of the beam with dimensions. Figure 3.2 shows the strand configuration, with 12 strands on the bottom and 2 strands on the top.

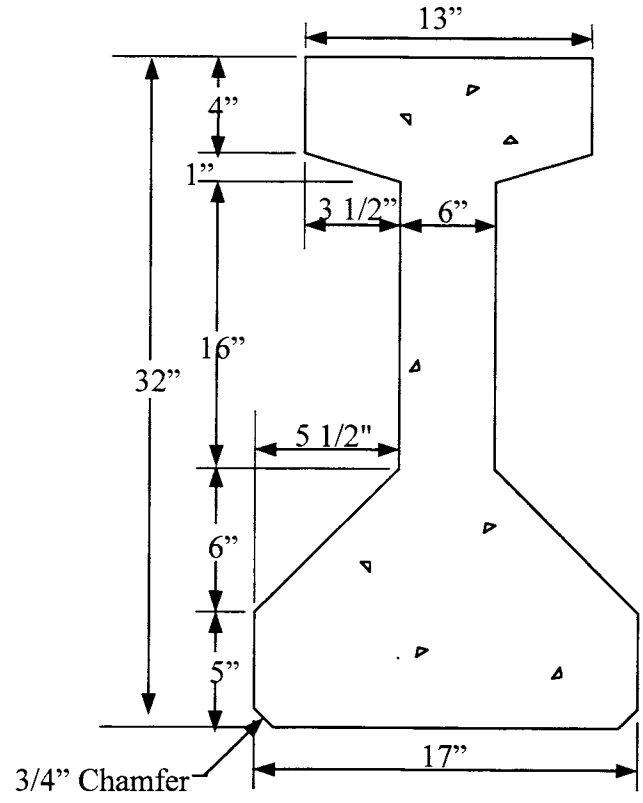

Figure 3.1. Cross-section of LXA-38 P/C beam.

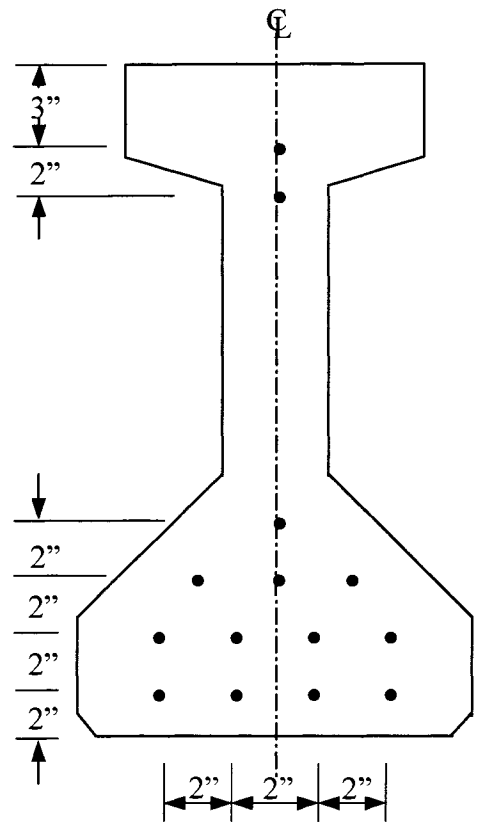

Figure 3.2. Strand Configuration of LXA-38 P/C beam.

3.1.1. Cast-in-place composite slab

A composite slab was cast in the lab to develop the full tensile strength of the CFRP repair material. The P/C beam with the composite slab more closely resembled a typical bridge in the field. The slab size that was chosen for this beam was 4 feet wide, spanning the length of the beam, and 8 inches thick; these dimensions were chosen after a literature survey of several DOT projects throughout Iowa. The maximum allowable spacing for this size of beam was 7 ft – 6 in, although most bridges in the state do not typically use this maximum allowed girder spacing. Using the AASHTO specifications, the effective slab width of the specimen was calculated to be 48 in. This was calculated as a function of the effective beam span, the slab depth (slab stiffness), and the beam spacing. The actual slab width was used as the effective slab width when calculating section properties of the composite cross-section.

Due to the instability of a larger slab, the 48 in. slab was decided upon even though it was somewhat conservative. The moment of inertia for a composite beam with a 7 ft – 6 in. wide slab is 22% larger than an identical beam with a 4 ft wide slab, which caused measured strain and deflection values to be slightly higher. Steel stirrups protruding from the original P/C beam, and the deliberate scoring of the concrete surface supplied the composite action of the beam and slab. The CIP slab is shown in Figure 3.3.

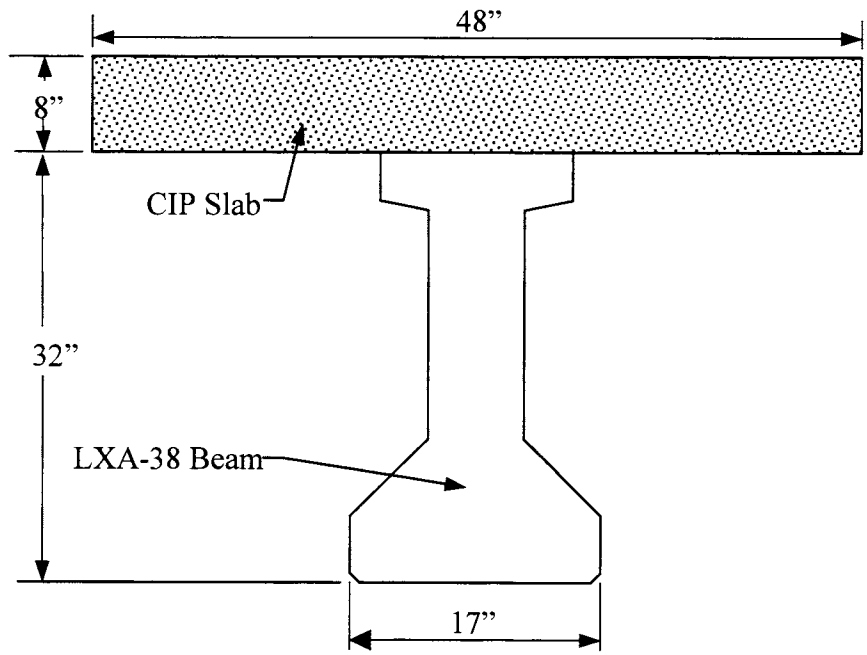

Figure 3.3. Dimensions of CIP concrete slab.

3.1.1.1. Formwork Detail

Wooden formwork for the slab was constructed in the lab using 2x4 and ¾ in. plywood. The 2x4 were used for the legs and transverse framework under the plywood. The legs were approximately 32 in. high. The legs were different lengths to conform to the natural ¾ in. camber of the beam. The transverse braces were spaced every 16 in. to prevent any deflection of the plywood while pouring. Concrete screws were installed to anchor the formwork to the beam; a cross sectional view of the formwork is shown in Figure 3.4. Only a few screws were used to prevent any unnecessary holes or accidents, and all of the plywood was coated with form oil before the steel reinforcement was set in place.

For the purposes of moving and loading the beam, 8 holes needed to be made in the slab, 4 on each side at particular spots. The easiest way to get the holes in the slab was to pour the slab with some sort of cylinders all ready in place, since drilling after the pour would require much more labor time and cause a bigger mess. The best cylinders available were 4 in. diameter PVC pipe sections, long enough to pass through the slab. Threaded rods, ½ in. in diameter, were used to hold the pipe sections in place during the pour. The rods were drilled through the plywood and held tightly on the top by a small wooden block. The wooden block also prevented any concrete from entering the inside of the PVC pipe. As with the plywood, the pipes had to be covered with form oil, and they were removed after the pour by twisting them out.

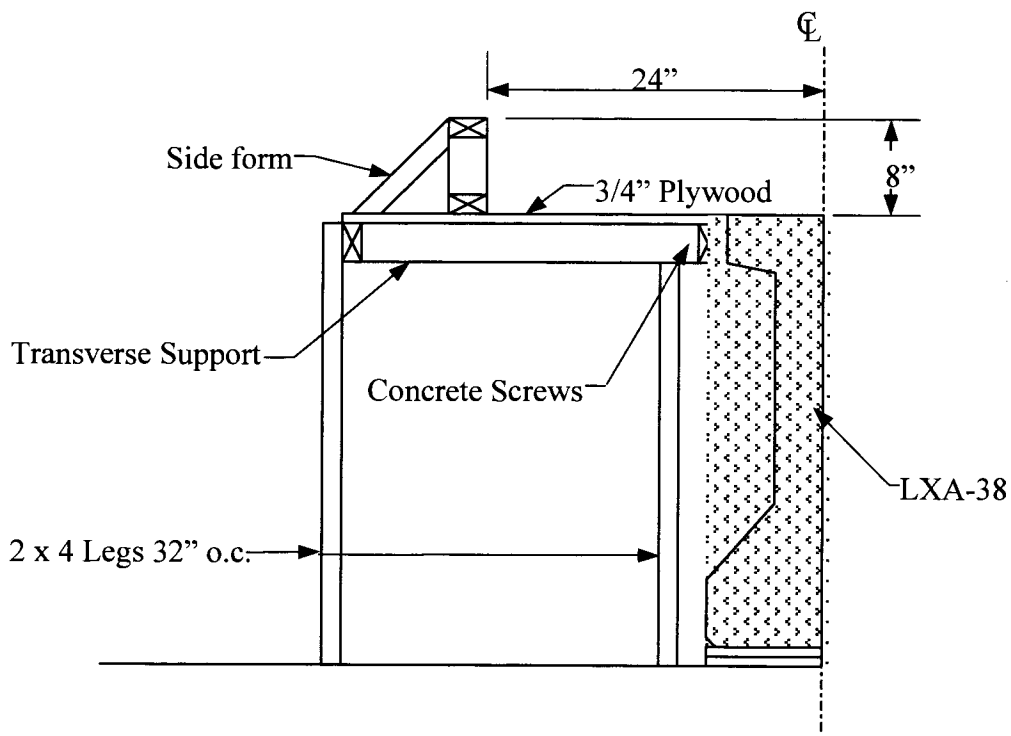

Figure 3.4. Formwork cross-section for R/C slab.

3.1.1.2. Slab Reinforcement

The R/C slab was poured according to AASHTO LRFD specifications, which called for #4 bars placed every 12 in. in both directions, longitudinal and transverse. The steel reinforcement was Grade 40 deformed bars, with shrinkage and temperature restraints being the controlling factors in the slab design. The reinforcement was placed on 6 in. high chairs.

The Iowa DOT provided the concrete, which was a standard mix, with 4,000-psi design strength. Standard industry practice was used for the pour, including a vibrator that was used to evenly distribute the mixture. Steel trowels were used to finish the top of the slab. Plastic tarps were used to cover the concrete for curing, along with burlap blankets to keep in the moisture.

3.1.2. Fatigue Conditions

The beam was subjected to cyclic loading to simulate actual highway loading. The setup for the fatigue portion of the test is shown in Figure 3.14. The lab setup required to accommodate the beam consisted of a large preexisting steel frame anchored to the lab floor. The frame consisted of two W-shaped steel beams about 25 feet long that ran parallel to each other seven feet apart, with other W-shaped beams providing bracing. The lab was not big enough to allow the P/C beam to be placed parallel or perpendicular to the frame. The only way the beam would fit was to skew it diagonally to the frame. This allowed for just enough room to walk around one end of the beam in order to maintain the functional capacity of the lab, although one end of the beam rested on the tie down floor and the other on the on grade slab.

Since the P/C beam had to be skewed, the actuators had to be skewed as well. Two hydraulic actuators were used to load the P/C beam; the actuators each had a 55 kip capacity. The actuators were attached to the frame using several large C-clamps. They were also braced in several directions, and welded to the frame to prevent them from moving from side to side. Small movements of the actuators did not appear to have a significant effect on the fatigue loading.

A cross-sectional view of the fatigue test is provided in Figure 3.15. A 10 ft steel spreader beam was used because the actuators were only 4 feet apart. It was not attached to the actuators to prevent any potential binding, and the spreader beam was supported by the pin and roller on top of the beam. The weight of the actuators kept the spreader from moving. During the fatigue testing, a minimum load of 2 kips was applied at all times to prevent any bouncing or movement of the spreader beam.

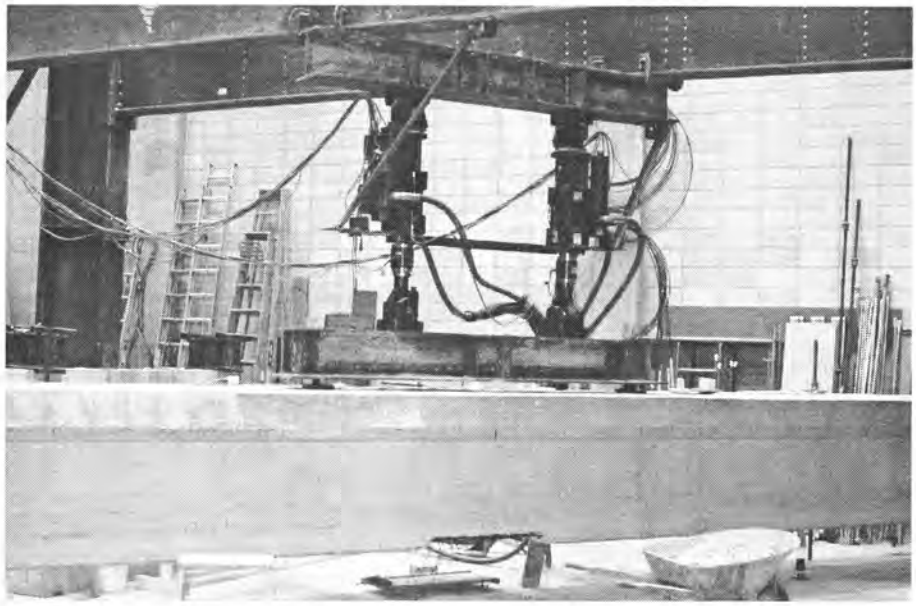

Figure 3.5. Fatigue loading setup.

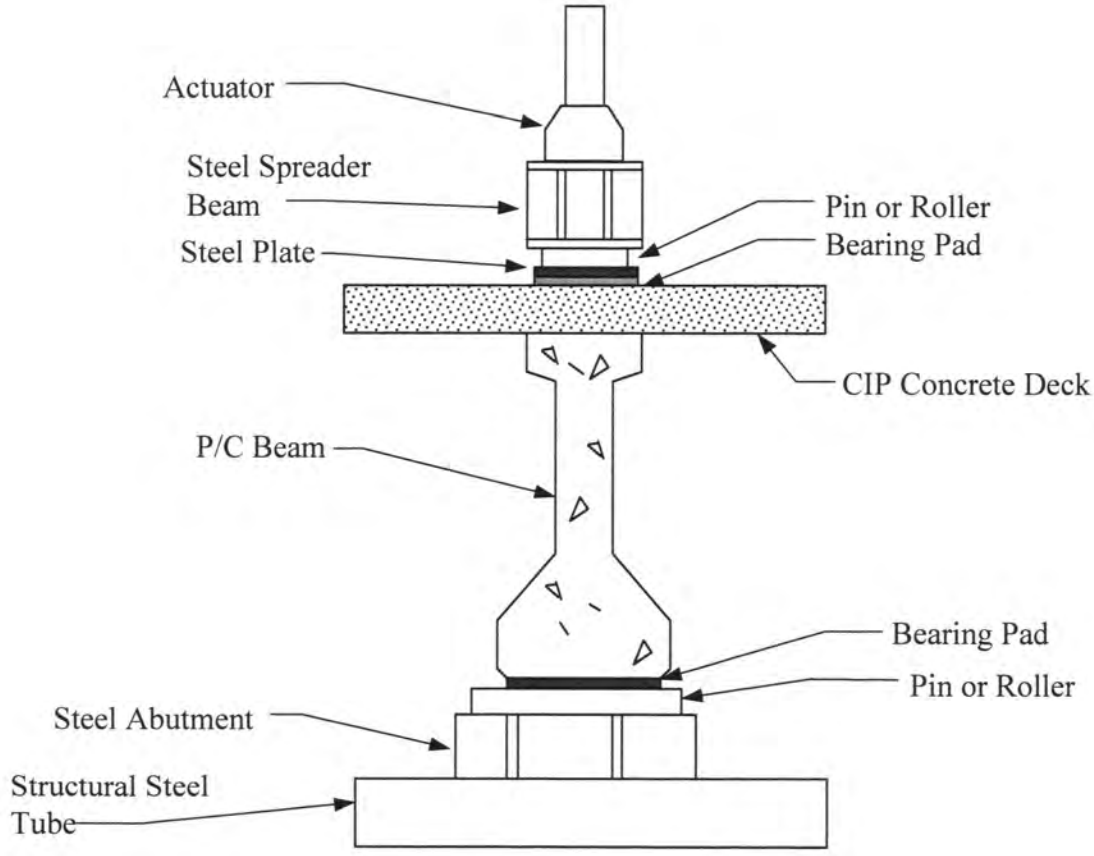

Figure 3.6. Cross section of fatigue loading setup.

3.1.3. Instrumentation

Instrumentation consisted of three different types of gages. Gages were placed on the concrete, the steel reinforcement and the CFRP. All of the gages were then fed into the data aquisition system, DAS.

3.1.3.1. Concrete gages

Six 2.4-inch type F-2400 concrete resistance gages were originally placed on the beam. Five gages were placed on top of the CIP slab, and one was placed on the bottom of the beam. Three of the gages were laid across the center of the slab at mid-span 18" apart. Two of the gages were laid on center, 56" from each end of the beam. These locations approximately corresponded to the termination points of the longitudinal CFRP. The one gage that was located on the beam was on the bottom flange at the center of the span. A top view of the concrete gages is shown in Figure 3.7.

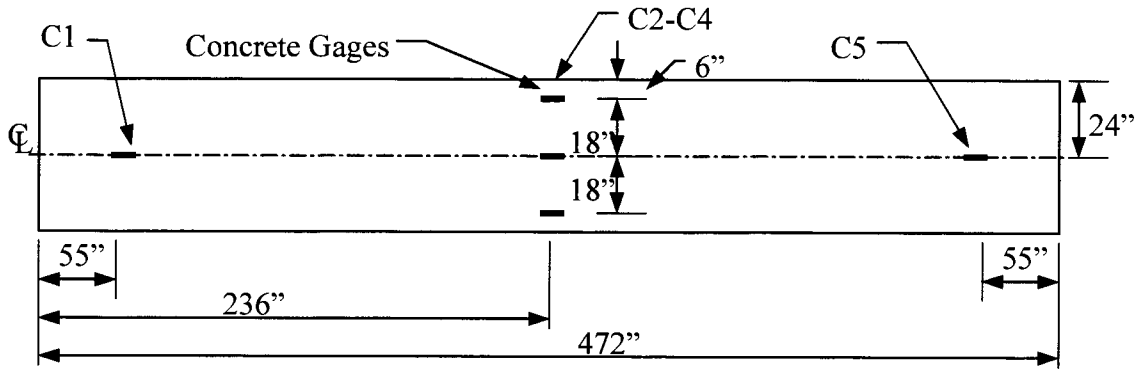

Figure 3.7. Concrete gage locations, plan view.

3.1.3.2. Prestressed gages

Eight steel resistance gages, type CEA-06-043UW-120, were placed on the prestressed strands after the concrete had been removed from the center of the beam. These gages were used to measure the prestressing forces in the beam. Two gages were placed on each strand near one end of the damage, which allowed the other end of the strands to be cut with an acetylene torch without damaging the strain gages. These gages are shown in Figure 3.8.

3.1.3.3. CFRP gages

A total of nine gages were positioned on the CFRP, six on the longitudinal CFRP, and three on the transverse wrap. Seven of the gages were placed symmetrically down the center of the CFRP, with the center gage actually on the wrap. The other two gages were placed on opposite sides of the bottom flange in the center of the beam. The CFRP gage layout can be seen in Figure 3.9, and an overall view of the setup and gage plans is shown in Figure 3.10

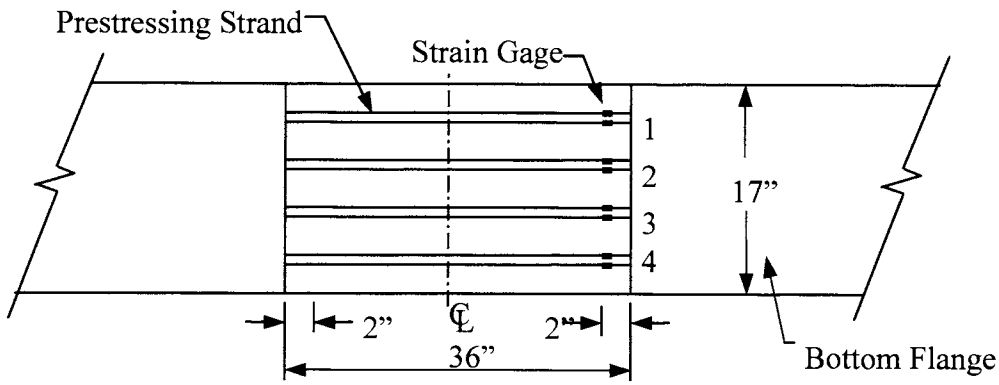

Figure 3.8. Prestressed gage locations.

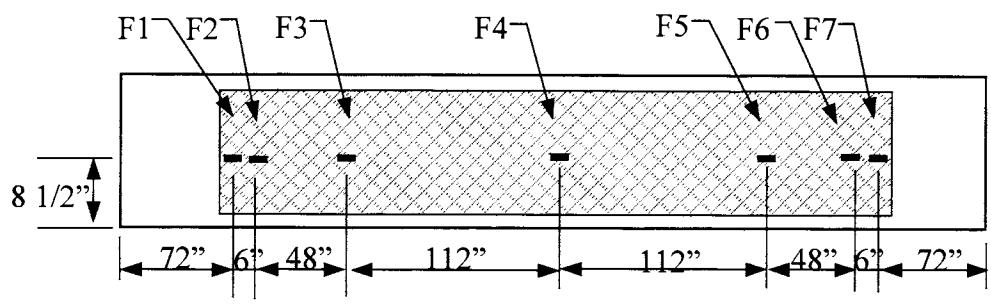

Figure 3.9. CFRP Gage locations.

3.1.4. Imposed Damage

Damage was inflicted to the beam to simulate a truck striking the beam as if it were a member in a bridge. The damage included removal of a section of concrete, and the cutting of two of the prestressing steel strands.

3.1.4.1. Removal of Concrete

A 3-foot section of concrete was removed from the center of the bottom of the P/C beam. The section was 4 inches deep measuring from the bottom. Four inches was chosen because that left the bottom four strands showing, while the next layer of four strands was still encased in concrete. The four inches taken out also allowed just enough room to be able to patch the damaged area. A large chipping hammer was used for the removal of the concrete, but significant care had to be taken so as not to sever any of the prestressing strands. The damaged section is shown in Figure 3.11, and a photograph of the damaged area is shown in Figure 3.12.

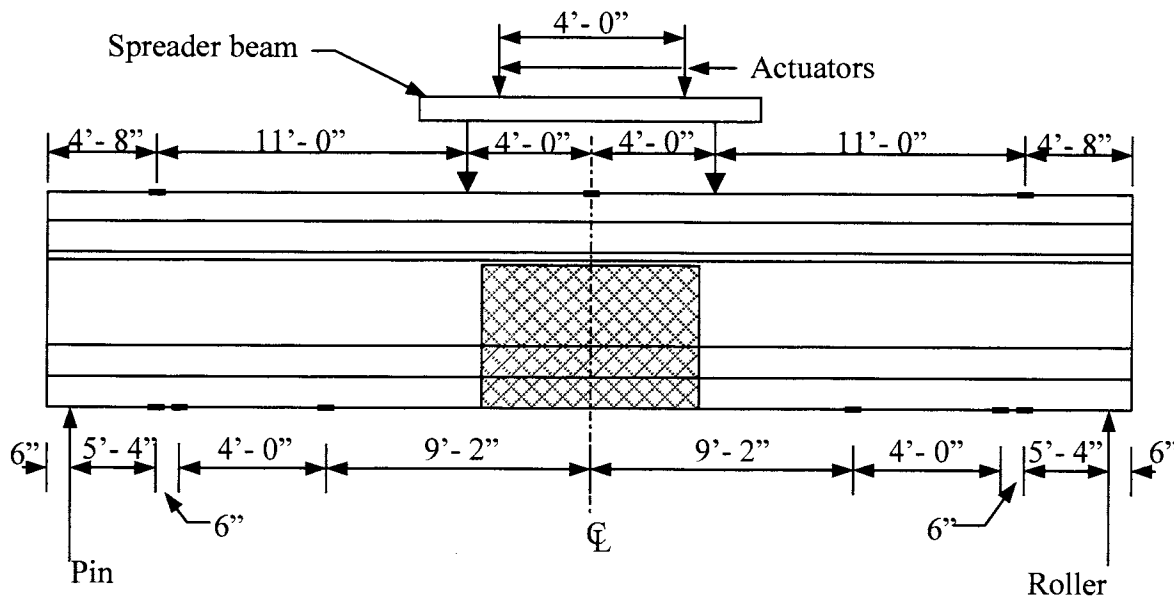

Figure 3.10. Overall gage locations.

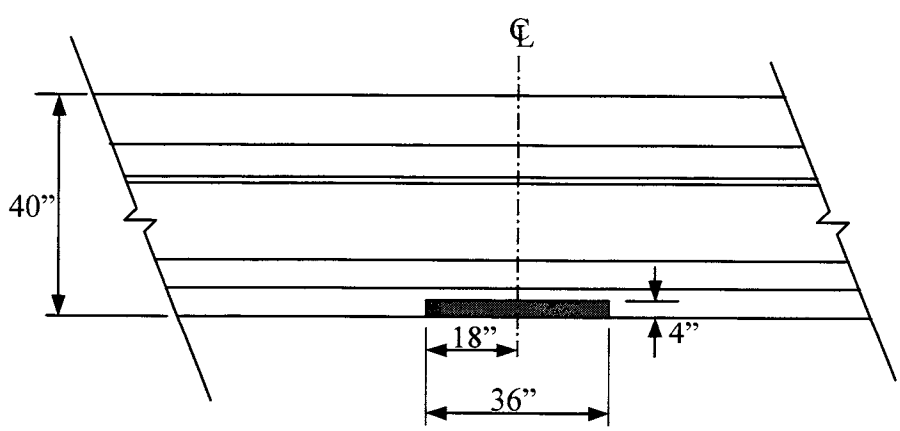

Figure 3.11. View of Damaged Concrete section.

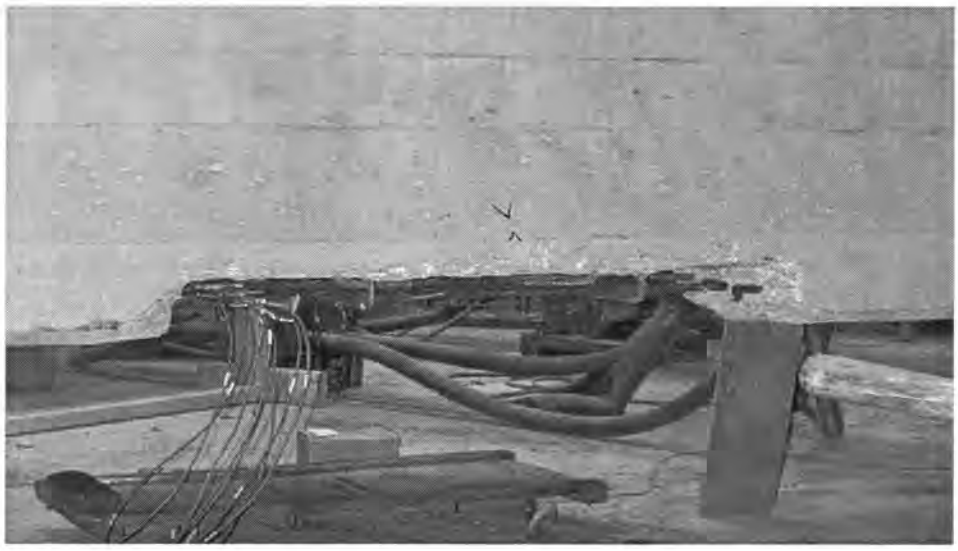

Figure 3.12. P/C beam with concrete removed.

3.1.4.2. Cutting of Prestressing Strand

Two of the twelve prestressing strands were cut, strands 3 and 4 in the diagram. This constituted 17% of the total area of steel. Once the concrete was removed, 2 strain gages were placed on each strand. The strands were then cut one by one using an acetylene torch. They were heated slowly to induce a slow severing, since violent kickbacks would not enhance the quality of the data. The strain in the strands was measured with no load on the beam three different times, before either strand was cut, after one strand was cut, and after both strands were cut. A photograph of the severed strands is shown in Figure 3.13.

3.1.4.3. Loading and Degradation

The P/C beam was loaded with a load range from 2 to 29 kips per actuator. The maximum moment induced was approximately 35% of the total moment capacity of the beam. The rate of loading was 0.70 cycles per second, and the loading was applied for 2.5 million cycles. Service load tests were run frequently, about 20 times throughout the cycling to identify any change in stiffness or strength. The CFRP was also visually inspected throughout the cycling to observe potential debonding. Table 3.2. lists the number of cycles carried out prior to each service test. Each degradation test involved setting the actuators so there were 2 kips total on the beam, then increasing the load to 58 kips while taking readings at 2 kip intervals.

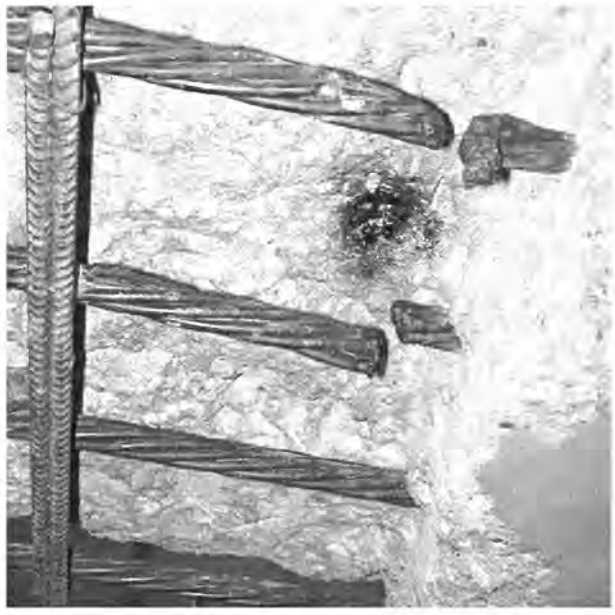

Figure 3.13. Strands after severing.

Other service load tests were also performed throughout the damage and repair process. A service test was performed after each of the following events: before any damage was done, after the concrete was removed, after the strands were cut, and after the longitudinal and transverse CFRP was applied. These tests were run from 0 to 25 total kips.

3.1.4.4. Ultimate Test Setup

Once repaired, the P/C was tested to failure to determine the ultimate load. The actuators used for the fatigue test did not have the capacity to completely fail the beam. Since the beam was skewed, it was also not possible to test through the tie down floor, thus the beam had to be lifted and moved to another part of the lab so the testing holes in the beam would line up with the holes in the floor.

The P/C beam was tested in four-point bending as shown in Figure 3.14. The abutments were each 2 W21 x 83 sections that had been welded together. The webs of the abutments had also been stiffened so as to take the tremendous concentrated loads. Bearing pads were placed on the abutments under the ends of the beam.

Table 3.1. Number of cycles at each degradation test.

Number of Test	Number of Cycles	Number of Test	Number of Cycles
1	0	11	899,430
2	64,960	12	958,140
3	115,500	13	1,092,200
4	176,180	14	1,189,610
5	288,060	15	1,361,150
6	330,170	16	1,526,420
7	384,740	17	1,641,800
8	441,240	18	1,769,340
9	694,600	19	2,049,910
10	786,780	Ultimate	2,528,930

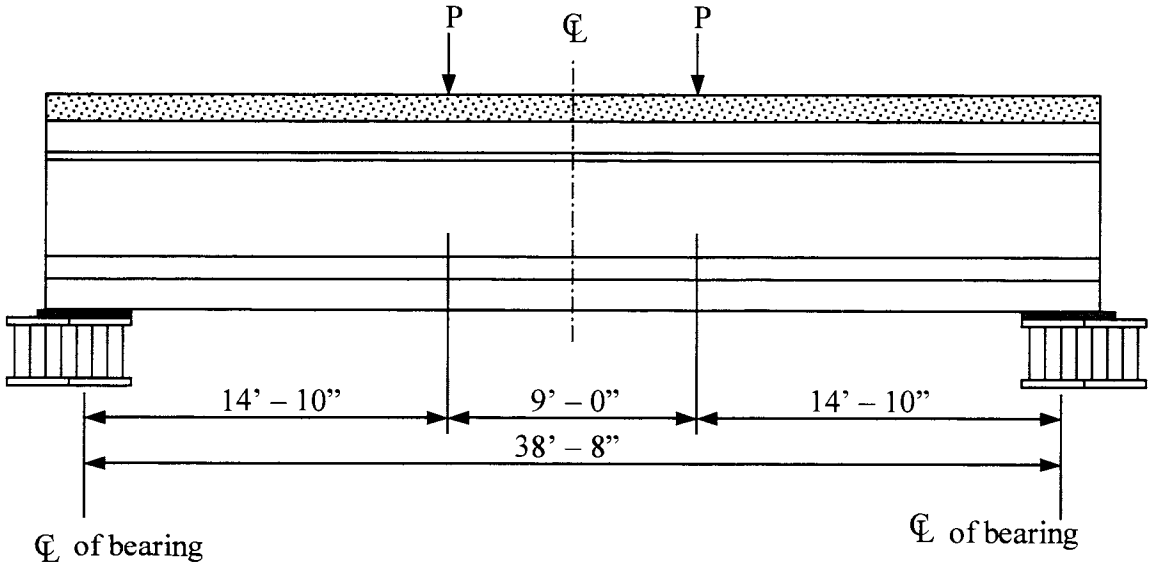

Figure 3.14. Side view of loading arrangement.

Load was applied using two hydraulic loading cylinders. The cylinders were connected to a hand pump via a splitting connector, used to keep a balance of load between the two loading cylinders. Tie down bars were secured to the floor, with structural tubing securely attached to the top of the bars. The load cylinders applied the load against tube, which loaded the beam. Load cells, neoprene pads, and steel plates were placed between the load cylinders and the beam, with the pads and plates used to lessen the concentrated loads. A cross section of the load set up is shown in Figure 3.15.

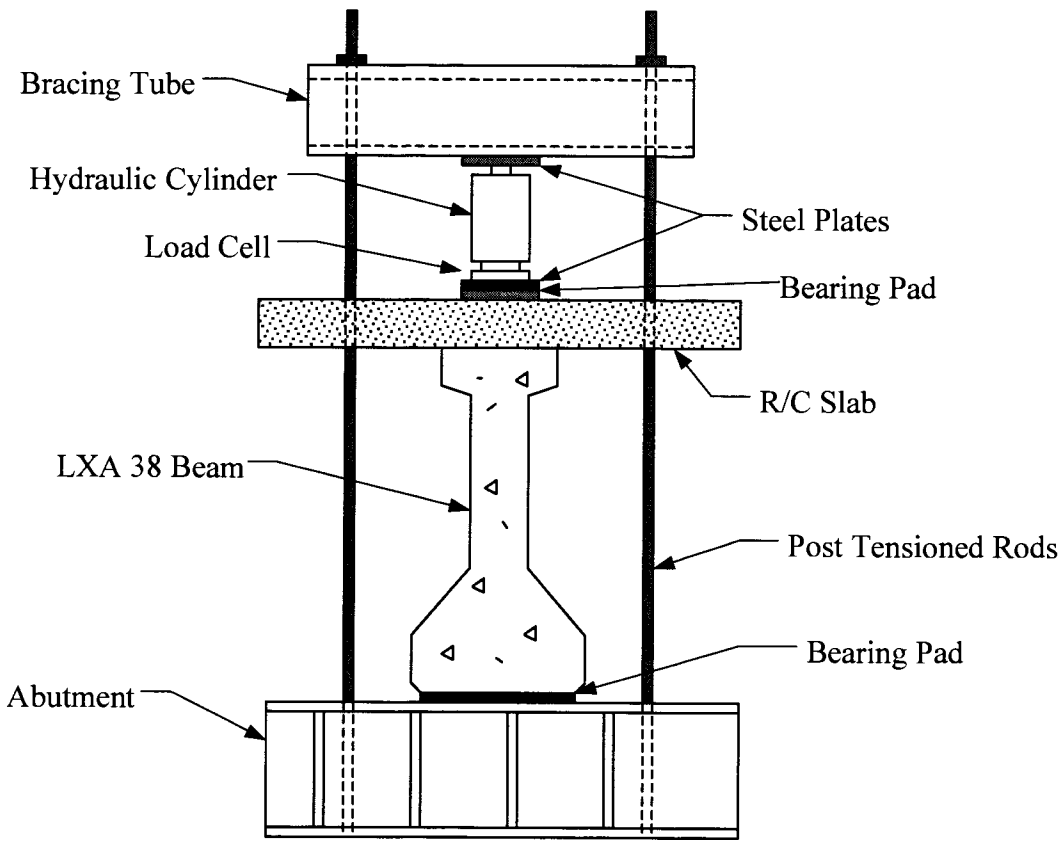

Figure 3.15. Ultimate load test setup.

3.2. Bridge Testing Program

The field portion of the program involved three bridges around the state of Iowa that had been damaged by overheight vehicles. The bridges were near Altoona, Osceola, and De Soto, Iowa. Each bridge was repaired using CFRP. Table 3.2 lists the bridge numbers and their location.

Table 3.2. Bridge locations and maintenance numbers.

	Approximate Bridge location	Bridge number
Bridge 1	Altoona, Iowa	7783.IL065
Bridge 2	Osceola, Iowa	2015.2L034
Bridge 3	De Soto, Iowa	2510.I.080

3.2.1. Altoona Bridge

Bridge 1 had six girders that all carried 4 spans. The 4 spans included a 36' approach span on the north side, a 46' exit span on the south side, and two 96.5' main spans that carry traffic south along IA Highway 65 over IA Highway 6, which runs almost perpendicular. The bridge consists of two travel lanes, a large shoulder lane on the outside, and a smaller shoulder on the inside of the roadway. An overall view of the bridge is shown in Figure 3.16, a schematic view is shown in Figure 3.17, and a cross section is shown in Figure 3.18.

Figure 3.16. Overall view of Altoona Bridge looking east.

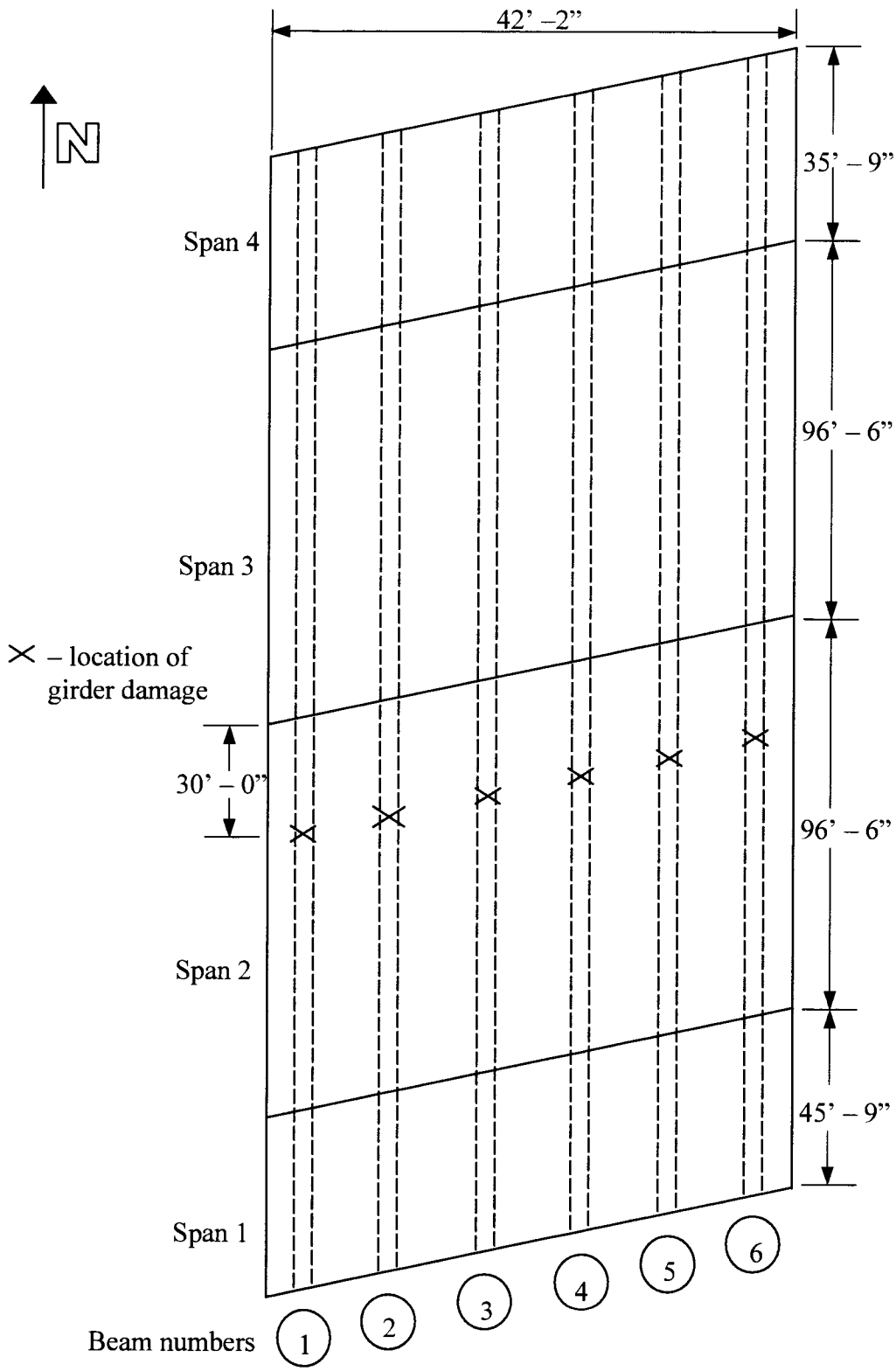

Figure 3.17. Dimensions of Altoona Bridge.

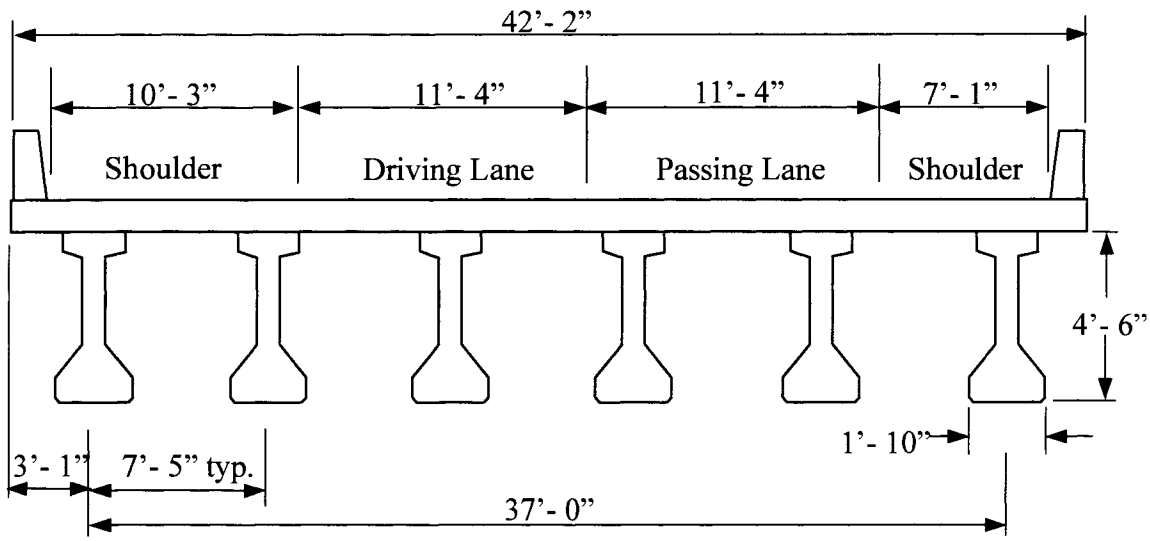

Figure 3.18. Cross section of Altoona Bridge.

3.2.1.1. Description of Damage

An overheight semi-tractor trailer being driven on Highway 6 from west to east impacted the west most girder of the bridge, damaging it slightly. This initial impact caused the truck's load to retract and then rebound back into the second girder. This impact caused greater damage, to the extent of two strands being severed and some concrete loss. The truck continued traveling under the bridge while the load scraped and superficially damaged the concrete of the remaining 4 girders. A more extensive damage report is located in Appendix B. Beam damage can be seen in the photographs of Figures 3.19 through 3.21.

3.2.1.2. Load Test Set up

The load test took two days to complete, with the first day consisting of instrumenting the bridge with strain gages. Displacement transducers were installed at midspan of span 2 on the second day, prior to the load testing. The strain gages were then left in place while the bridge was repaired, but the displacement transducers were removed. Following the repair of the bridge, new strain gages were installed where they had been torn down and the test was repeated.

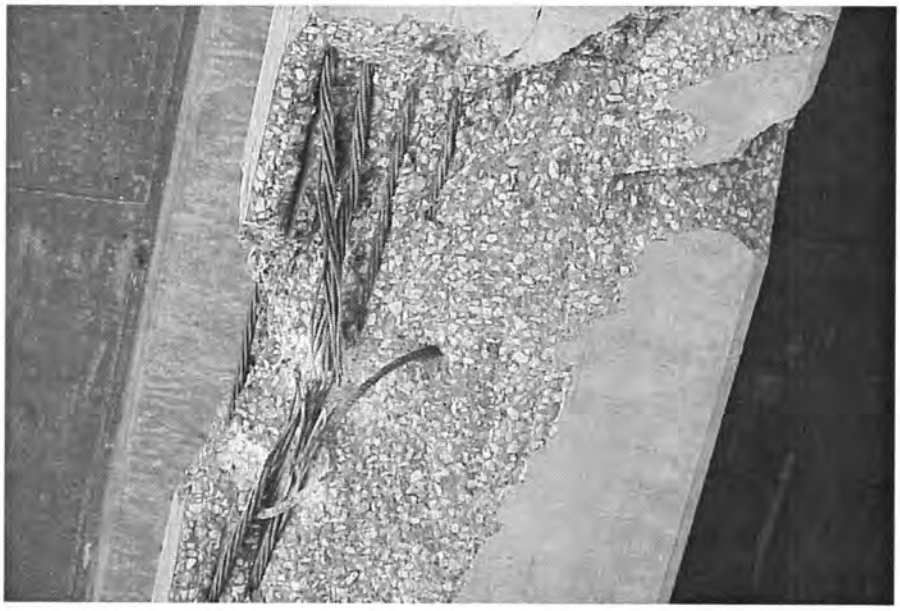

Figure 3.19. Photograph of the damage to Beam 2 in the Altoona Bridge.

Figure 3.20. Photograph of the damage to Beam 1 in the Altoona Bridge.

Figure 3.21. Photograph of the damage to Beam 5 in the Altoona Bridge.

3.2.1.2.1 Instrumentation

Concrete strain gages were placed in several different positions on each of the 6 girders. The gages were glued according to the methods described in the gage manual. The gages were covered with enamel, thin rubber strips, and aluminum tape (see Figure 3.22) to protect them from the elements, as they would remain on the bridge for several months.

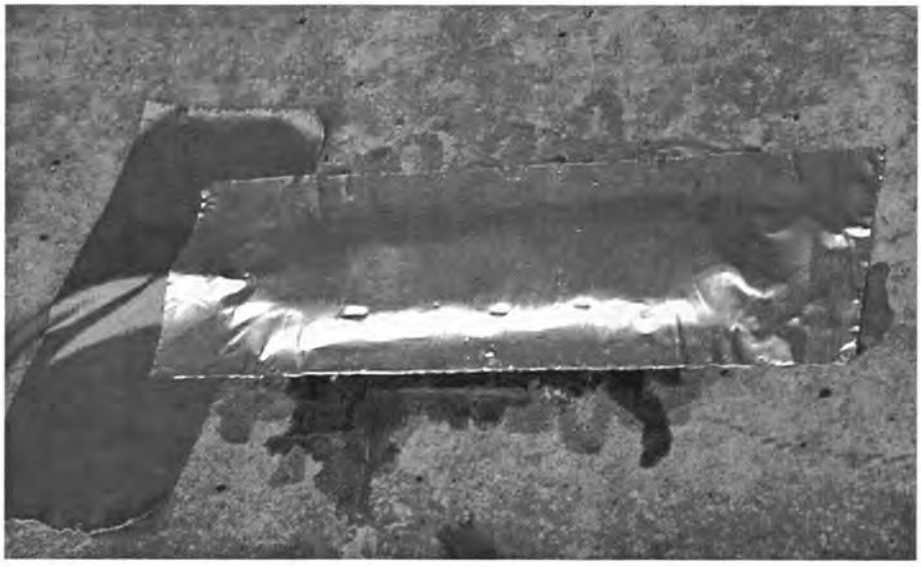

Figure 3.22. Photograph of weather protecting tape over a strain gage on the Altoona bridge.

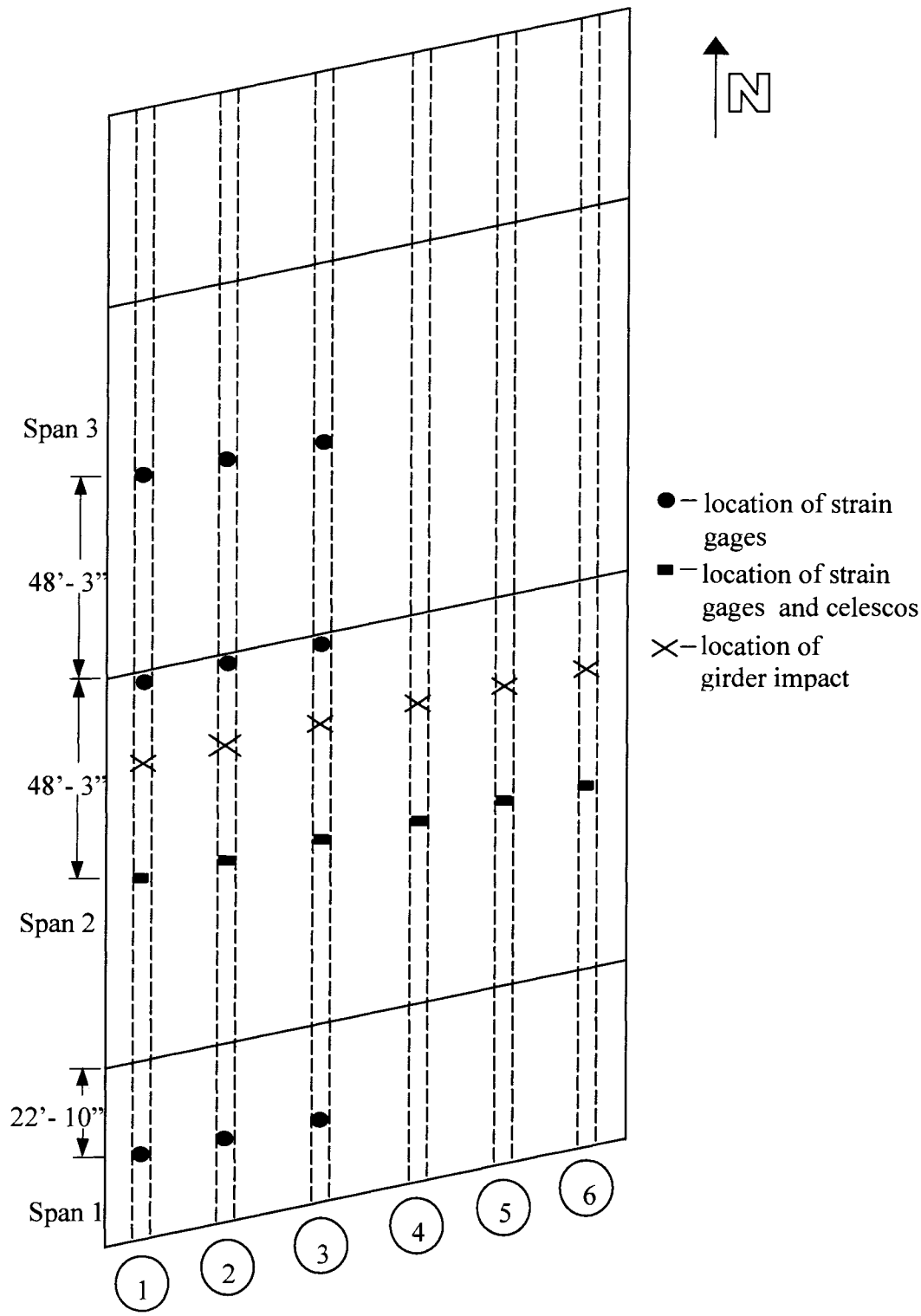

Figure 3.23. Location of strain gages and deflection transducers on the Altoona Bridge.

The strain gage and deflection schematic is shown in Figure 3.23. Six strain gages where placed on girders 1, 2, and 3. These were the girders that surrounded the most heavily damaged area, Girder 2. The eastern three girders, girders, 4, 5, and 6, each had two gages.

For girders 1, 2, and 3, one gage was placed on the side of the bottom flange at mid-span of span 1, the south span. Two gages were placed at mid-span of span 2, with one gage placed on the side of the top flange, and one on the side of the bottom flange. Two more gages were placed near the north pier of span 2 in the same configuration that was just mentioned, which was done so the damaged area would have gages on either side of it. Finally, 1 more gage was placed on the side of the bottom flange at mid-span of span 3.

Girders 4, 5, and 6, had two gages each. The gages were on the side of the top flange and the side of the bottom flange and were set at mid-span of span 2. These gages made it possible to find the centroids of girders 4, 5, and 6. Deflections were measured on all of the beams at the mid-span of span 2 with celesco type string potentiometer transducers.

3.2.1.2.2 Load Trucks

The trucks used for the static and dynamic load tests were Standard DOT 3-axle dump trucks filled with sand. The weights and dimensions for each of the four trucks can be found in Table 3.4, with the accompanying figure (Figure 3.24). Dimensions are listed to the nearest one tenth of a foot. Trucks 1 and 2 were used for loading during the original test while trucks 3 and 4 refer to the trucks from the second test. The center of gravity of the trucks was taken to be at the center of the rear tandem axle.

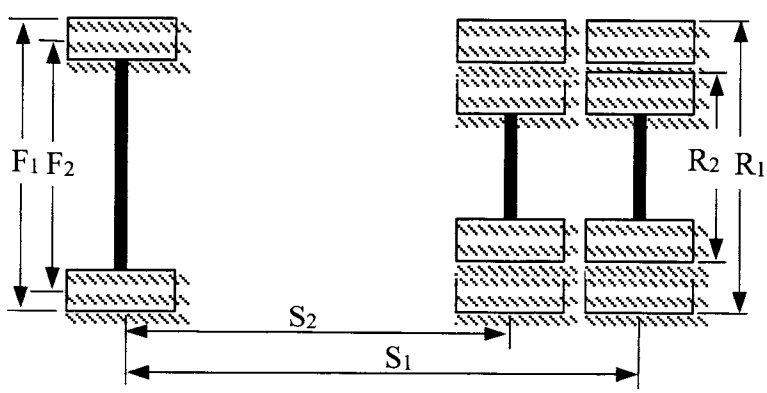

Figure 3.24. Dimensions of the trucks used in the Altoona bridge test. (see Table 3.3)

Table 3.3. Weights and dimensions of trucks.

Truck	Truck Number	Weight (lbs.)	F_1 (ft)	F_2 (ft)	R_1 (ft)	R_2 (ft)	S_1 (ft)	S_2 (ft)
1	A29244	53,800	8.0	7.0	8.0	6.0	18.5	14.5
2	A29532	48,400	8.0	7.0	8.0	6.0	18.5	14.5
3	A29244	46,180	8.0	7.0	8.0	6.0	18.5	14.5
4	A25857	47,220	8.0	7.0	8.0	6.0	19.0	15.0

3.2.1.3. Static and Dynamic Test Procedures

Two tests were conducted on this bridge; before and after repair. Both a static test and a dynamic test were conducted. The dynamic test was performed to provide a better indication of the bridge continuity.

3.2.1.3.1 Static Test Procedure

A static load test was conducted using various load cases. The purpose was to get reliable transverse strain and deflection data. The static load tests were performed in the midst of moving traffic. One or two lanes (including the shoulder as a lane) were blocked off at a time, while an open lane allowed traffic to continue to flow over the bridge. Although traffic continued to flow, all test readings were taken when the bridge was free of traffic.

The strain gages were zeroed when there was no traffic or trucks on the bridge or the approach spans. The trucks were positioned in the marked positions corresponding to the 32 different load cases. Strain and deflection data were taken for a series of approximately five of the load cases in series, and then the gages were zeroed again. All of the measurements were taken when there was no traffic on or near the bridge; the procedure was repeated until data had been collected for all load cases. The procedure for the static tests remained consistent from the damaged bridge test to the repaired bridge test.

3.2.1.3.2 Load Cases

There were 32 different load cases used for the static portion of the test (see Table 3.4 and Figure 3.24) involving one or two trucks. The positions were chosen to produce positive and negative moment data. For the cases that involved two trucks, trucks were either placed side-by-side in adjacent lanes, front to back in the same lane, or in the same lane at different

points of the spans (i.e. positions 1 & 3, 2 & 3, etc.). Photos of the trucks in side-by-side and front to back positions are shown in Figure 3.26 and 3.27. The load cases are listed in Table 3.5, and the lanes and dimensions of the cross-section are shown in Figure 3.25.

Table 3.4. Listing of load cases.

Load Case	Lane(s)	Truck(s)	Span(s)	Location
1	1	1	1	1/2
2	1	1	2	1/4
3	1	1	2	1/2
4	1	1	2	3/4
5	1	1	3	1/2
6	2	1	1	1/2
7	2	1	2	1/4
8	2	1	2	1/2
9	2	1	2	3/4
10	2	1	3	1/2
11	1 & 2	1 & 2	1	1/2
12	1 & 2	1 & 2	2	1/4
13	1 & 2	1 & 2	2	1/2
14	1 & 2	1 & 2	2	3/4
15	1 & 2	1 & 2	3	1/2
16	1	1 & 2	1 & 2	1/2
17	1	1 & 2	1 & 3	1/2
18	1	1 & 2	2 & 3	1/2
19	1	1 & 2	2 & 2	1/2
20	2	1 & 2	1 & 2	1/2
21	2	1 & 2	1 & 3	1/2
22	2	1 & 2	2 & 3	1/2
23	2	1 & 2	2 & 2	1/2
24	3	1	1	1/2
25	3	1	2	1/4
26	3	1	2	1/2
27	3	1	2	3/4
28	3	1	3	1/2
29	3	1 & 2	1 & 2	1/2
30	3	1 & 2	1 & 3	1/2
31	3	1 & 2	2 & 3	1/2
32	3	1 & 2	2 & 2	1/2

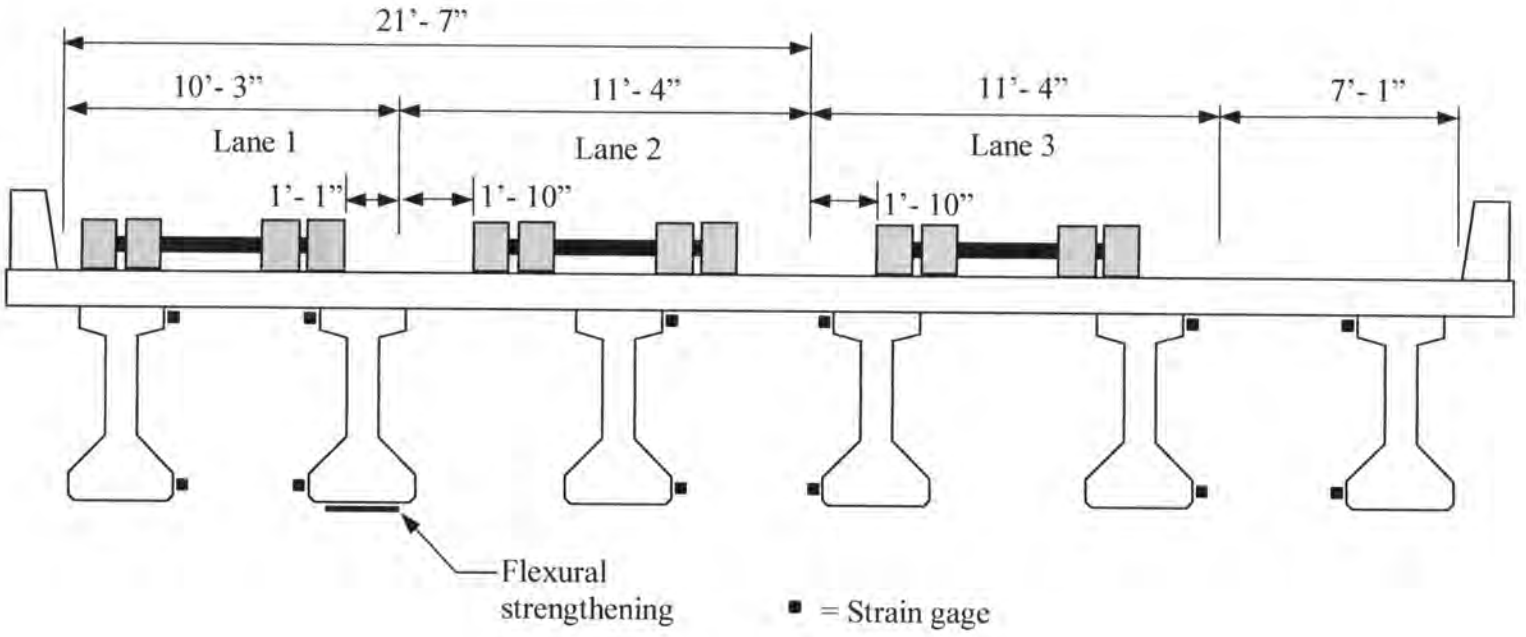

Figure 3.25. Truck lanes used in the Altoona Bridge Test

Figure 3.26. Photograph of trucks in Lane 1 and 2 in the Altoona Bridge test.

Figure 3.27. Photograph of trucks in Lane 3 in the Altoona Bridge test.

3.2.1.3.3 Dynamic Procedure

The same strain gage and deflection schematic from the static procedure was used for the dynamic procedure. Several trials were measured at different speeds, with one truck traversing the bridge at a time. The different speeds included several crawl runs

(approximately 3-8 mph) and some faster runs (approximately 30-35 mph), with several ambient vehicles traveling highway speeds (65-70 mph) also measured. The dynamic tests helped to check the continuity of the gages as loads crossed the bridge, as well as confirming the data from the static tests.

3.2.2. Osceola Bridge

The second bridge tested, Bridge 2, has eight prestressed concrete beams and carries traffic west on Highway 34 over Interstate 35 north and southbound near Osceola, Iowa. The bridge is a two-lane bridge, both westbound, and includes two main spans and two approach spans (see photo in Figure 3.28). The approach span from the east is 48'- 7" long. The next span, which carries traffic over northbound I-35, is 64'- 7" long and is the span that sustained the impact damage. The span that carries traffic over southbound I-35 is 56'- 3" long, and the exit span is 48'- 7" long. A schematic of the bridge can be seen in Figure 3.29, and a cross section of the bridge is shown in Figure 3.30.

Figure 3.28. Overall view of the Osceola Bridge looking southwest.

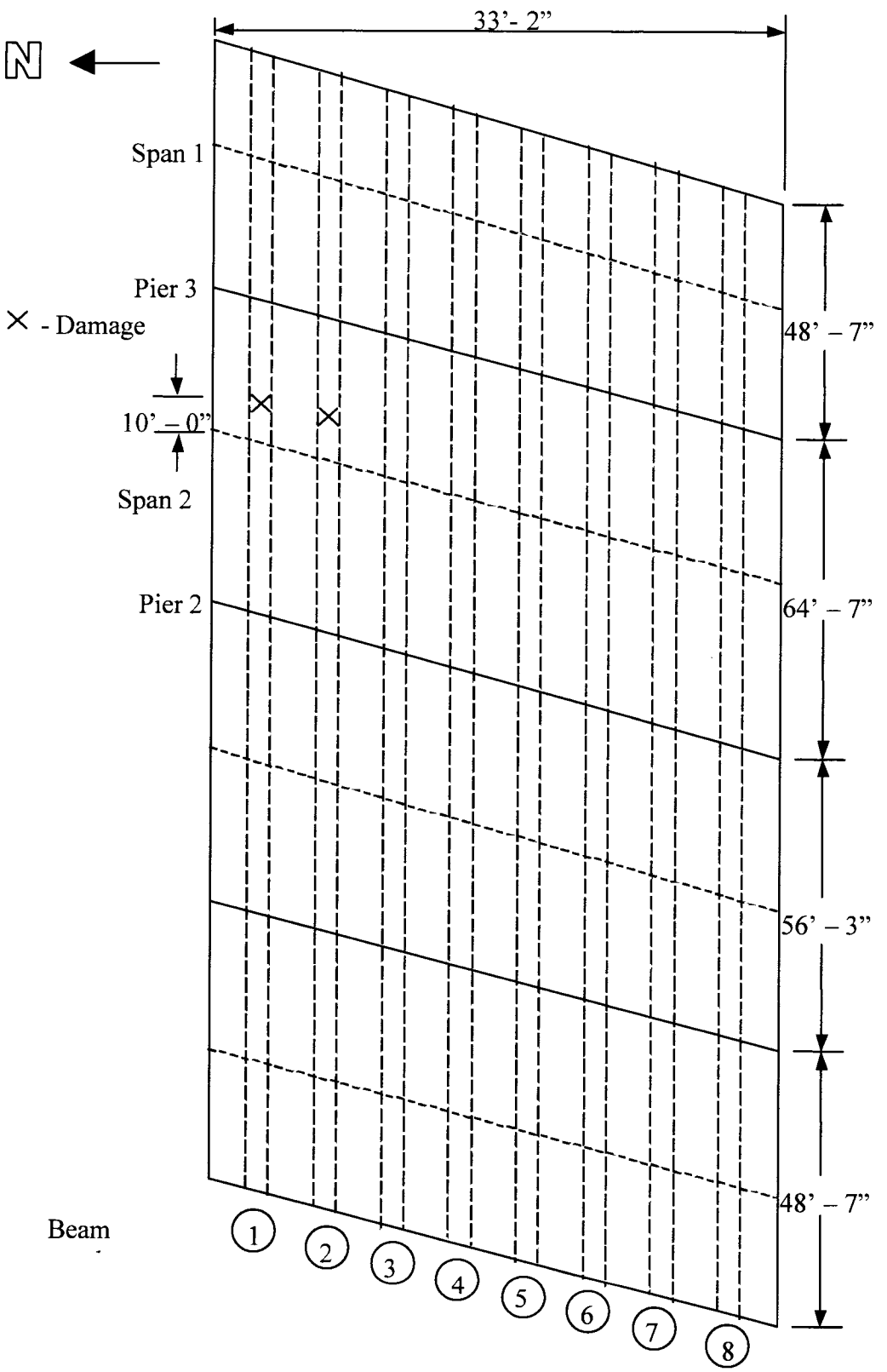

Figure 3.29. Dimensions of Osceola Bridge.

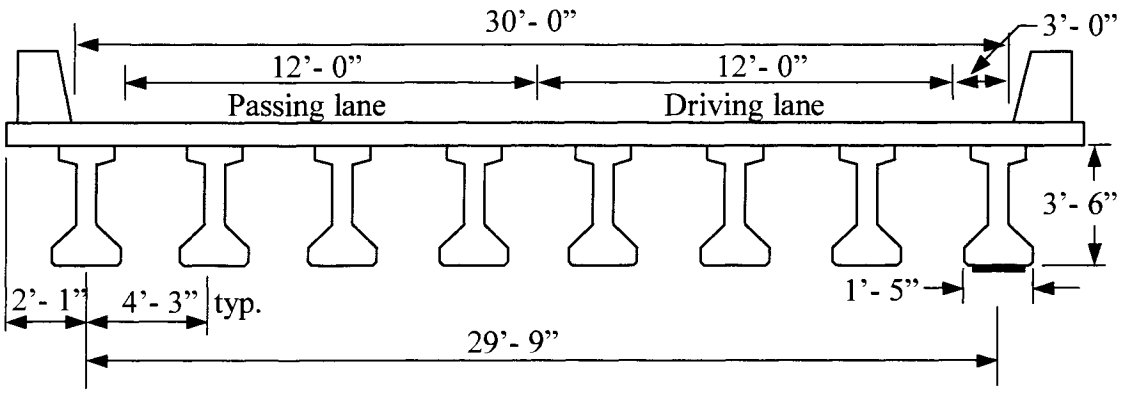

Figure 3.30. Cross section of Osceola Bridge.

3.2.2.1. Description of Damage

The bridge incurred some damage due to an overheight piece of machinery being transported on a semi-tractor trailer. The vehicle was traveling northbound on I-35. The equipment cleared the southernmost six beams, but due to the grade of the highway, the two beams on the north side were struck. The 2nd beam sustained some concrete spalling but no steel damage. The 1st beam incurred the most damage with significant concrete spalling as well as one prestressed steel tendon being severed. The diaphragm between the 1st and 2nd girders near the impacted area also lost some concrete. Figures 3.31 and 3.32 show two of the damaged areas. Appendix B offers a more complete damage report.

3.2.2.2 Instrumentation

Instead of using regular resistance type strain gages, a newer testing system was used. The new system called BDI-STS, Structural Testing System by Bridge Diagnostics, Inc., was used for this test. This system consists of up to 64 strain transducers that are applied to a bridge or other structure in a fraction of the time needed to apply standard foil strain gages. The strain transducers are place in position, and then they are fastened using a quick drying adhesive. All of the gages are then connected to the main data collection system, which the n produces the strain results by measuring the tiny displacements as a general resistance gauge would. A typical BDI gage on the bottom flange of a girder is shown in Figure 3.33.

Figure 3.31. Photograph of the damage to Beam 1 in the Osceola bridge.

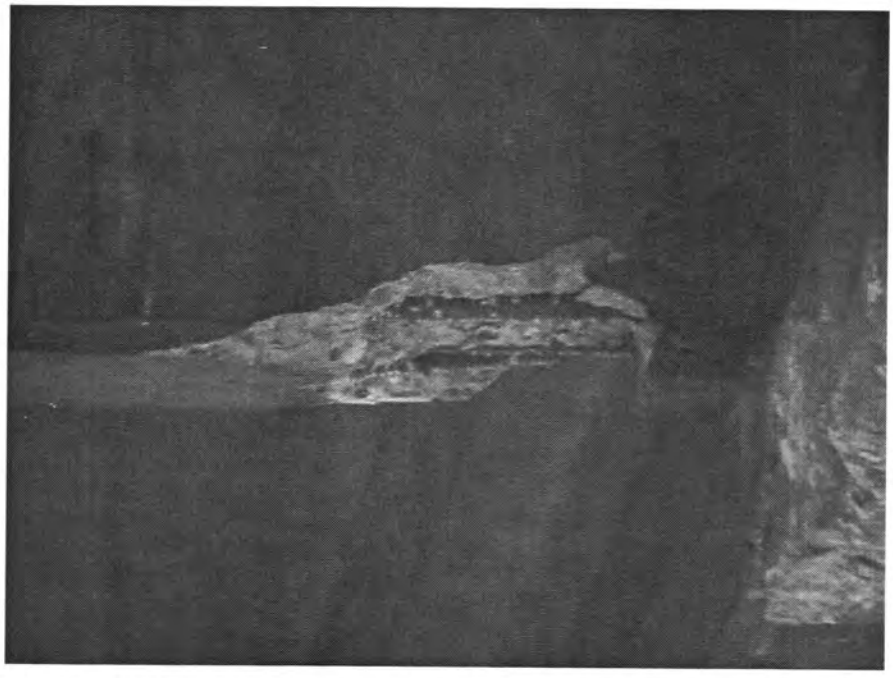

Figure 3.32. Photograph of the damage to the diaphragm in the Osceola bridge.

Figure 3.33. Close-up of BDI gage on the Osceola bridge.

Sixteen BDI gages were used in the instrumentation. One gage was placed on the side of the top flange, and one on the bottom of the bottom flange for each of the eight beams. The gages were all placed 3 feet west of the existing bridge diaphragm, which allowed for the easiest gage placement while traffic was flowing under the bridge. The damaged area was located about 3 feet east of the diaphragm, in the center of the driving lane for I-35. Figure 3.35 shows the instrumentation cross-section for the testing.

3.2.2.3. Trucks

One standard DOT 3-axle dump truck filled with sand was used for this test. The center of gravity was assumed to be in the center of the two rear axles. The front axle weighted 13,120 lbs., the rear axles weighed a combined 34,340 lbs., for a total weight of 47,460 lbs. Figure 3.34 shows the layout and dimensions of the truck.

3.2.2.4. Procedure

A total of ten rolling tests were performed for the testing of this bridge. The rolling tests consisted of a single truck driving about 5 to 8 mph. along a predetermined straight line. There were five different positions across the transverse direction, with two trials run for each position. These positions will be called 1-5 during the discussion, starting from the

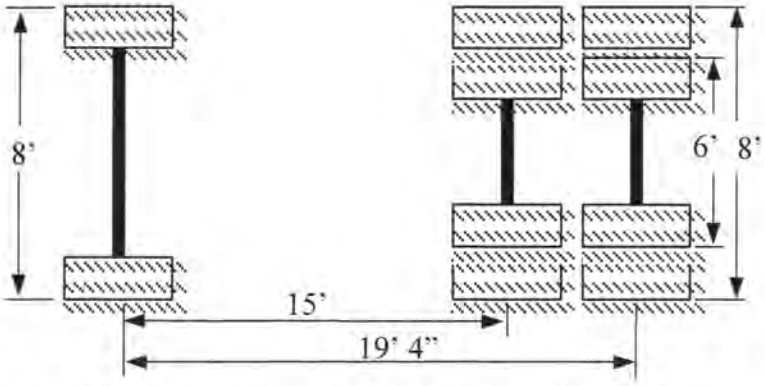

Figure 3.34. Dimensions of truck used in Osceola bridge test.

north. A cross section of the bridge including the truck lanes is shown in Figure 3.35, and a gage schematic is shown in Figure 3.36.

Before the test, the truck was fixed with the BDI auto-clicker that attached near the front left wheel. This device detects a reflective surface that marks every wheel revolution. Before every test, vice-grip pliers with a reflective surface connected would be attached to the front left wheel. The auto-clicker would then click every time the reflective surface would pass it, which allowed for easy determination of spacings and distances when looking at the final data plots.

For each test, the truck was rolled into place right up to the edge of the first approach span. The reflective pliers were attached to the top of the wheel and the truck was backed up one complete wheel revolution, which was 10.8 ft. When the truck started moving, the data acquisition device was activated.

Traffic was stopped before the bridge while the rolling tests were done. One person walked in front of the truck to ensure that it kept rolling in a straight line along the pre-measured lanes, while another person walked alongside the truck to watch the auto-clicker and prevent any malfunctions. The rolling speed of the truck was approximately 8-10 mph. When the truck had exited the bridge, the gages were reset and traffic was allowed to go over the bridge again. Two identical trials were run back to back in each position before the truck was moved to a new lane. After all ten trials were completed, the gages were removed and the bridge was ready to be repaired.

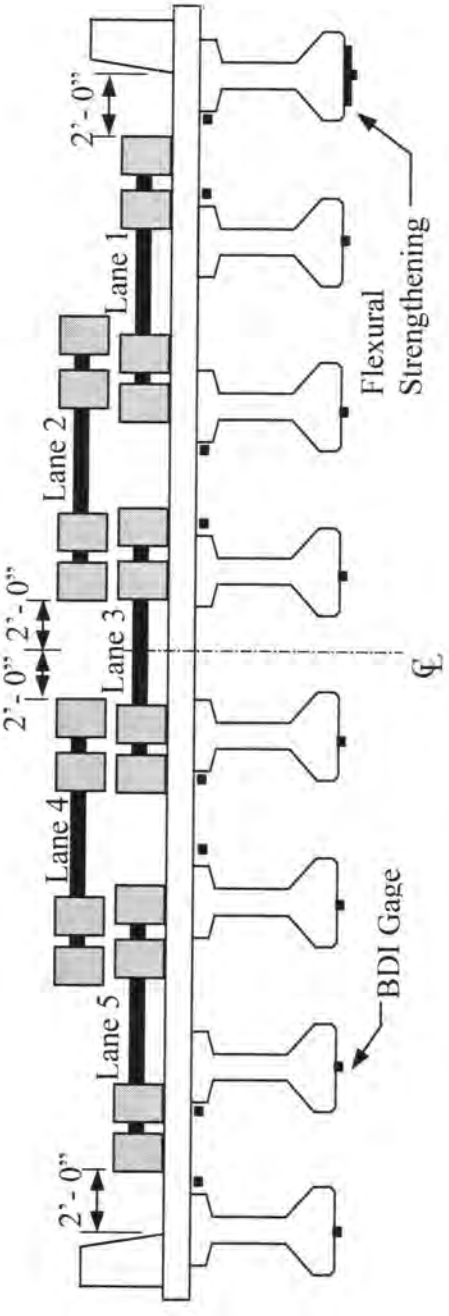

Figure 3.35. Truck lanes and gage positions used in Osceola Bridge test.

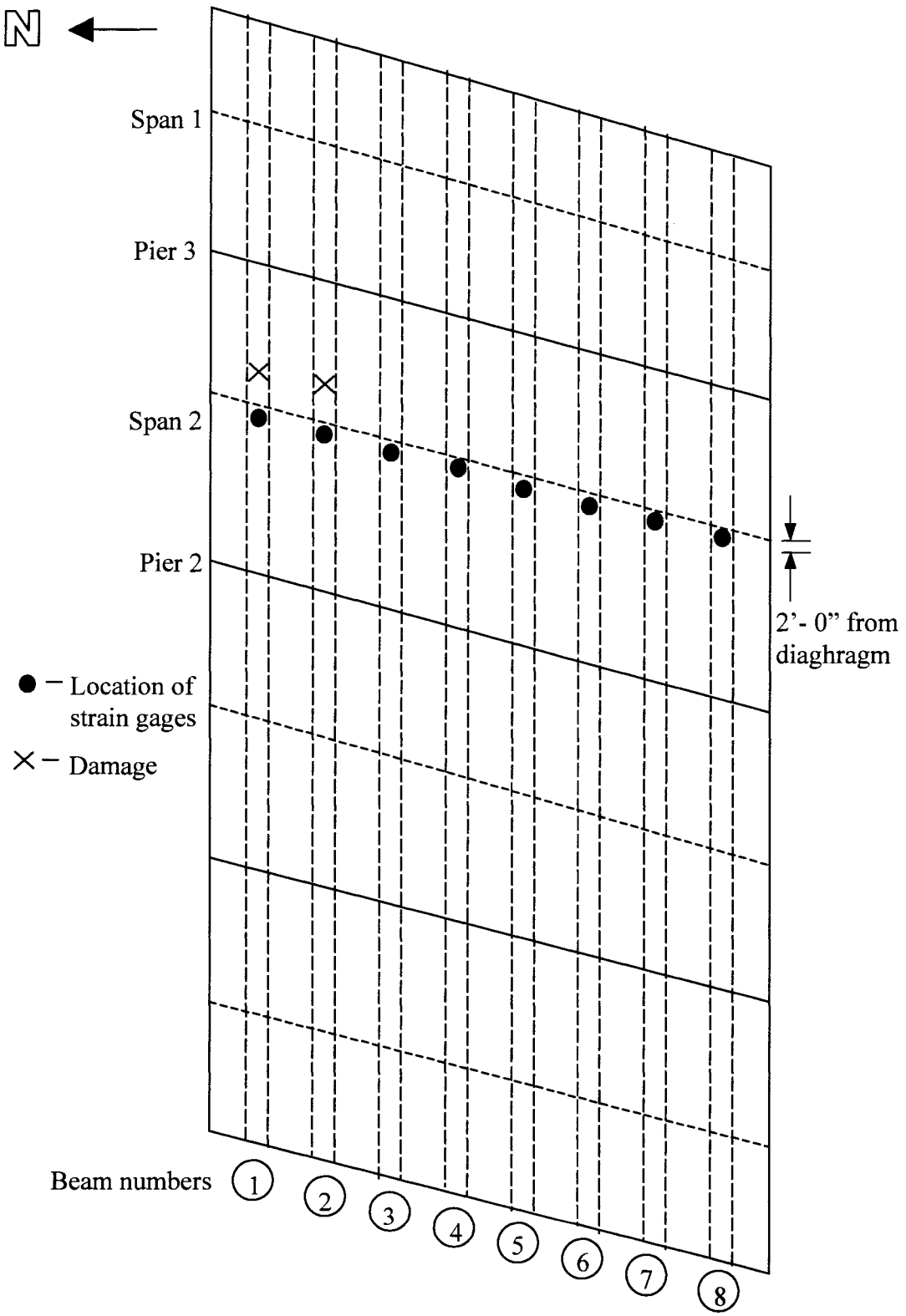

Figure 3.36. Gage schematic of Osceola Bridge.

3.2.3. De Soto Bridge

Bridge 3 has nine prestressed concrete beams and carries traffic west on Interstate 80 over Highway 169 north and southbound near De Soto, Iowa. The bridge is a two-lane bridge, and includes two main spans and two approach spans. The first approach span is 34'- 9". Both main spans are 68'- 9", and the exit span is 39'- 0". The bridge accommodates two 12'- 0" travel lanes as well as a wide shoulder on the driving lane side. An overall view of the bridge is shown in Figure 3.37, a schematic view is shown in Figure 3.38, and a cross section is shown in Figure 3.39.

Figure 3.37. Overall view of De Soto Bridge looking southeast.

3.2.3.1. Description of Damage

The bridge incurred some damage due to an overheight vehicle traveling south on Highway 169. The vehicle missed the seven northernmost beams and struck the final two, Beams 8 and 9. Beam 9 sustained significant concrete loss and also lost a prestressing tendon. Two of the damaged areas are shown in Figure 3.40 and 3.41. Appendix B contains a more thorough report of the damage.

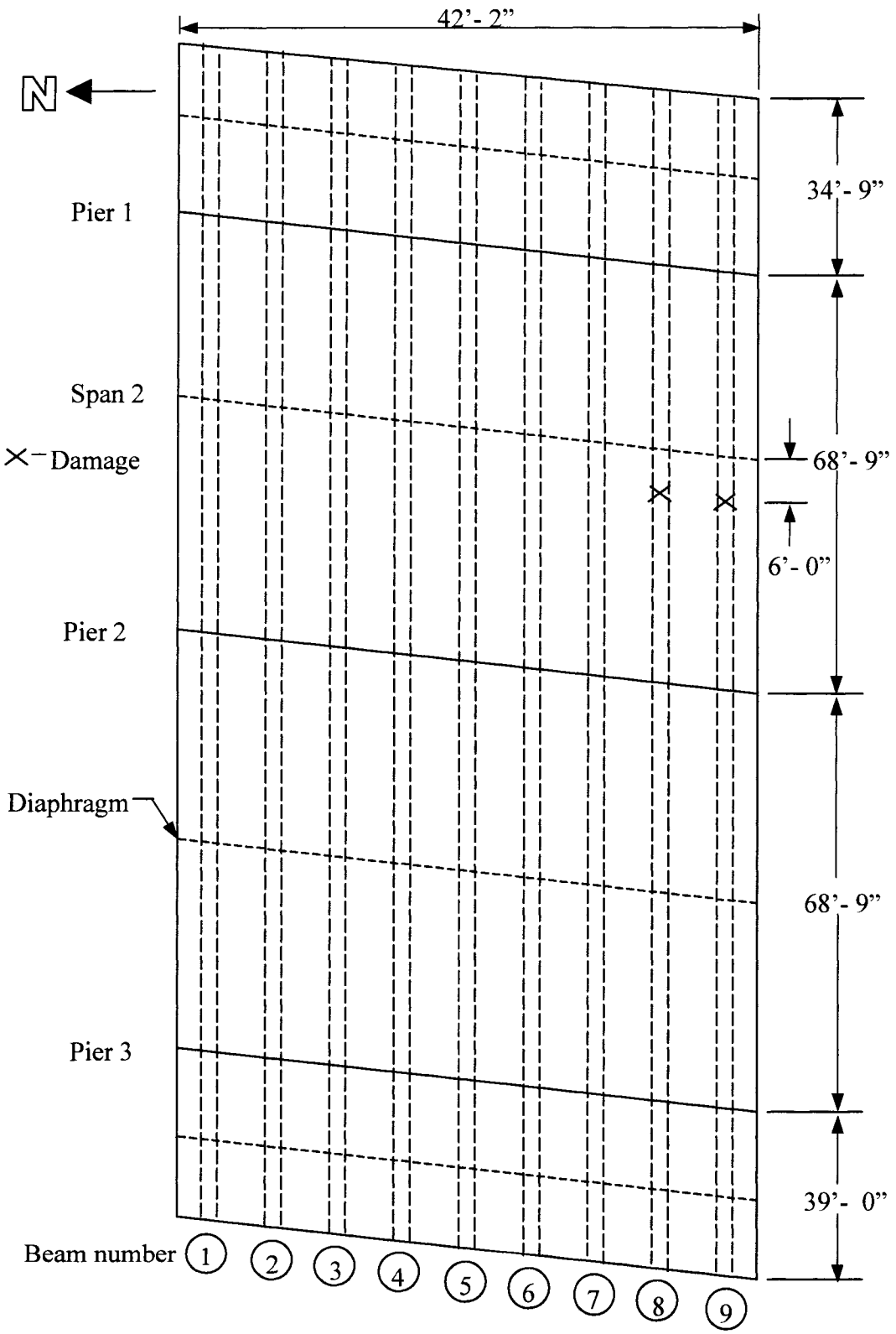

Figure 3.38. Dimensions of De Soto Bridge.

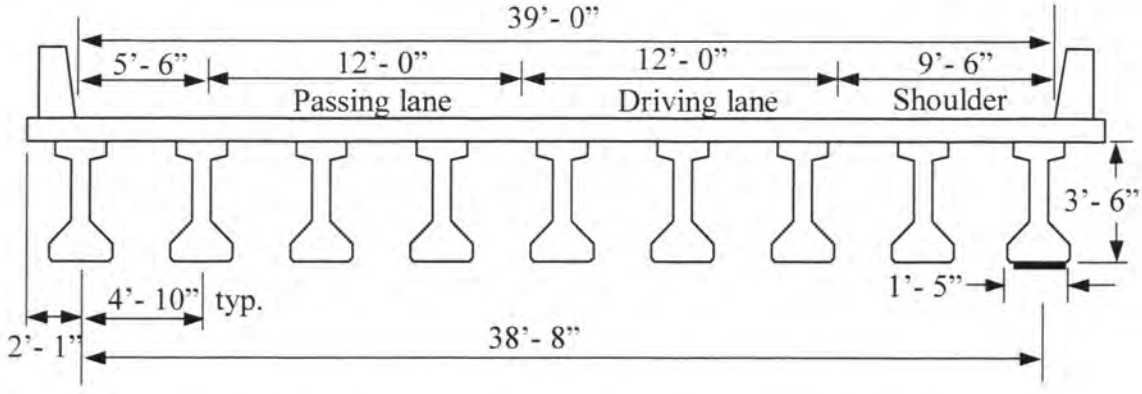

Figure 3.39. Cross section dimensions of De Soto Bridge.

Figure 3.40. Photograph of severed prestressing strand on Beam 9 in the De Soto bridge.

3.2.3.2. Instrumentation

The BDI-STS, Structural Testing System by Bridge Diagnostics, Inc., was used for running this test. This system was also used for the Osceola bridge test and is described in section 3.2.2.2. Eighteen BDI gages were used in the instrumentation. One gage was placed on the side of the top flange, and one on the bottom of the bottom flange for each of the nine beams (see Figure 3.43). The gages were all placed 1 foot west of the existing bridge diaphragm. The damaged area was located about 3 feet west of the diaphragm, in the center of the driving lane for Highway 169. Figure 3.44 shows the gage schematic.

Figure 3.41. Photograph of severed prestressing strand in the De Soto bridge.

3.2.3.2.1 Trucks

One standard DOT 3-axle dump truck filled with sand was used for this test. The center of gravity was assumed to be in the center of the two rear axles. The front axle weighed 15,060 lbs. and the rear axles weighed a combined 34,140 lbs., for a total weight of 49,200 lbs. Figure 3.42 shows the layout and dimensions of the truck.

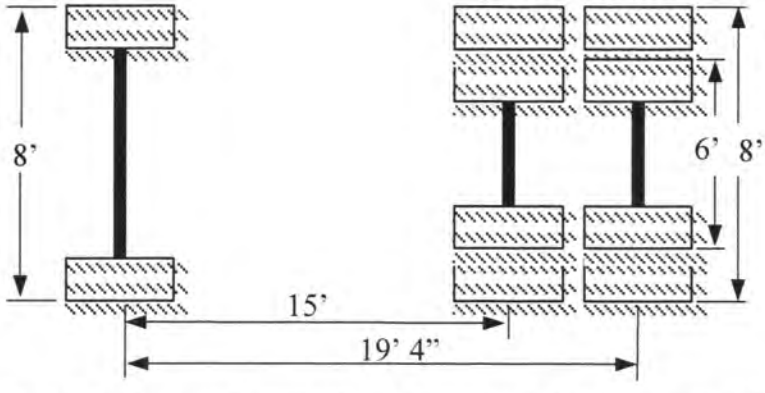

Figure 3.42. Load truck dimensions from De Soto Bridge test.

3.2.3.3. Procedure

Six rolling tests were done for the testing of this bridge. The rolling tests consisted of a single truck driving about 8 mph. in each lane and along the left barrier of the bridge, called

Load Lanes 1 through 3. There were three different positions across the transverse direction, with two trials run for each position. The truck positions are shown in Figure 3.44.

For each trial, the truck started back about one quarter mile. The driver would then maintain speed trying to avoid any bouncing of the truck. Traffic was only blocked along the lane in which the truck was driving, since traffic could not be stopped along the busy interstate highway. The gages started reading on a command based on visual position. When the truck was nearing the first approach, a radio call started the readings. When the truck had exited the last span, another called was used to stop the gages. When the truck had exited the bridge, the gages were reset. Two identical trials were run back to back in each position before the truck was moved to a new lane. After all six trials were completed, the gages were removed and the bridge was ready to be repaired.

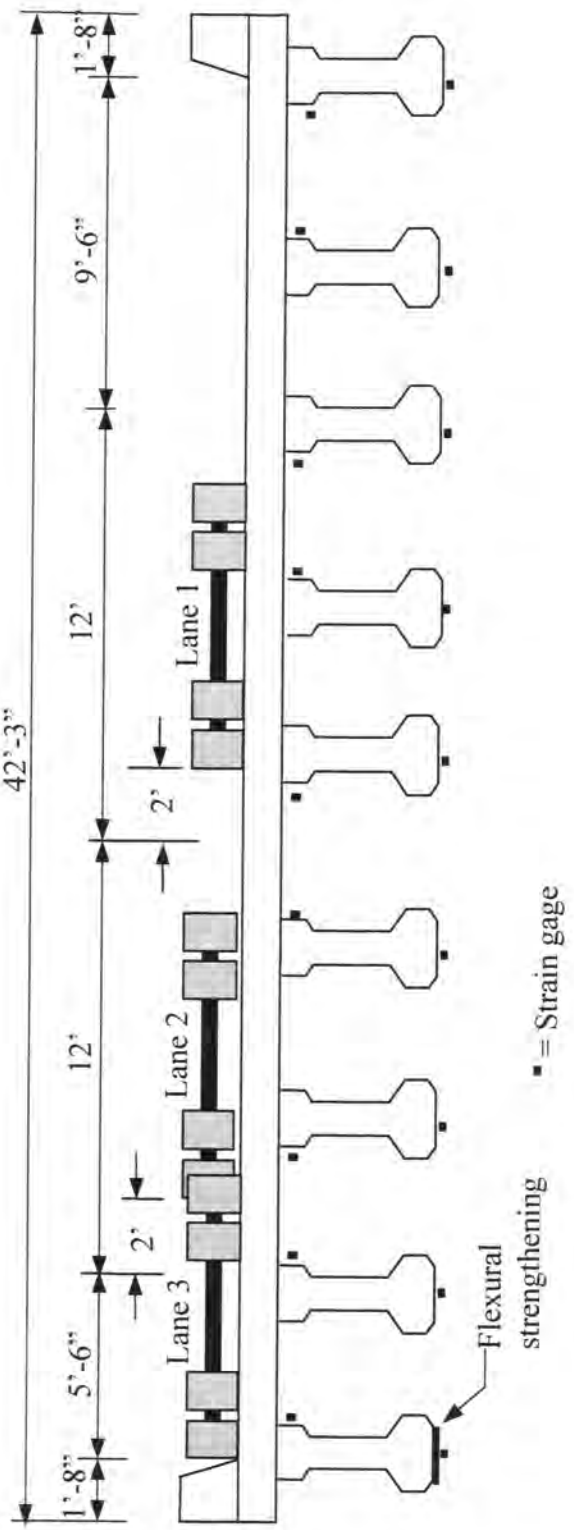

Figure 3.43. Instrumentation cross-section of the De Soto bridge.

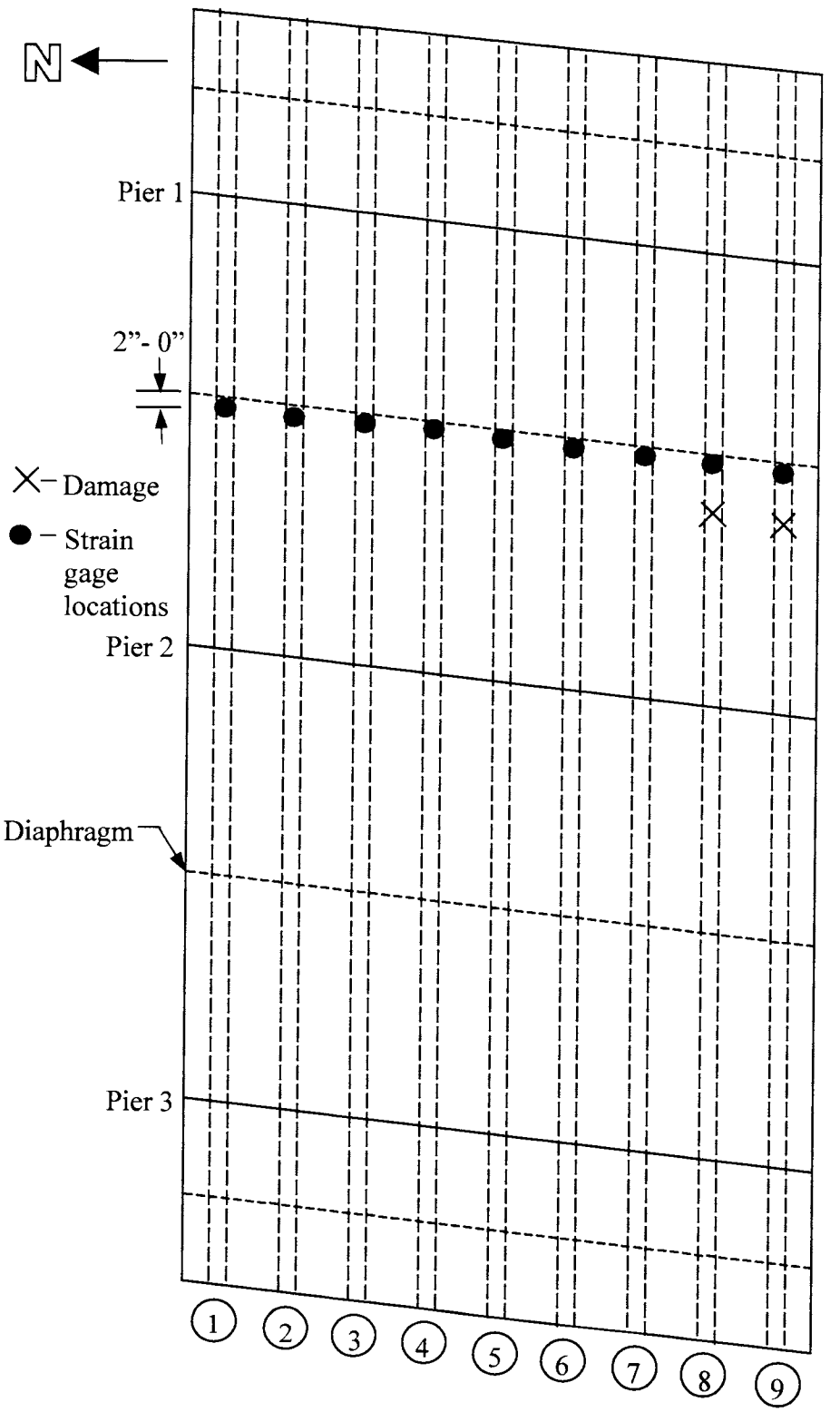

Figure 3.44. Strain gage schematic for the De Soto Bridge.

4. REPAIR OF DAMAGED P/C LABORATORY AND FIELD BEAMS

There are usually four main facets to a CFRP repair. The first facet is a mortar patch, which restores the original shape of the flange of the damaged beam. The second aspect is the longitudinal CFRP sheets, which restore some of the lost strength to the damaged beam. The third facet is very similar to the second and does the same job, but it consists of CFRP plates instead of sheets. The final facet of a repair job consists of a transverse CFRP wrap that helps to contain the mortar patch and slows flexural cracking.

4.1. Patch

The purpose of the mortar patch is to reform the original flange shape to allow for the installation of the CFRP. The CFRP requires smooth edges for proper adhesion. Usually a mortar good for overhead applications is chosen. The patch material selected for the repair of the laboratory beam was EMACO S88 CI. The patch material properties, as well as the CFRP system description can be found in Appendix 1. Similar materials were used for the field repairs.

4.1.1. Patch Installation

The installation procedure described comes from the patch installation in the laboratory. Field installation follows a similar procedure with slight variances in tools, standards, etc. The only major difference is that a beam in the field would be injected with epoxy prior to the patch being installed. This was done for the three bridges in the field. The rest of the patch installation is somewhat uniform.

4.1.1.1. Formwork

Wooden formwork was needed to reform the flange of the P/C beam. The three components of the formwork included pieces of ¾ in. plywood, stiffened by 2x4 in. boards of similar length. One of the sections included a side form, which was also made of ¾ in. plywood. Each of the plywood boards was a couple inches longer than the damaged area and was attached to the bottom flange using concrete screws in each corner. The holes for the concrete screws were measured and drilled beforehand with an electric hammer-drill. Form

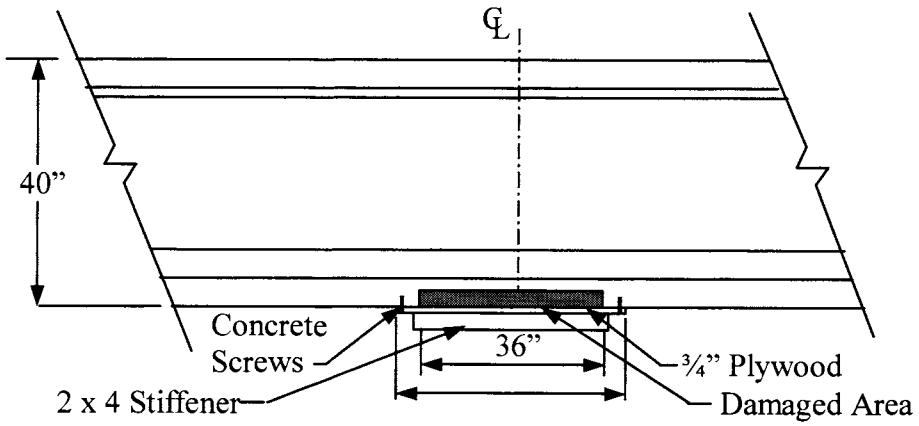

Figure 4.1. Diagram of formwork used for patch installation.

oil was lathered on the plywood before the mortar was set in place; Figure 4.1 shows a schematic of the formwork.

4.1.1.2. Installation

The patch procedure was discussed in the installation bulletin provided and was followed carefully to ensure proper strength and performance. Since all of the concrete was already chipped out, the patch installation began with the mixing of the mortar. One 55 lb. bag of the EMACO S88 CI was mixed at a time and was mixed with 0.9 gallons of water as suggested by the manufacturer. The mortar was mixed in a clean 5-gallon bucket, and an electric hammer-drill with a mixing bit was used to mix the mortar for 5 minutes. Another 0.1 gallons of water was added while mixing to get the desired consistency. While the mortar was being mixed, the existing concrete was saturated with water to prevent it from drawing moisture from the mortar. The concrete was subsequently sprayed intermittently with water to keep it saturated throughout the patching process.

Once the mortar was mixed thoroughly, the next step was to apply a bond coat to the existing concrete surface. A bond coat consisted of thoroughly scrubbing a thin layer of mortar into the saturated concrete surface with a stiff-bristled brush. Once the bond coat was applied, the first of the three forms was attached. The mortar was then scooped out of the bucket with a hand trowel and was shoveled into place against the side form. Mortar was added until the area between the form and the bottom of the concrete was almost full. When no more mortar could fit, the second form was screwed into place. This process was

continued until all the forms were in place and could hold no more mortar. The hand trowel was used to smooth out the mortar at the open-ended area of the formwork into a suitable flange. Throughout the patching process, more mortar was mixed as needed.

4.2. CFRP Sheet Installation

The techniques for installing CFRP sheets in the lab are virtually the same as the techniques used on bridges in the field. The technique described is for the laboratory beam, but the process is the same for beams in the field, there are just more beams. A short description of the materials is provided in Appendix A along with the patch material properties. The design/application manual in the appendix also shows the field installation procedures.

4.2.1. Longitudinal CFRP

The patch was allowed to cure for two days before the formwork was removed and the MBrace system was installed. The patch was ground down with a hand grinder to match the exact shape of the flange. Sharp edges of the existing flange where also rounded off to increase the contacting surface in order to avoid air pockets. Once the patch and original concrete formed a continuous profile, the beam was ready to be prepared. Before the primer could be applied, the concrete surface was roughened. All of the concrete that was to come in contact with the epoxy was roughened using a hand grinder and concrete/masonry grinding wheel. A dust collection unit was used to minimize the dust on the beam, which would need to be wiped off anyway, and to prevent small particle inhalation by other laboratory workers. After the grinding was completed, the leftover dust was wiped off the beam with a damp rag.

The carbon fiber strips were cut into their desired lengths after the beam had been cleaned. A scissors was used to cut the material. The carbon fiber was cut into 94 ½ and 44 ¼ in. lengths, and the strips were also cut down from their nominal 20-in. width to a width of 14 inches, which was 1 ½ in. smaller than the bottom flange. The strips were covered with plastic to avoid getting dust on them.

The primer consisted of a two-part epoxy and was mixed in a small plastic bucket according to the manufacturer's instructions. It was mixed in a 3/1 ratio with a hammer-drill

and mixing attachment. The primer was poured into a painting tray for ease of application. A clean, medium sized paint roller was used to apply the primer. A generous amount of primer was rolled onto the roller each time, but the roller was not overloaded because this could cause the primer to drip during overhead applications. The primer was applied somewhat quickly since it has a 20-minute working time at room temperature. Working quickly did not negatively affect the epoxy strength, since the entire area was thoroughly covered.

After the primer was applied, the second step was to apply the putty. Since the test beam was new and had never been in the field, there was no reason to use the MBrace putty. The purpose of the putty is to fill bug holes and other small cracks. Had the putty been needed, it would have been applied directly over the wet primer. The putty was used on the damaged bridges though (see appendix). The test beam had virtually no cracks so this step was skipped in the laboratory and the next step was started immediately.

The MBrace Saturant is also a two-part epoxy and was mixed immediately after the primer was applied. It was mixed the same way as the primer, in a small bucket with a hammer-drill and mixing bit in the same 3/1 ratio. A single layer was applied using a clean paint roller. The working time of the saturant is 45 minutes at room temperature, so the saturant was also applied quite quickly while making sure the entire surface area was covered. The next step was to apply the carbon fiber sheets.

The carbon fiber strips were set directly onto the wet saturant. The strips were laid starting at one end and moving toward the other end. A 6 in. overlap was used, although only a 2 in. overlap was required. The strips were pressed onto the saturant with gloved hands at first. After all of the carbon fiber strips were stuck in place, a ribbed roller was used to better work the carbon fibers into the saturant. The ribbed roller was rolled along the direction of the fibers to prevent any damage that could occur by rolling across them. After the final run with the ribbed roller, one more check was made to smooth out any wrinkles or air pockets.

Thirty minutes after the original carbon fiber layer was laid down, a second layer of saturant was spread over the existing carbon fiber. Another layer of carbon fiber strips was then laid down in the new tier of saturant in a similar fashion as the previous layer of strips.

The second layer of carbon fibers strips was staggered at half intervals from the first layer as shown in Figure 4.2. The A strips were 94 ½ in. strips, and the B strips were 44 ¼ in. strips.

The bridges in the field were repaired in the same fashion as the described beam. Variances only occurred in the lengths of the repaired beams, as well as the number of beams. The bridges also included the putty step while it was skipped in the laboratory.

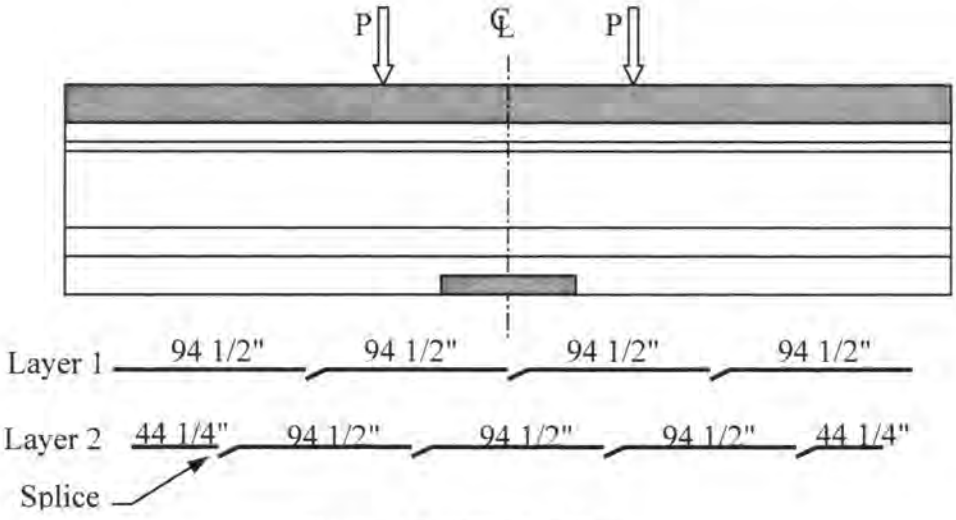

Figure 4.2. CFRP splices.

4.3. CFRP Plates

CFRP plates were only attached to one beam, Beam 2, of the Altoona bridge, and none of the Osceola or De Soto beams. The CFRP plates used on the Altoona bridge were Sika CarboDur plates. Sika CarboDur is a pultruded (CFRP) laminate designed for strengthening concrete, timber and masonry structures. CarboDur is bonded onto the structure as external reinforcement using Sikadur 30 epoxy resin as the adhesive. The plates are very high strength, lightweight, non-corrosive, and relatively easy to install. They come in unlimited lengths and have a high modulus of elasticity. The design tensile strength is 406 ksi.

After the patch had cured, the plates were adhered to the bottom flange of Beam 2. The epoxy resin was applied using flat trowels to the entire length of the beam, while the 4-inch plates were run through a tool that applied the resin to it. The 75 feet of plate was then

hoisted to the underside of the beam and stuck to it using gloved hands by two laborers, both on lifts. A rubber roller was run along the length of the plates to enhance the bond. The entire process was repeated three more times until the bottom of the flange had four plates covering it. The wraps were then installed according to the method described in section 4.4.

4.4. CFRP Wrap

A CFRP wrap was adhered to the center of the P/C beam to help contain the patch. The wrap extended 40 in. both ways from the center of the beam, which was the entire length of the patched area. Five strips were cut to cover this area; three were left their nominal 20 in. wide, and two were cut down to 10 in. The sizes were chosen to avoid the wires from the prestressed strand gages that stuck out from the patch. All of the strips were approximately 6 ft. long to allow them to cover the entire bottom flange and reach up to cover the entire web leaving only an inch from the bottom of the top flange.

The longitudinal strips were allowed a day to cure before the wrap was added. The transverse strips were applied the same way that the longitudinal strips were. Primer was applied to the web and side of the bottom flange. The bottom of the flange already had the longitudinal strips so it did not need to be primed again. The entire area was covered with saturant and the strips were set in place. The ribbed roller was used to get rid of air pockets. Another layer of saturant was put on to finish the wrap. Figure 4.2 shows the layout and dimensions of the transverse wrap, and Figure 4.3 shows a cross section of the transverse wrap.

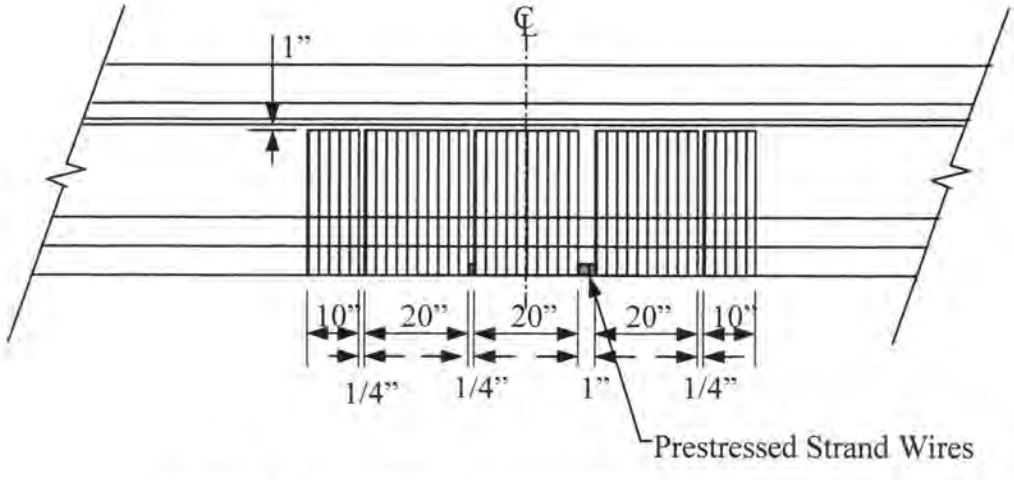

Figure 4.3. Layout and dimensions of transverse wrap.

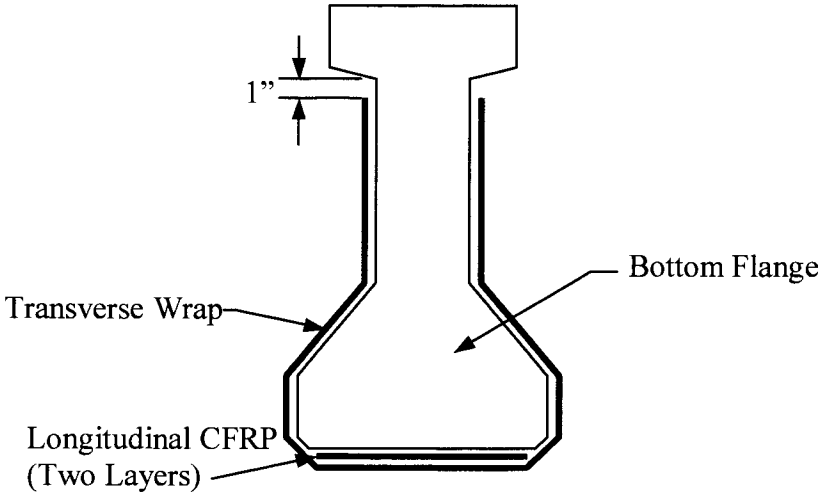

Figure 4.4. Cross-section of longitudinal and transverse wrap.

5. LABORATORY AND FIELD TEST RESULTS

Results and analysis of the four tests performed during the course of this research are presented in the following section. One P/C beam was damaged, repaired, and tested in the laboratory, and three bridges that had been damaged were load tested in the field, one near Altoona, IA, one near Osceola, IA, and a third near De Soto, IA. The three bridges were subsequently repaired using CFRP; only the Altoona bridge was retested after the CFRP strengthening system was installed. All the repairs consisted of the application of concrete patches followed by the installation of CFRP, either plates and/or fabric. The results of these tests are presented in the following sections.

5.1. Laboratory Beam

The laboratory beam was damaged and repaired using CFRP as described in Chapter 3. Two layers of longitudinal CFRP sheets, 30 ft long, were attached to the bottom flange of the beam with epoxy, followed by transverse wrap that was then wrapped around the bottom of the beam. The wrap extended from just under the top flange on one side of the web to just under the top flange of the other side of the web in the center portion (7.67 ft) of the beam.

5.1.1. Service Tests

Service tests were performed before and after the prestressing strands were cut as described in Chapter 3. Two tests were performed on the undamaged beam, followed by another after the concrete was removed and two prestressing strands were cut. As shown in Figure 5.1, a service load of 25 kips, which is lower than the cracking load for this beam, was applied. Data were taken at intervals of 1 kip. Once the concrete area was removed, it was difficult to get a good center deflection reading, thus the quarter point deflections are presented in Figure 5.1. The deflection increased slightly (0.002 in.) due to the cutting of the tendons and removal of the concrete.

The stiffness of the undamaged beam (as determined using the secant modulus definition at the highest service load of 25 kips) was 107.1 kips/in. The damaged beam had a stiffness of 103.7 kips/in, which indicates a decrease of 3.1% that can be attributed to the damage. The stiffnesses are smaller than those obtained for similar beams tested previously; this is due to the steel tubing that was used as supports for the simply supported beam.

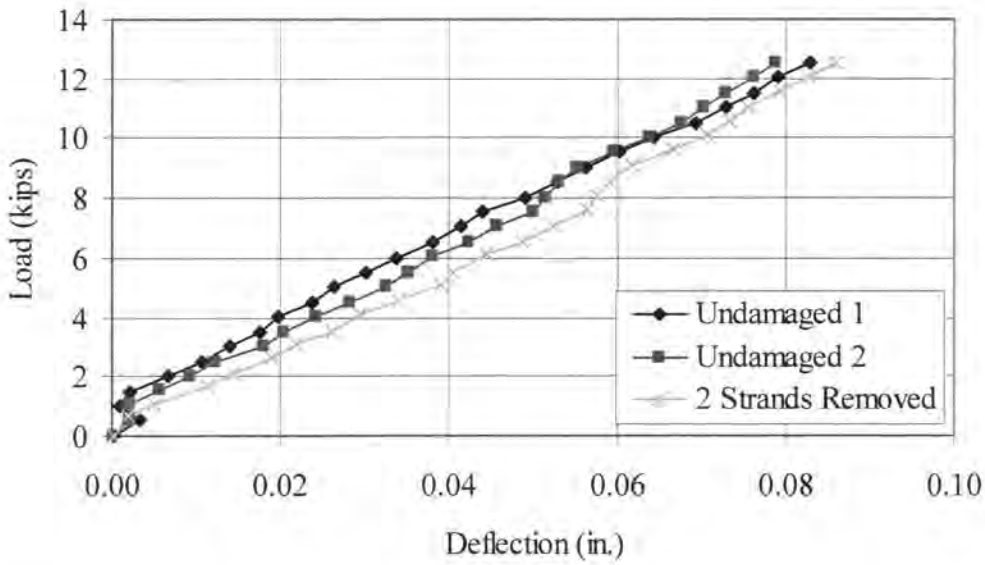

Figure 5.1. Load vs quarter point deflection in laboratory beam during strand removal.

During loading, the steel tubing deflected and this altered the deflections that were used to calculate the stiffnesses. The steel support deflections were measured during subsequent tests. Celescoes were later installed near the supports to measure support deflection so it could be subtracted from the mid-span and quarter point deflections. The final stiffness of the repaired beam (which includes the effects of the support deflections) with the patch and CFRP was 114.07 kips/in.

5.1.2. Degradation

The beam was cyclically loaded with a loading range of 2 to 58 kips at a rate of 0.7 cycles per second. The maximum load (58 kips) was not high enough to crack the beam. (This load range was based on information from previous static load tests that was misinterpreted; thus, the load range was half of what was desired. Unfortunately this error was discovered after the cyclic loading was completed.) Cyclic loading was stopped and service tests were performed every third day after approximately 150,000 cycles. The test was terminated after 2.2 million cycles of loading. The centerline deflections from three of these service tests, approximately a million cycles apart, are shown in Figure 5.2. It was

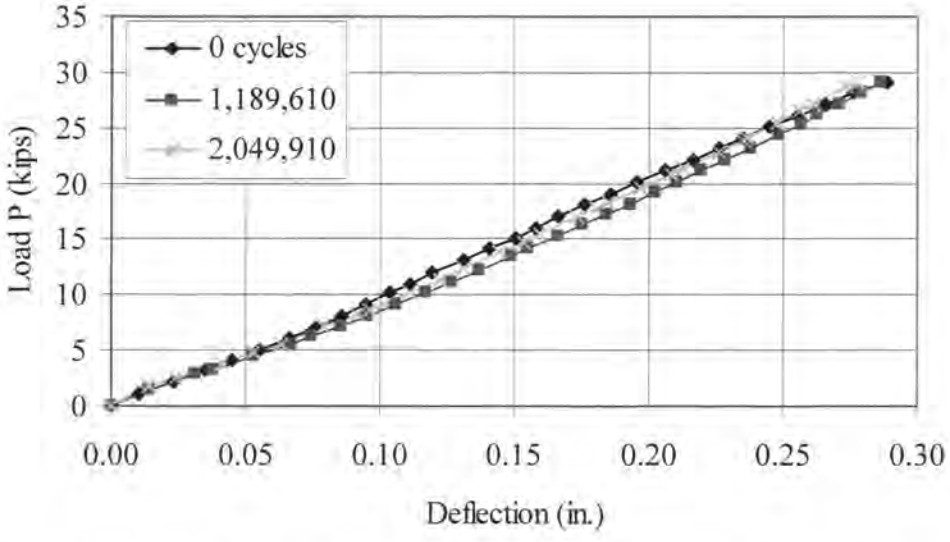

Figure 5.2. Load vs. centerline deflection in laboratory beam after 0, 1, and 2 million cycles.

clear that there was no degradation due to the cyclic loading, also there was no noticeable debonding of the CFRP due to the loading.

5.1.3. Ultimate Test

After completing the cyclic loading and the service tests, the beam was statically loaded to failure. The ultimate load test deflection results are presented in Figure 5.3; cracking of the beam occurred at approximately 44 kips. With increased loading, the CFRP sheets began to make popping noises at approximately 75 kips. The maximum load reached was 89.4 kips per actuator before a major drop in load occurred. Failure resulted when the CFRP and epoxy caused the concrete to delaminate. Concrete was attached to the CFRP after failure indicating that the epoxy bond was not the cause of the failure.

The mid-span deflection just prior to failure was 3.61 inches. The total applied load of 178.8 kips was greater than the maximum load measured in previous tests of similar CFRP reinforced beams. A similar beam tested with the same longitudinal CFRP and a wrap only around the bottom flange of the beam, (not extending up the web), reached 167.2 kips before failure. Thus, the additional wrap length on the web more than likely increased the failure load. This repaired beam was more ductile than previously repaired beams as it reached a deflection of 3.61 in. before failure occurred. The largest deflection at failure for the

previous tests was approximately 3.0 in. As shown in Figure 5.4, the deflections were symmetrical about the centerline of the beam prior to failure, which reflects the symmetric loading conditions and symmetric behavior of the beam and repair system.

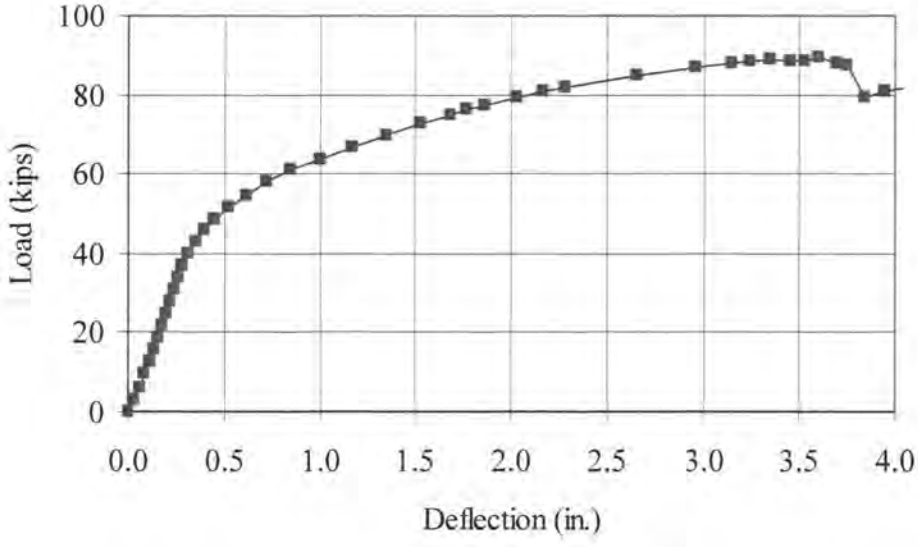

Figure 5.3. Load vs. centerline deflection in laboratory ultimate load test.

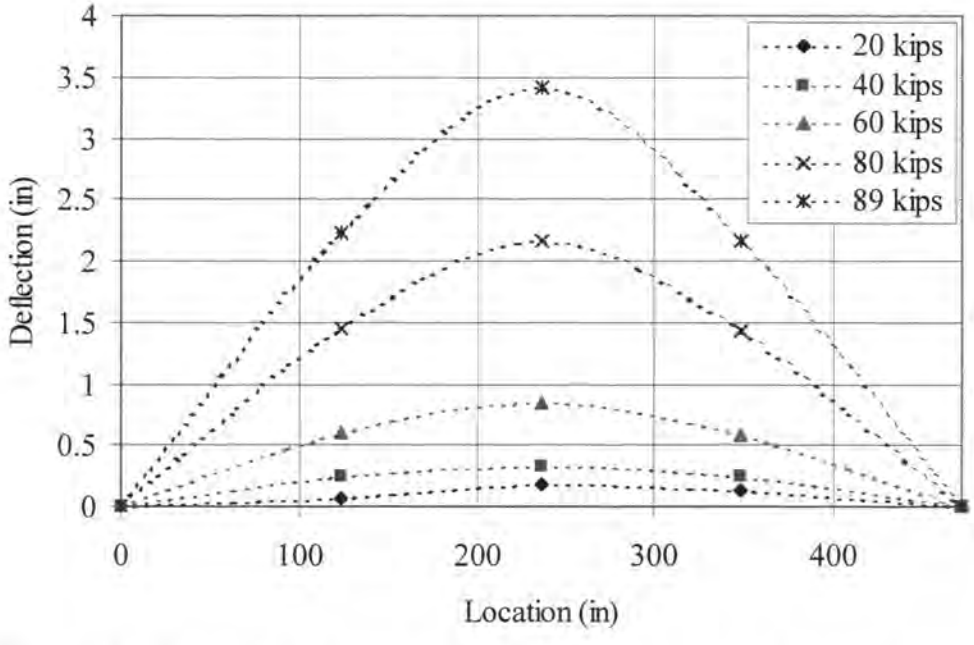

Figure 5.4. Vertical displacements along the length of the laboratory beam.

5.1.3.1. Strains

The strains in the longitudinal CFRP reached a maximum of 5,850 MII at the failure load, while the maximum strains measured in previous laboratory beam ultimate tests were 5,300 MII or less. The full web wrap previously described prolonged the delamination, thus allowing the beam to reach higher loads. The design strain for the CFRP sheets as stated by the manufacturer was 16,700 MII. Obviously, with the CFRP only reaching 35% of its design tensile capacity, it was not the cause of failure. The longitudinal strains in the CFRP are shown in Figure 5.5.

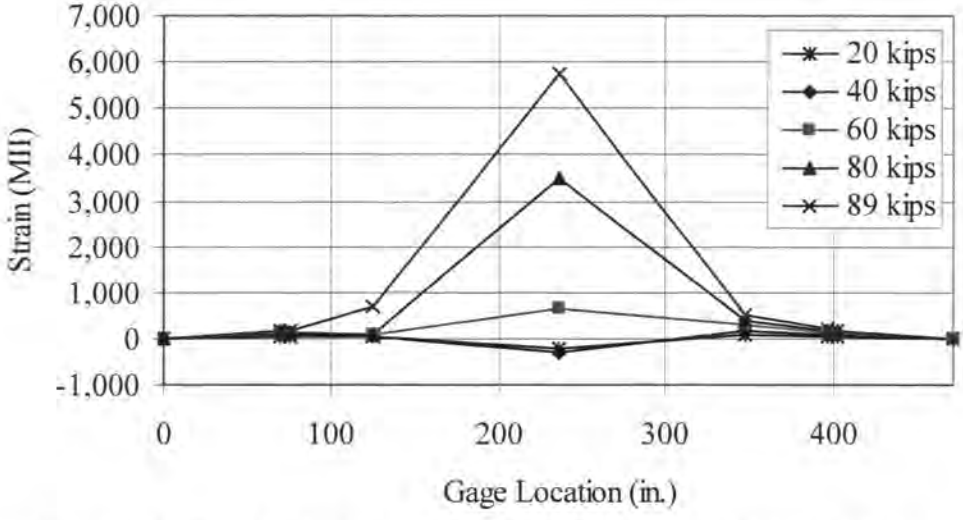

Figure 5.5. Tensile strains along the CFRP sheets in laboratory beam.

The strains appear to be quite symmetric under the symmetric loading conditions, although at one of the quarter points, the increase in strain from the 80 kip load to the 89 kip load looks larger than the increase at the other quarter point. This strain increase could be an indicator of an eventual failure mode. The strains near the termination points of the CFRP were still quite low, 194 MII at failure, therefore, debonding near the end of the CFRP was not a cause of failure.

Strain distribution through the depth of the composite beam is shown in Figures 5.6 through 5.8, where the top of each graph is the top of the concrete deck. As seen in Figure 5.6, the neutral axis location at the center of the beam was 7 in. below the top of the deck

during the final stages of loading, while the neutral axis location at the quarter points was approximately 15 in. from the deck top throughout the test. The extreme compression fiber of the concrete at the centerline of the beam reached a strain of 1,350 MII indicating that the concrete's full compressive strength had not been reached.

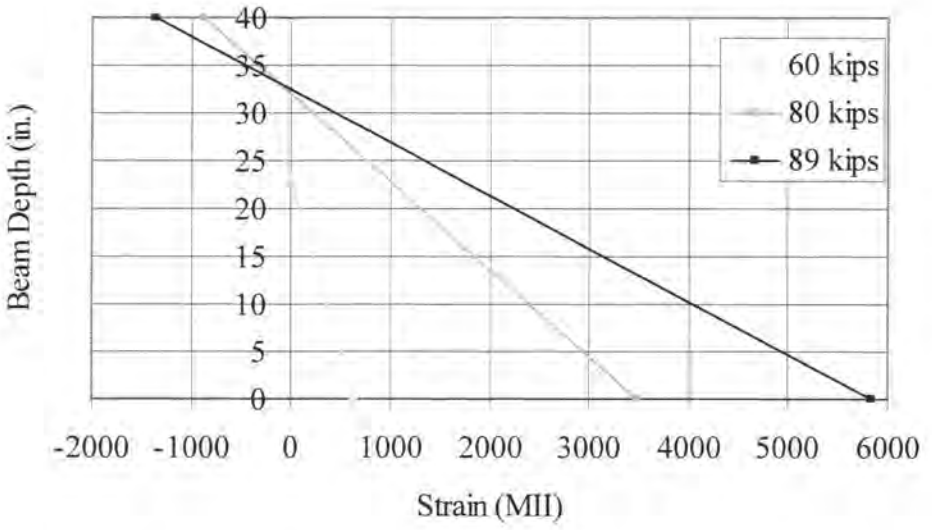

Figure 5.6. Strain distribution at centerline of laboratory beam.

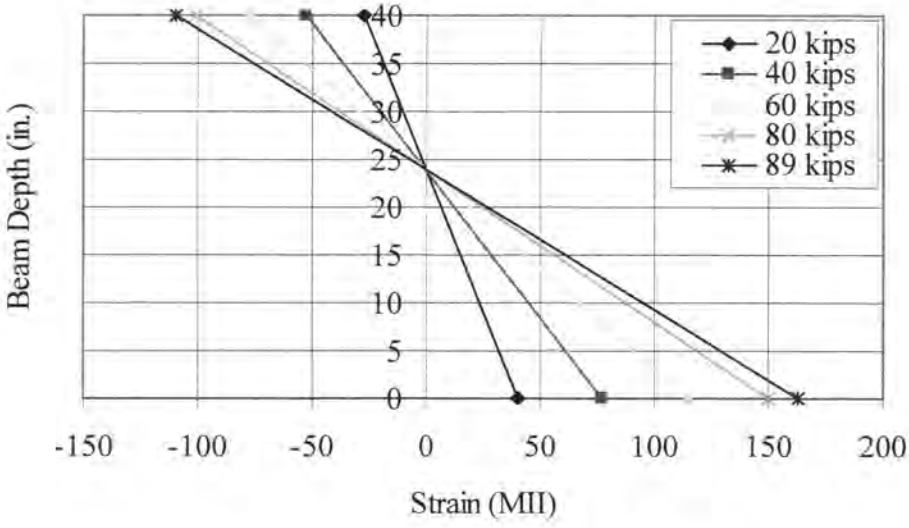

Figure 5.7. Strain distribution at left quarter point of laboratory beam.

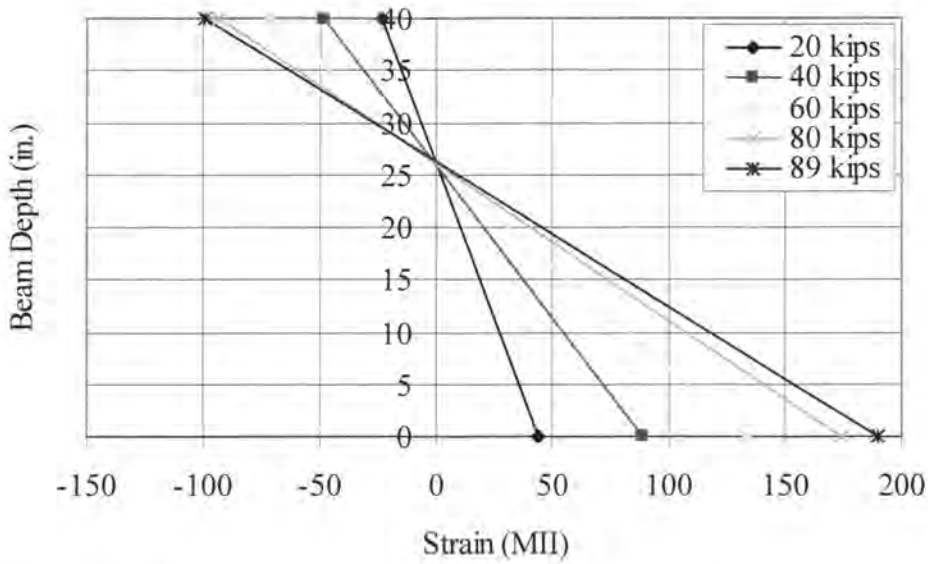

Figure 5.8. Strain distribution at right quarter point of laboratory beam.

5.1.4. Summary of Beam Results

Table 5.1 shows the moment values based on statics, using the ultimate load of 89.0 kips to calculate the moments. P_{live} was the actual maximum load at each load point during the ultimate test. M_{live}, the moment due to the live load was calculated from the maximum load (P_{live}) and added to the dead load moment (M_{dead}), based on beam weight, to find M_n, the ultimate moment capacity. Table 5.2, which shows the predicted moment strengths, shows that the beam reached 98.3% of its expected capacity by reaching 1,455 ft-kips when it was predicted to reach 1,480 ft-kips.

Table 5.1. Moment results from beam tests.

	P_{live} (kips)	M_{live} (ft-kips)	M_{dead} (ft-kips)	M_n (ft-kips)	% of Undamaged Beam Strength
Beam (2 Sheets & Jacket)	89.0	1,320	135	1,455	102.3%

Table 5.2. Predicted nominal moment strengths.

Beam Description	P_{live} (kips)	M_{live} (ft-kips)	M_{dead} (ft-kips)	M_n (ft-kips)	% of Undamaged Beam Strength
Undamaged Beam	86.7	1,286	135	1,421	100.0%
Damaged Beam	70.3	1,042	135	1,177	82.8%
Strengthened Beam	90.7	1,345	135	1,480	104.2%

5.2. Altoona Bridge Test Results

Two tests were performed on the damaged bridge over Highway 6 near Altoona. The first test (Fall, 2000) was conducted after an over-height vehicle had damaged the bridge. The second test (Spring, 2001) was performed after the damaged area had been repaired with a mortar patch, epoxy injections, carbon fiber plates, and a carbon fiber wrap described in Chapter 4. The tests consisted of a static portion, with 32 different load cases, and a dynamic portion.

5.2.1. Damaged Bridge Test

The initial testing was performed weeks after the bridge had been damaged. No repair, retrofit, or epoxy injections had taken place prior to this testing. The results from these tests are compared to results of the following test, which was performed after the bridge had been repaired.

5.2.1.1. Transverse Behavior

Figures 5.9 through 5.11 show strains and deflections at mid-span of the damaged bridge for Load Cases 13, 19, and 23 (see Table 3.4). Two loaded trucks were placed at various locations along the bridge to measure the strain and corresponding deflection in the beams prior to the CFRP repair. The trucks weighed a combined 102,200 lbs (see Table 3.3). The plots reference the static load cases shown in Table 3.4; these load cases were chosen because they caused the largest strains and deflections at mid-span from two truck loading. The data plots in all three cases show a nearly normal distribution of load among all the beams, except for jump or dip in strain visible on all three strain plots. Several factors were considered when trying to explain the behavior of the structure but no conclusion was finally settled upon. Initially a faulty strain gage was suspected, but an extra strain gage was placed near the existing gage on Beam 5 and it produced similar results, so the abnormal strain curve was left without a logical explanation. The bridge must have been distributing the load in an unusual fashion.

A distribution factor (based on design assumptions) of 0.66 was calculated for the bridge using the 1996 AASHTO LFD Bridge Design Specification with one lane loaded. A

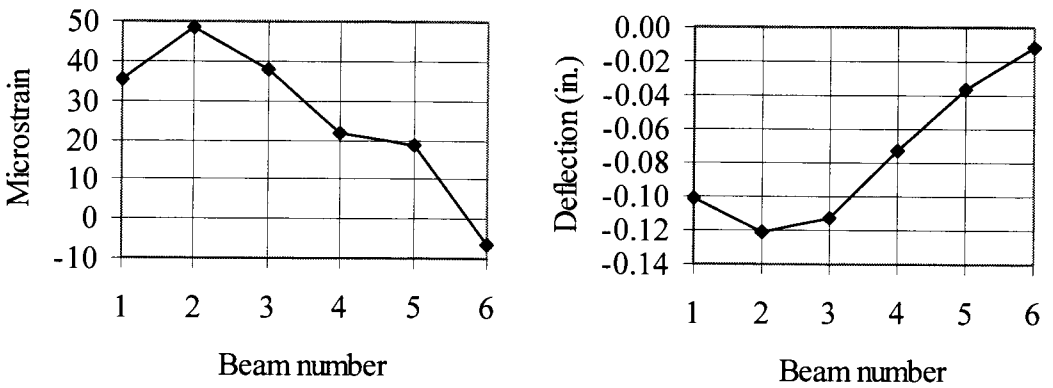

Figure 5.9. Strain and deflection in the Altoona bridge for Load Case 13.

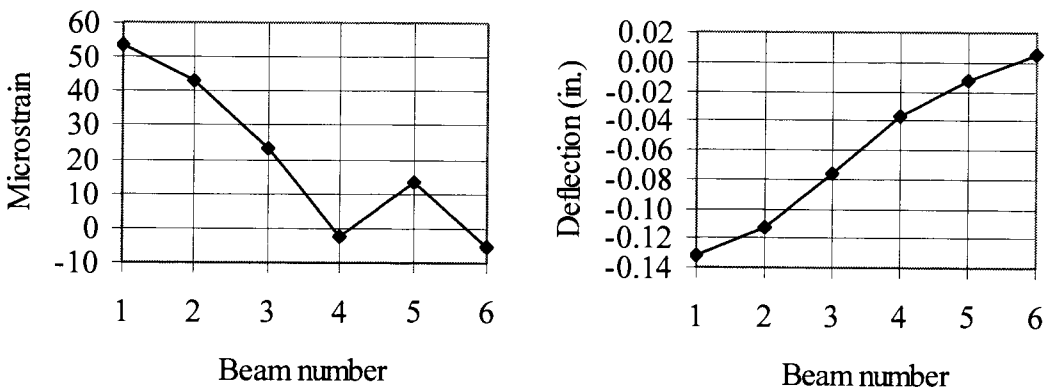

Figure 5.10. Strain and deflection in the Altoona bridge for Load Case 19.

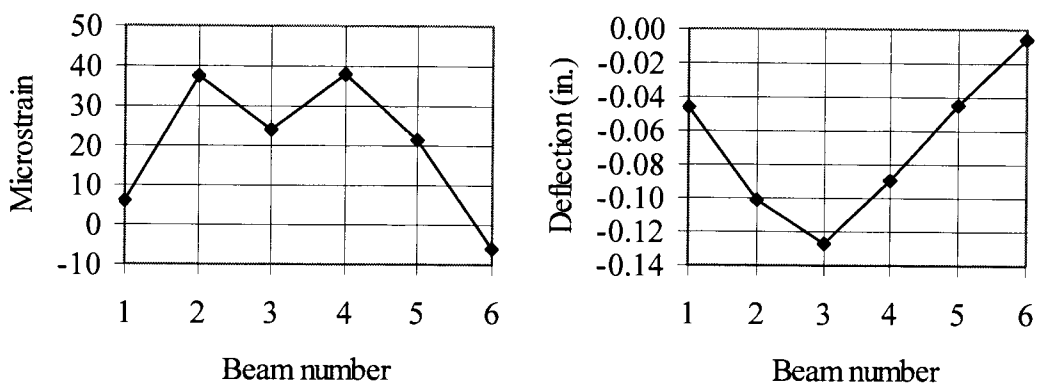

Figure 5.11. Strain and deflection in the Altoona bridge for Load Case 23.

value of 0.31 was computed in Beam 2 from the strain readings of the damaged bridge test, and a value of 0.27 was computed from the deflection data for the same beam. These values were taken from the results from Load Case 13, which caused the highest strains in Beam 2. The actual load distribution factor of the bridge was lower than the design distribution factor. The maximum strain Beam 2 reached was 49 MII which is much less than the 185 MII that was calculated using the AASHTO distribution factor, so it appears that the other beams could be assuming some of the load or that the distribution factor is quite conservative.

5.2.1.2. Longitudinal Behavior

Figure 5.12 through 5.14 show the strain at the center of span 2 as a function of truck position for a single truck placed at five locations along the length of the bridge, and when both trucks were side-by-side at the same five locations. By doing this, the behavior of the more heavily damaged girder can be compared with two girders that only incurred concrete damage. The five positions were the midpoint of span 1; ¼, ½, ¾ points of span 2; and midpoint of span 3. For all three girders, the strains are either zero or negative when the truck was positioned in Span 1 or 3, showing some moment continuity in the girders. The strains were the largest in the most heavily damaged girder (Beam 2), reaching almost 50 MII, but this can be attributed to the location of the wheel load, which was almost directly over Beam 2, and not the damage.

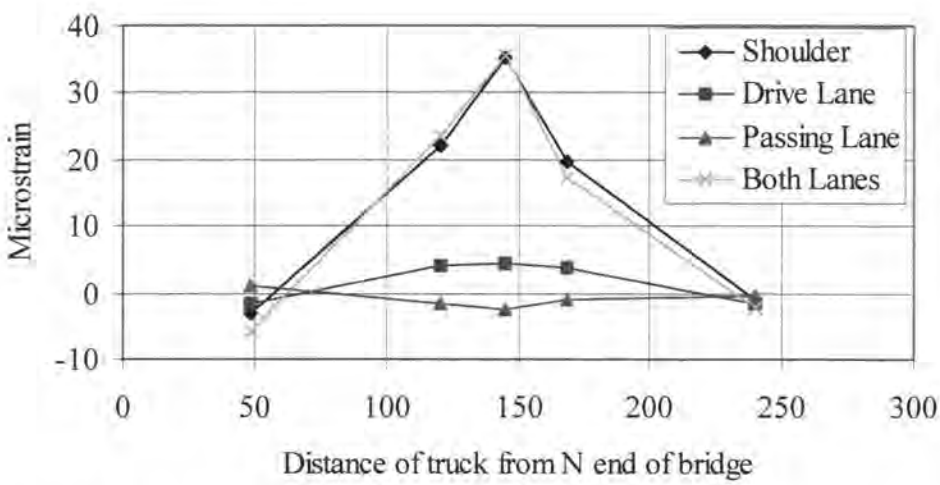

Figure 5.12. Strains in Beam 1 at the center of Span 2 in the Altoona Bridge.

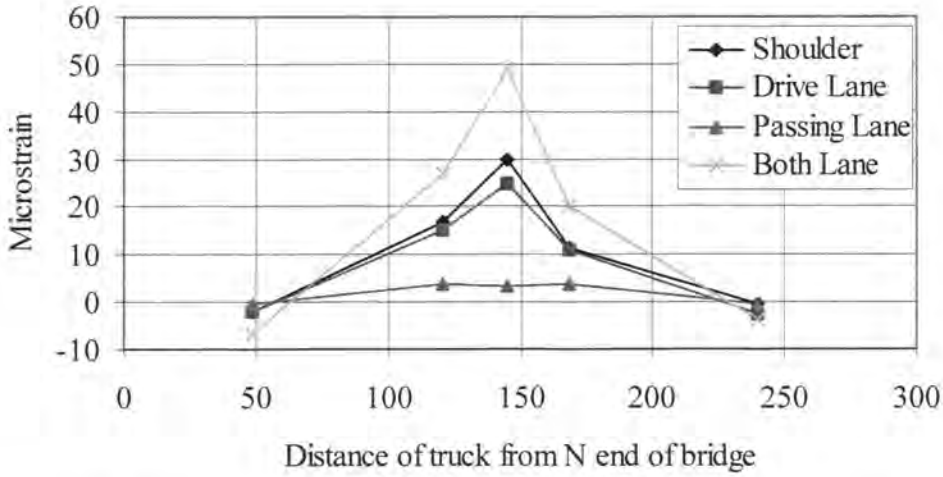

Figure 5.13. Strains in Beam 2 at the center of Span 2 in the Altoona Bridge.

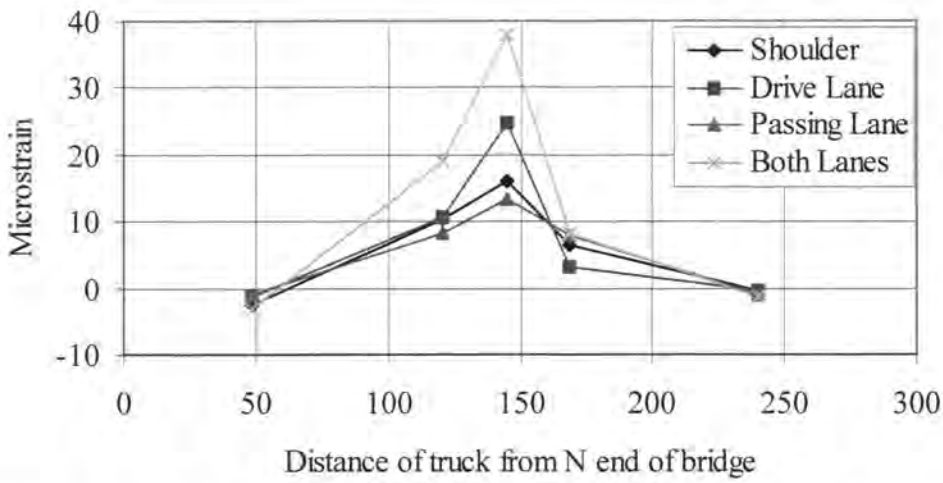

Figure 5.14. Strains in Beam 3 at the center of Span 2 in the Altoona Bridge.

5.2.2. Comparison Plots

After the second test was completed and the results were analyzed, a comparison was made between the data from each test to observe the changes in the behavior of the bridge due to the addition of CFRP. The plots for the transverse behavior were used for the comparison. After comparing the transverse data, it was determined that a comparison of the longitudinal behavior would be unnecessary.

5.2.2.1. Transverse Behavior

Figures 5.15 through 5.17 show the strains and deflections for the damaged and repaired tests for the three load cases mentioned in section 5.2.1.1, Load Cases 13, 19, and 23. Since the trucks used for the repaired bridge test weighed slightly less than the trucks used for the damaged bridge test, it was necessary to normalize the strain and deflection data. The normalization was based on the truck loads. For plotting comparisons, all the strains and deflections of the repaired bridge test were multiplied by 1.0942 to represent a 9.42% difference in total weight.

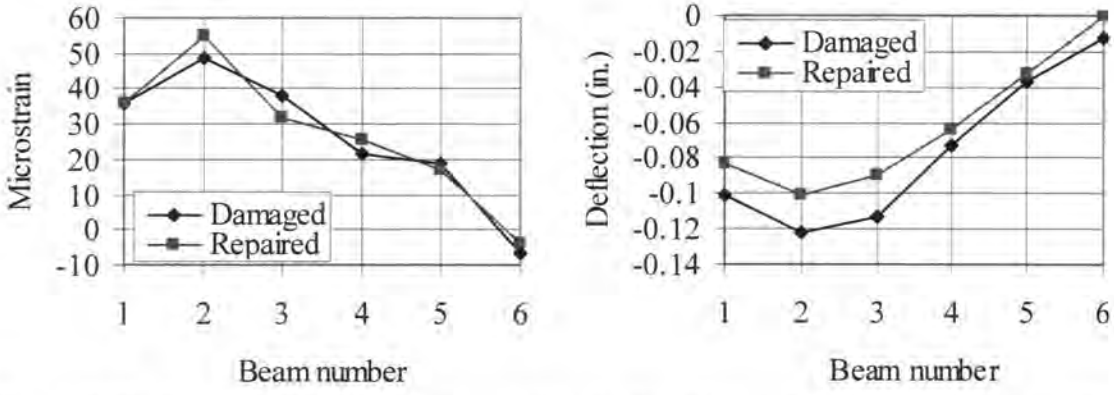

Figure 5.15. Strain and deflection comparison in the Altoona bridge for Load Case 13.

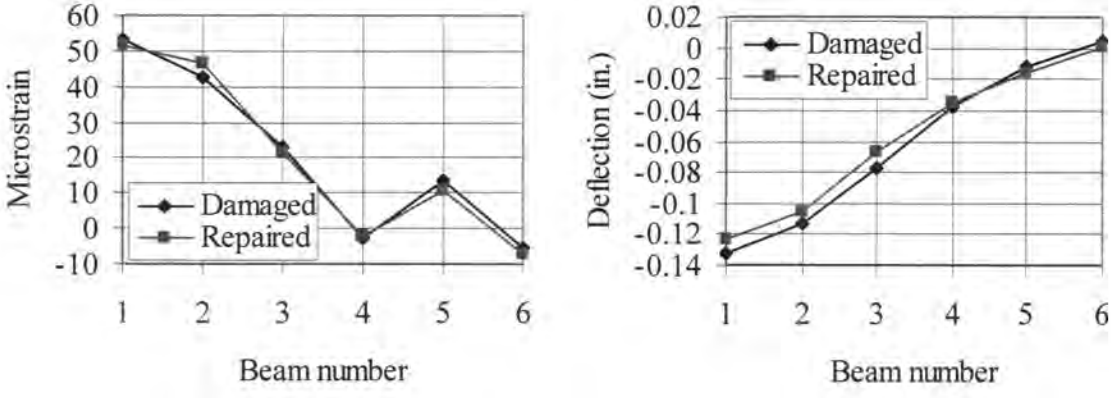

Figure 5.16. Strain and deflection comparison in the Altoona bridge for Load Case 19.

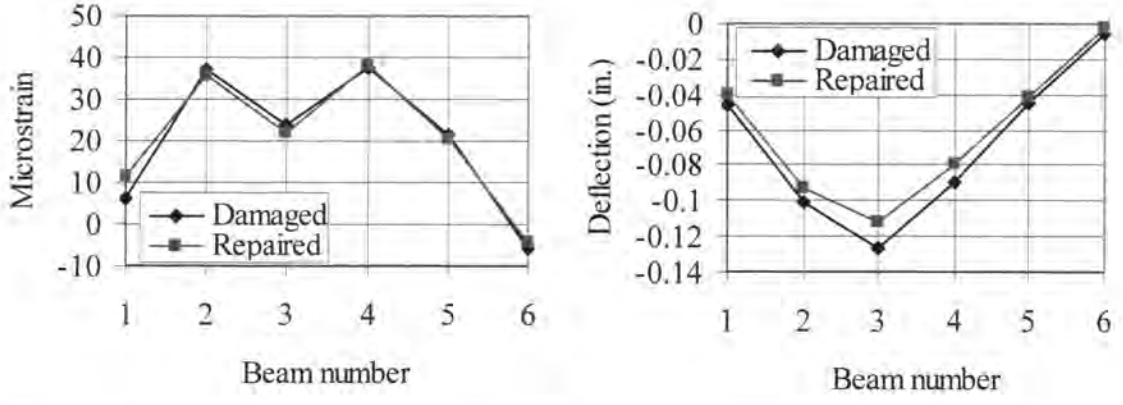

Figure 5.17. Strain and deflection comparison in the Altoona bridge for Load Case 23.

As shown in figures 5.15 through 5.17, the deflection in some of the beams decreased by up to 20%, which could be due to the repair or the positioning of the load trucks during the testing. The strain distribution also appears to have changed slightly, although the unusual jumps and dips evident in the first test are still observed in the repaired bridge test. In all three strain plots, the repaired Beam 2 has slightly higher strains than in the damaged tests, while Beam 3 has slightly lower strains. The addition of the CFRP plates slightly increased the stiffness of the repaired beam causing it to attract more of the load than in the first test. The plates slightly increased the moment of inertia approximately 5%, but the decrease in strain due to this increase was only calculated to be approximately 1%. The load factor computed from the strains of the bridge test was 0.32, and the load factor computed from the deflections was 0.27. The load factor computed from the strain increased with the addition of the CFRP, while the load factor computed from the deflection data stayed the same as the first test.

5.3. Osceola Bridge Test Results

The damaged bridge carrying IA Highway 34 over US 35 was tested in a series of rolling tests using a standard IA DOT tandem axle truck. Strains were measured using the BDI-STS system of gages described in Chapter 3. One strand on Beam 1 was completely severed, and this bridge was not retested after it was repaired.

5.3.1. Transverse Behavior

Figures 5.18 through 5.20 show the transverse behavior during the loading for load lanes 1, 3, and 5; the two outside lanes and the center lane. The loaded truck traveled five different loading lanes for the test, making each pass twice. Using the auto-clicker of the BDI system, the center of the bridge could be found. The BDI gage on Beam 4 was giving consistently high strain readings about 1.75 times higher than it should, indicating that it may have been placed on a microscopic crack or there was a problem with the gage. Thus the readings from that gage were left off the plots. Both trials of each load position are shown on the plots to show the consistency.

The strains in the extreme outside beams for the center load case, Load Lane 3, were quite small ranging from 3 to 7 MII. The damaged beam did not appear to exhibit any abnormal behavior, as it appeared to behave almost symmetrically to the beams on the opposite side of the bridge, which were undamaged. The strains in the beams at the center of the bridge only reached a maximum of 23 MII, and the highest measured strain in the bridge was 30 MII. This level of strain is extremely small for beams this large and is nothing that should cause any worry or indicate that the bridge is in any danger of failure.

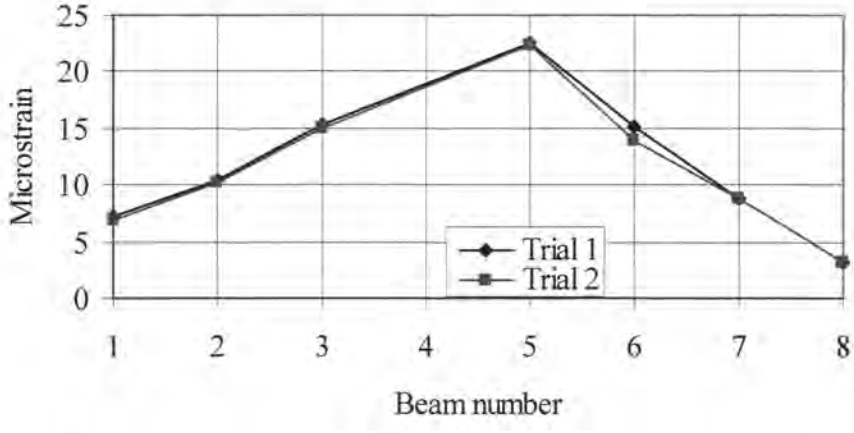

Figure 5.18. Strain at midspan of the Osceola bridge for Load Lane 3.

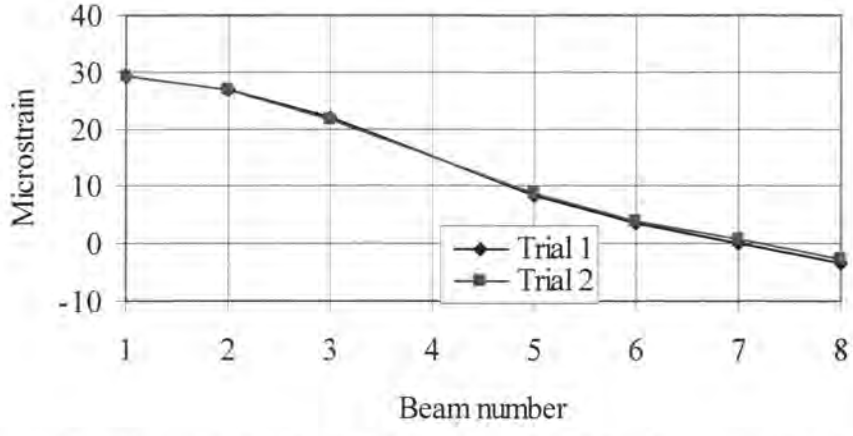

Figure 5.19. Strain at midspan of the Osceola bridge for Load Lane 1.

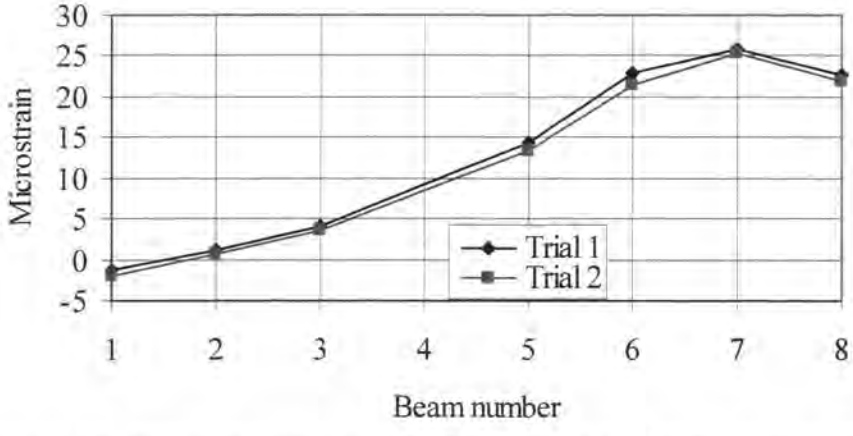

Figure 5.20. Strain at midspan of the Osceola bridge for Load Lane 5.

A distribution factor of 0.39 was calculated for this bridge using the 1996 AASHTO LFD Bridge Design Specification manual. A value of 0.28 was computed in Beam 1 from the strain readings of the damaged bridge test for the northernmost truck loading, which caused the largest strains in the damaged beam. The calculated factor is higher than the actual factor, which shows that the undamaged beams were assuming more of the load, or the distribution factor used by AASHTO is quite conservative.

5.4. De Soto Bridge Test Results

The damaged bridge carrying Interstate 80 over Highway 169 was tested in a series of rolling truck tests using a standard IA DOT tandem axle truck. The test was very similar to the Osceola bridge test, where again strains were measured using the BDI-STS system of

gages. One strand of Beam 9 was completely severed, and the bridge was not retested after it was repaired.

5.4.1. Transverse Behavior

Figures 5.21 through 5.23 show the transverse strain behavior of the nine beams during the loading for all three load positions. The loaded truck traveled three different loading paths for the test, making each pass twice. The load lanes included the center of the driving lane, the center of the passing lane, and the shoulder on the passing lane side. Beam 9 was the damaged beam, which was on the south side under the passing lane shoulder.

The highest strain recorded for any of the load cases was less than 50 MII, and were always located in the beam directly below the loaded lane. The highest strain in Beam 9 when the trucks were in the normal traveling lanes, (driving and passing lanes), was less than 12 MII. The damaged beam did not appear to have higher strains than would be expected on an undamaged bridge, since Beam 9 behaved similarly to Beam 1 for symmetric loading conditions. It can be concluded that the loss of only one strand out of nine beams is fairly insignificant for service loads.

A distribution factor (based on design assumptions) of 0.44 was calculated for this bridge using the 1996 AASHTO LFD Bridge Design Specification manual. A value of 0.30 was computed in Beam 9 from the strain readings of the bridge test for Load Lane 3, the left shoulder loading, which caused the largest strains in the damaged beam.

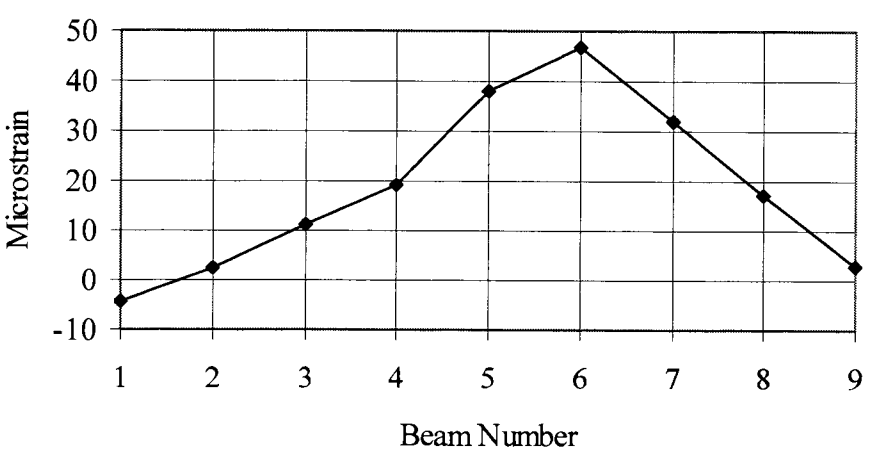

Figure 5.21. Strain at midspan in the De Soto bridge for Load Lane 1.

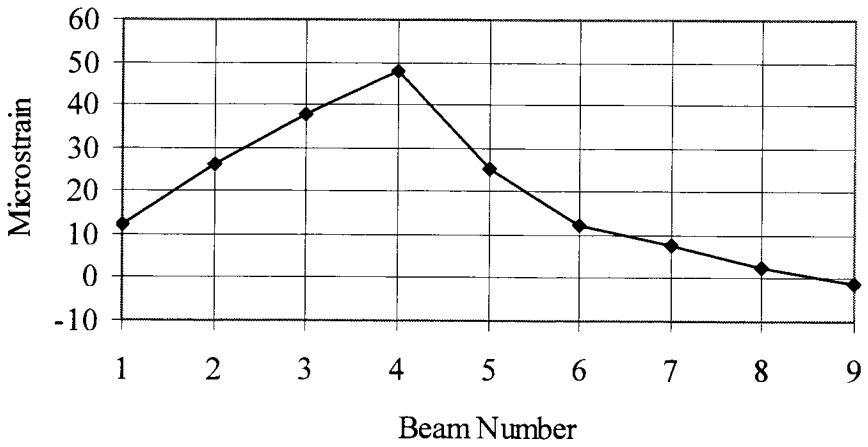

Figure 5.22. Strain at midspan in the De Soto bridge for Load Lane 2.

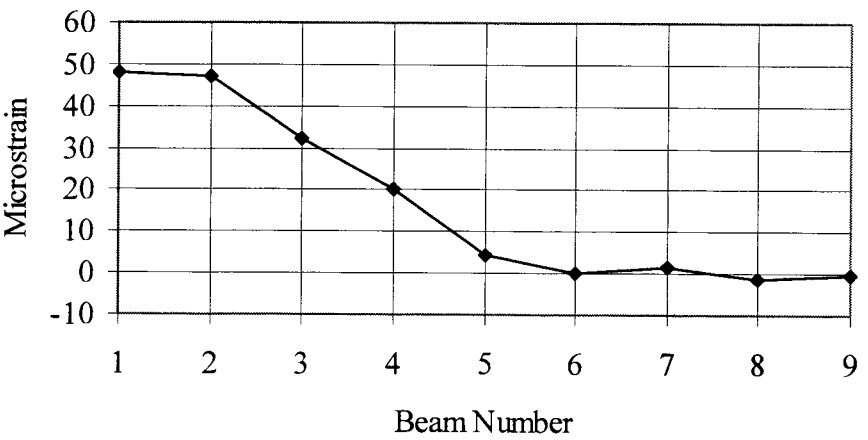

Figure 5.23. Strain at midspan in the De Soto bridge for Load Lane 3.

5.4.2. Longitudinal Behavior

Figure 5.24 shows three different beams from three different trials. The beams plotted were the beams most directly beneath the left tire of the loaded truck. Beam 1 is plotted for the first shoulder run, S1, Beam 3 is plotted for the first pass lane run, P1, and Beam 5 is plotted for the first drive lane run, D1. The jaggedness of the figure was due to the truck bouncing somewhat on the bridge during the trial runs. Notice that all three beams

achieve almost the same strain levels. The first beam had the highest strain, but it was on the outside where the strain distribution was not as good as the distribution is for the inside beams. This can also be seen in the transverse plots, Figure 5.23, where only half of the bridge is taking the shoulder truck load.

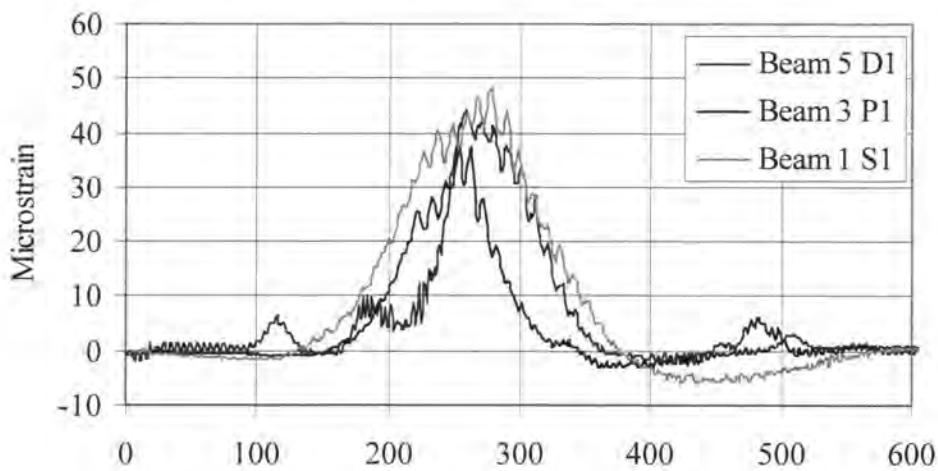

Figure 5.24. Strain at midspan of Beams 1, 3, and 5 in the De Soto bridge .

6. SUMMARY AND CONCLUSIONS

6.1. Summary

In this study, a full-sized P/C beam was damaged and three P/C field bridges that had been damaged and subsequently repaired with CFRP. The goal was to determine the effects of the repair/strengthening process on the structural behavior of the P/C beams. As part of the research, a literature review was also conducted to examine the recent findings from any similar testing.

In the laboratory, a full-sized P/C beam was damaged to replicate impact damage from an overheight vehicle to a bridge. The beam was repaired using current CFRP technology and was subjected to cyclic service level loads to simulate bridge traffic. The beam was then statically tested to failure to observe the effects of the cyclic loading on the repair. Results were compared to previously collected data on three similar repaired beams that did not undergo the cyclic loading.

From the many bridges in Iowa that have been struck by overheight vehicles, three were repaired as part of this investigation. The southbound I-65 bridge near Altoona, the westbound IA-34 bridge near Osceola, and the westbound I-80 bridge near De Soto all had significant concrete loss on one or more beams, as well as at least one severed prestressing strand. Repair strategies were developed so the moment capacity from the severed strand(s) could be restored by CFRP. CFRP also has the functional capacity of preventing the mortar patches from falling out onto the highways below. All three bridges were load tested using weighted DOT tandem axle trucks prior to repair. The Altoona bridge was also tested after the repair was complete to observe any differences in the bridge's behavior.

Photographic and written documentation were taken during the repair of the IA-34 bridge near Osceola. This documentation was used to create a CFRP application guide for aid in any future bridge repairs. A design aid was also put together using manufacturer's suggested design guidelines as well as input from other sources. These materials were assimilated to assist other engineers in the design of similar repairs.

6.2. Conclusions

Carbon fiber repair methods are an effective method for repairing and strengthening damaged bridges. Due to the extremely high strength to weight ratio, the installation process is relatively quick and easy. Traffic control costs are lower due to the speed of the repair. Since the repair techniques are relatively new, the design/application guide developed will be very helpful when teaching the new techniques. This guide will also be helpful in the design of a given bridge repair. With continued usage and perfection of the design techniques involved, CFRP repair design time can be reduced thus increasing the cost effectiveness of the repair. The following conclusions can be drawn from this investigation:

- Transverse CFRP jackets helped develop the longitudinal CFRP sheets and prevented debonding. More importantly, the jackets helped to confine the patch material under service or over-loads. This is especially important in the field where falling patch material from a repaired bridge can damage traveling vehicles and/or cause serious injuries to the traveling public.
- CFRP can restore reduced moment capacity. While a steel jacket may contain patched concrete, it does not have the tensile strength of CFRP in restoring beam strength.
- Distribution of loads among beams was always better than the AASHTO distribution factor predicted. The damaged beams carried a smaller percentage of the total load than predicted and were subjected to less stress than was predicted using the distribution factor.
- Beam deflections were reduced in the bridge tests as much as 20%. The deflections decreased up to 0.02 in. for the most heavily loaded beams. Deflection decreases although slight, were noticed in several of the load tests on the Altoona Bridge.
- Bridge closure following impact damage is probably unnecessary when only one or two strands in a P/C beam are damaged. The data from the bridge tests showed that the damaged bridges behaved like undamaged bridges when distributing load among the beams.

- The use of design aids including design templates for CFRP can reduce design times.
- The excellent corrosive and fatigue properties of CFRP reduce future inspection and rehabilitation time.

7. FURTHER INVESTIGATION

A number of issues were discussed during the course of this investigation including CFRP repairing/strengthening capabilities, bridge load distribution, and transverse jackets. Tests were performed on one P/C beam in the laboratory and three P/C bridges in the field. Several conclusions were drawn about the capabilities of CFRP for beam repair as well as load distribution characteristics of damaged bridges. Some issues seemed to need further investigation and are listed below.

- Of the three bridges tested, the Altoona bridge incurred the most damage, which consisted of 5 severed strands. It was evident from the testing that this minor amount of damage did not seriously compromise the integrity of the bridge. It could have remained in service for quite some time with no noticeable effects. Further study is needed on bridges with extreme damage. To fully utilize the strength of CFRP, bridges with damage requiring replacement need to be tested to see if replacement can be avoided by utilizing CFRP. Of the three bridges tested for this investigation, the patch containment is probably the best benefit received.
- Anchorage issues for CFRP should be investigated further. In the P/C beam ultimate test, the CFRP reached barely one third of its tensile capacity before delamination occurred resulting in failure. In order to maximize the effectiveness of CFRP, anchorage systems need to be developed that would prevent premature debonding and delamination, allowing the design strength of the CFRP to be neared.
- Perhaps an in depth study of the reserve capacity of damaged beams should be done for aid in deciding on repair policies. Some repairs could possibly be cheapened or avoided simply by realizing the capacity that damaged beams have. If costly replacement or CFRP repair can be avoided, it should be investigated.

APPENDIX A

DAMAGE REPORTS

ALTOONA

Beam #1- At the impact point, concrete was spalled from the bottom flange for approximately 24 inches in the longitudinal direction, 7 inches in the vertical direction on the bottom flange west face, and 10 inches in the transverse direction. Approximately 2 ½ inches of concrete was missing at the deepest point. One prestressing strand was severed and there was one exposed stirrup. There was no evidence of cracking in the beam.

Beam #2- This was the most severely damaged beam. At the impact point, concrete was spalled from the bottom flange for approximately 48 inches in the longitudinal direction, the entire vertical face of the bottom flange and approximately 5 inches of the sloped west face, and transversely across the entire bottom of the bottom flange. Approximately 4 inches of concrete was missing at the deepest point. Five prestressing strands were exposed, and two more were severed. On the west face of the beam, one crack was located at the web and top flange interface and extended from approximately 8 ft. off of the face of the middle pier diaphragm to near the face of the centerline diaphragm. This crack was approximately $1/16^{th}$ to $3/32^{nd}$ inches wide at its widest point. Another crack extended from the bottom flange near the middle pier diaphragm, diagonally across the web, and met the top crack at approximately 23 ft. from the pier diaphragm. Four cracks extended diagonally across the bottom of the bottom flange and diagonally across the face of the bottom flange and along the web and bottom flange interface. These cracks were located at approximately 15, 18, 21, and 25 ft north of the centerline of the impact area. Sounding of the web in this area with a hammer produced a slightly different ring, indicating possible hollow areas. There were several other longitudinal cracks on the web of the west face. On the east face of the beam, one crack was located at the web and top flange interface and extended from the face of the centerline diaphragm to within 9 ft of the face of the middle diaphragm. There were a couple of other longitudinal cracks on the web of the east face.

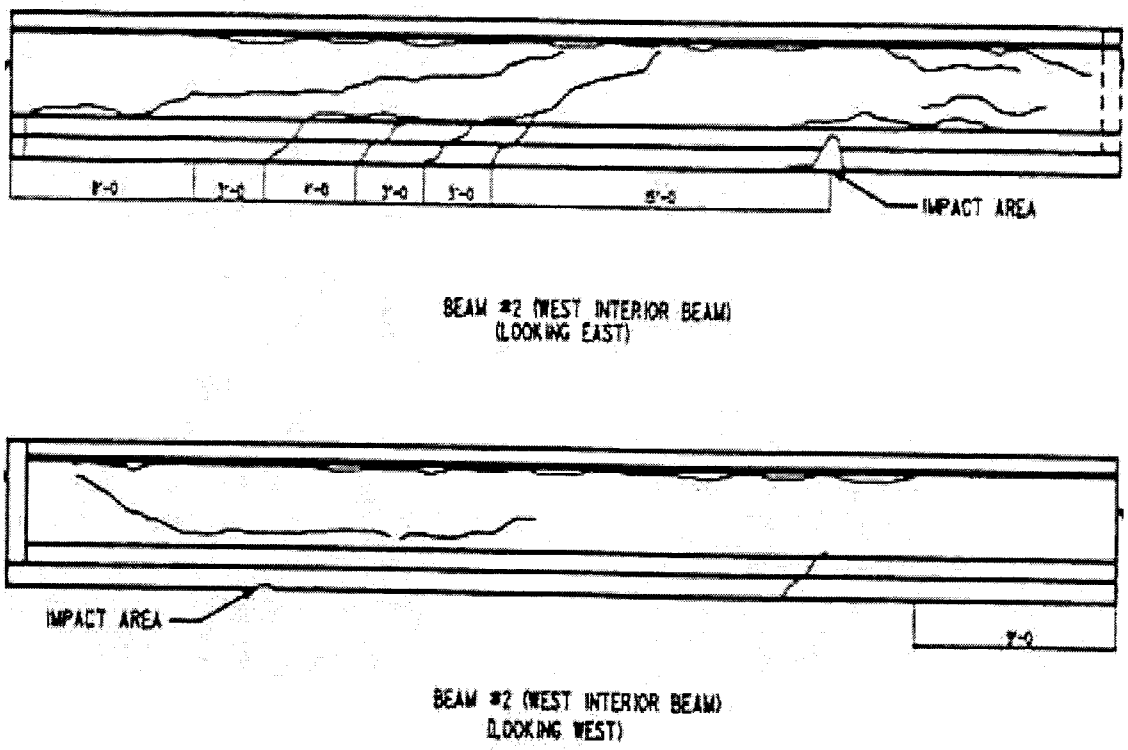

Figure A24. Altoona beam #2 damage drawings.

Beam #3- At the impact point, concrete was spalled from the bottom flange for approximately 26 inches in the longitudinal direction, 7 inches in the vertical direction on the bottom flange west face, and 10 inches in the transverse direction. Approximately 2 ½ inches of concrete was missing at the deepest point. One prestressing strand was severed and there was one exposed stirrup. On the west face of the beam a crack was located at the web and top flange interface and extended approximately 10 ft from the centerline of the collision area toward the middle pier.

Beam #4- At the impact point, concrete was spalled from the bottom flange for approximately 18 inches in the longitudinal direction, 6 inches in the vertical direction on the bottom flange west face, and 9 inches in the transverse direction. Approximately 2 inches of concrete was missing at the deepest point. One prestressing strand was partially exposed and it appeared gouged. There was no evidence of cracking in this beam.

Beam #5-At the impact point, concrete was spalled from the bottom flange for approximately 32 inches in the longitudinal direction, 6 inches in the vertical direction on the

bottom flange west face, and 10 inches in the transverse direction. Approximately 2 ½ inches of concrete was missing at the deepest point. One prestressing strand was severed. There was a crack on both sides of the beam at the web and top flange interface that extended from approximately 10 ft. off of the middle pier diaphragm face to about 5 ft past the centerline of the impact point.

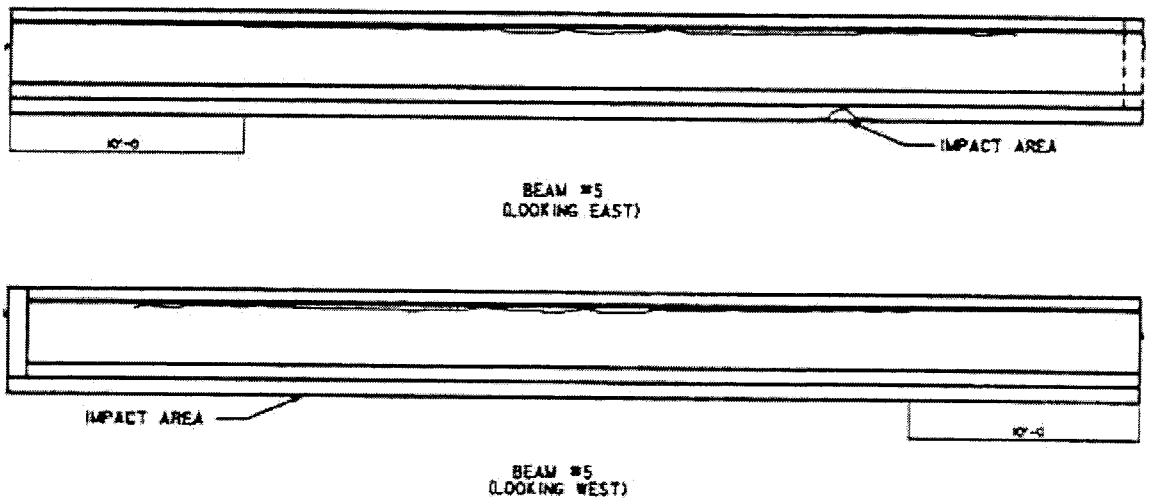

Figure A25. Altoona beam #5 damage drawing.

Beam #6-At the impact point, concrete was spalled from the bottom flange for approximately 45 inches in the longitudinal direction, 6 inches in the vertical direction on the bottom flange west face, and 10 inches in the transverse direction. Approximately 2 inches of concrete was missing at the deepest point. One prestressing strand was exposed and partially severed, and there were two exposed stirrups. There was also a crack starting at about 5 ft from the impact point, intersecting the top crack, and extending diagonally to the interface of the web and bottom flange at the centerline diaphragm.

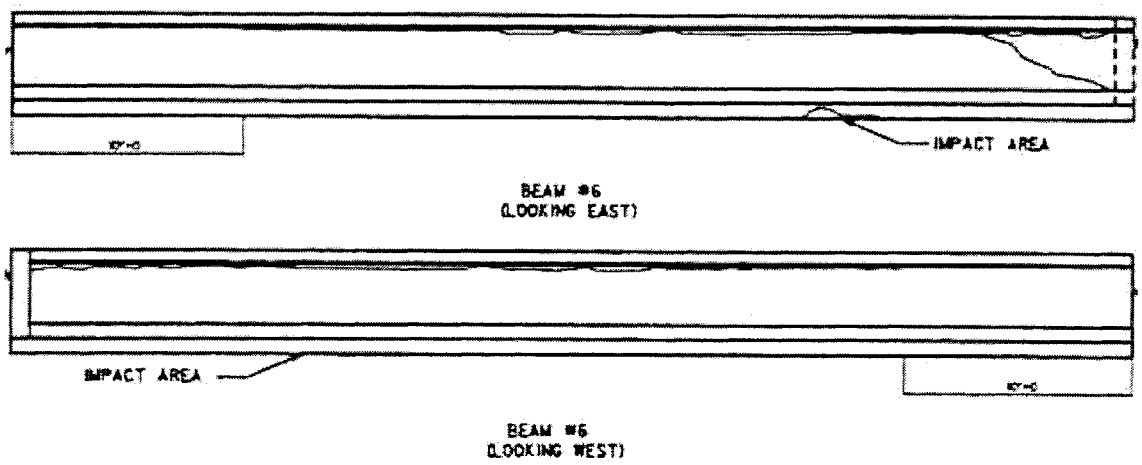

Figure A26. Altoona beam #6 damage drawing.

OSCEOLA

Beam #1- This beam was the most severely damaged of the two beams. Two strands were severed in the bottom layer of strands. There was a large hollow area in the bottom flange at the impact zone. A portion of the hollow area appeared to be cracked completely through from the top most edge to the bottom edge. This area was most likely being held in place by the strand that was running through it. The web was cracked along the top flange interface, on both sides of the beam, for a distance of approximately 25 ft over the impact zone. There was a hairline crack at the beam and diaphragm interface with a spall in the bottom of the diaphragm exposing the coil ties that connected the bottom flange to the diaphragm. On the north exterior face of the beam there was horizontal hairline cracking in the web at the impact zone. There was a diagonal crack staring in the bottom flange 12 ft from the east bearing, extending back towards the east bearing and stopping near the center of the web. The diagonal crack did not appear on the interior face of the beam.

Beam #2- Beam #2 had some minor spalls on the bottom flange and a large spall on the north side of the bottom flange. The large spall was approximately 2 ½ inches deep, partially exposing 2 to 3 strands and reinforcing steel. No cracking in the web was seen. Other spalls were ¾ to 1 inch deep with no reinforcing exposed. A drawing from the damage report is shown in Figure A27.

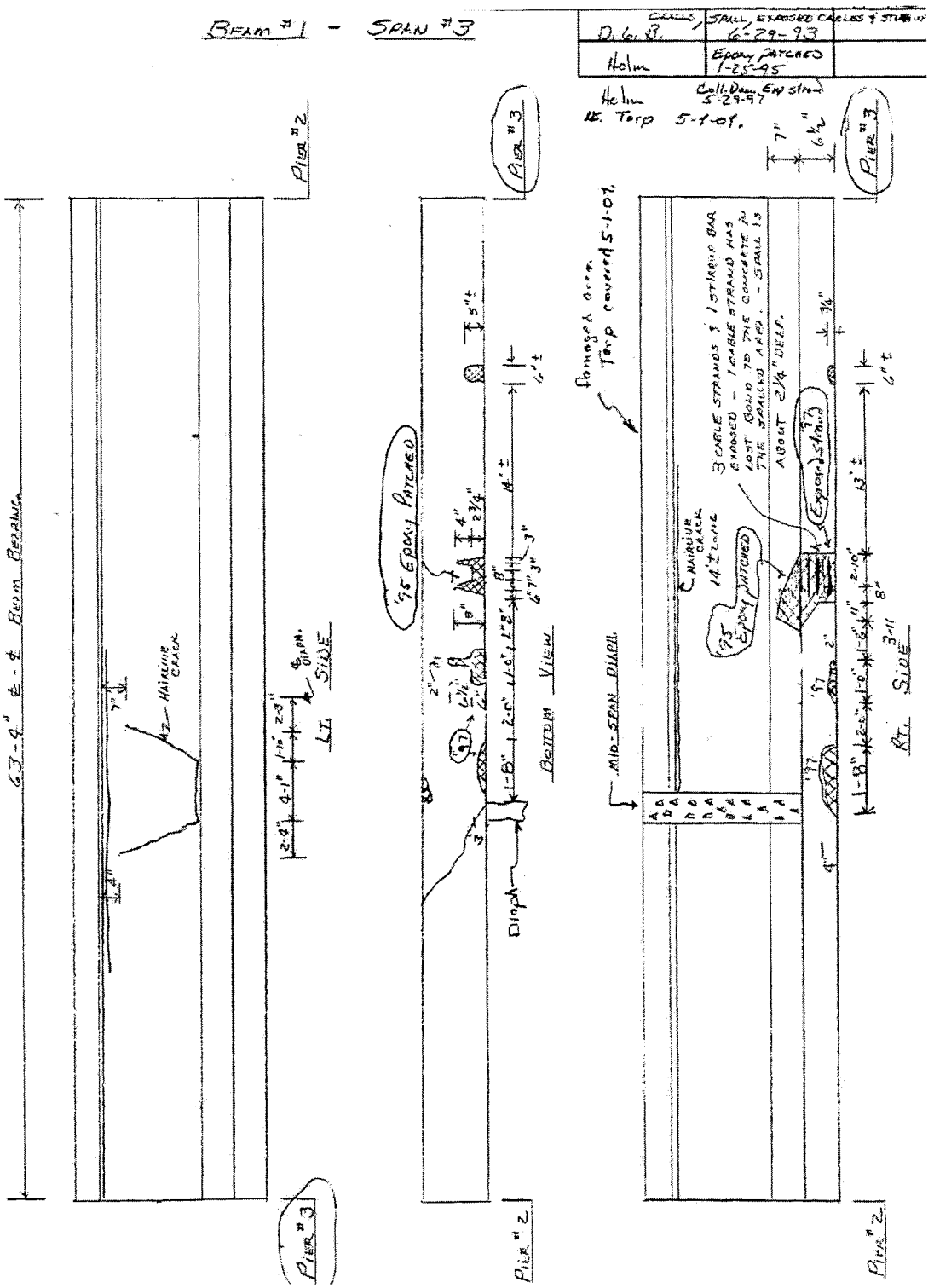

Figure A27. Osceola damaged beam drawing.

DE SOTO

Beam #1- This beam was the only beam to sustain major damage. A southbound vehicle struck the southernmost beam but virtually missed the other beams before it. The bottom strand on the north side of the beam was completely severed and another strand was almost totally visible. Three strands were also visible on the south side where concrete had broken away. There were several cracks along the bottom of the beam propagating from the impact zone. There was also a 1/8 inch crack that extended for several feet just below the top flange that was visible on both sides of the beam. A page from the damage report is shown in Figure A28.

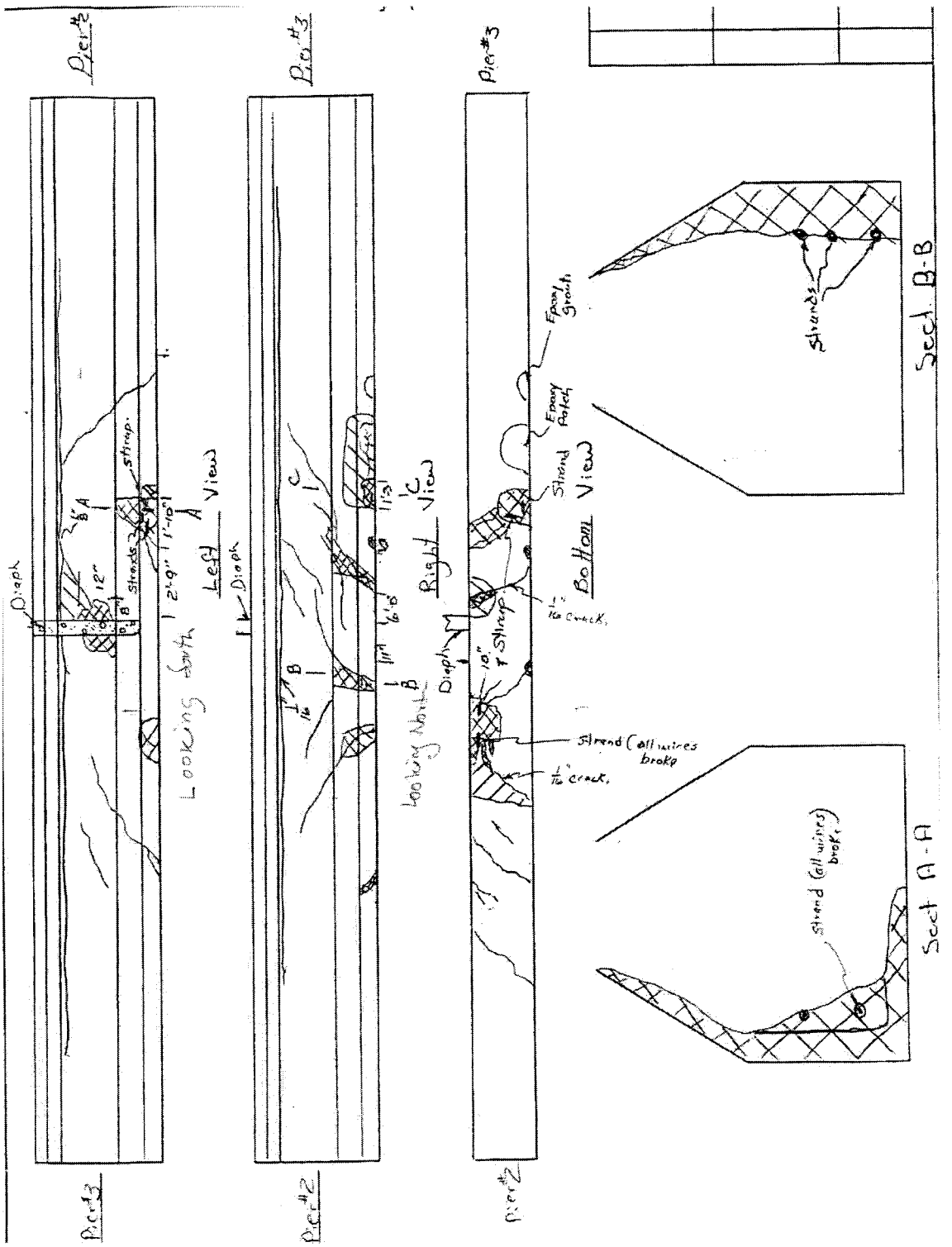

Figure A28. De Soto damaged beam drawing.

APPENDIX B

DESIGN/APPLICATION GUIDE

Design for Fiber Reinforced Plastic repair to a Prestressed Concrete Beam

Designing a CFRP repair system for a damaged prestressed beam can be somewhat confusing if the designer is not familiar with the design procedures This guide is intended to aid in the design process and will provide some step-by-step instructions as well as examples of previous designs.

1) Design is based on the Master Builders product CF 130 High Tensile Carbon

2) All highlighted values need to be entered manually

$kip := 1000 \cdot lbf$

$ksi := 1000 \cdot psi$

STEP 1: List all values needed for analysis of prestressed beam.

Area of beam.	$A_c := \blacksquare \cdot in^2$
Height of beam.	$H := \blacksquare \cdot in$
Area of prestressing steel.	$A_{ps} := \blacksquare \cdot in^2$
Prestressing steel strength.	$f_u := \blacksquare \cdot psi$
Distance from top of concrete that is in compression to centroid of prestressing steel in composite section.	$d := \blacksquare \cdot in$
Distance from centroid of beam to bottom of non-composite section.	$Y_b := \blacksquare \cdot in$
Slab thickness.	$t_s := \blacksquare \cdot in$
Gross beam moment of inertia.	$I_g := \blacksquare \cdot in^4$
Slab concrete strength.	$f'_c := \blacksquare \cdot psi$
Beam concrete strength.	$f'_{cbeam} := \blacksquare \cdot psi$
Distance from bottom to centroid of prestressing strands .	$Y_s := \blacksquare \cdot in$
Moment on beam when FRP is installed.	$M_{initial} := \blacksquare \cdot ft \cdot kip$ (100% Dead Load + 25% Live Load)
Effective prestress force when FRP is installed.	$P_e := \blacksquare \cdot lbf$
Modulus of elasticity of prestressing strand.	$E_p := \blacksquare \cdot ksi$
Effective slab width.	$b := \blacksquare \cdot in$

Transformed section modulus for the bottom of the beam only. $S_{beam} := \blacksquare \cdot in^3$

Section modulus for the composite beam and slab at the bottom of the beam, with the slab concrete transformed to equivalent beam concrete. (E_{slab}/E_{beam}) $S_n := \blacksquare \cdot in^3$

Section modulus for the composite beam and slab at the bottom of the beam, with the slab concrete transformed to equivalent beam concrete for long term loading. (E_{slab}/E_{beam})/3 $S_{3n} := \blacksquare \cdot in^3$

Section modulus for the composite beam and slab at the top of the beam, with the slab concrete transformed to equivalent beam concrete. (E_{slab}/E_{beam}) $S_{n\_top} := \blacksquare \cdot in^3$

Section modulus for the composite beam and slab at the top of the beam, with the slab concrete transformed to equivalent beam concrete for long term loading. (E_{slab}/E_{beam}) $S_{3n\_top} := \blacksquare \cdot in^3$

Transformed section modulus for the top of the beam only. $S_{top} := \blacksquare \cdot in^3$

FRP Material Properties

Thickness of fiber sheet $t_f := \blacksquare \cdot in$

Design strength $f_{fu} := \blacksquare \cdot psi$

Design strain $\varepsilon_{fu} := \blacksquare \cdot \frac{in}{in}$

Tensile Modulus $E_f := \blacksquare \cdot psi$

STEP 2: Determine the existing flexural capacity based on original section properties and determine the loss of capacity due to damage.

Determine Ultimate Moment capacity of beam before damage/deterioration using section properties.

$$Mu_{original} := \blacksquare \, ft \cdot kip$$

Determine Ultimate Moment capacity of beam after damage/deterioration.

$$Mu_{existing} := \blacksquare \, ft \cdot kip$$

Calculate loss in capacity :

$$M_{loss} := Mu_{original} - Mu_{existing} \qquad M_{loss} = \blacksquare \, ft \cdot kip$$

STEP 3: Using the M_{loss}, estimate the number of sheets of FRP that will be needed based on the additional tensile force required to restore the original moment strength.

Tension to be recovered = T

$$T := \frac{M_{loss}}{0.9 \cdot d}$$

Area of FRP needed:

$$A_f := \frac{T}{0.9 \cdot 0.85 \cdot f_{fu}}$$

Nominal sheet width is 24 inches. The FRP is easy to cut into smaller widths such as 3, 4, 6, 8, or 12 inches.

Width of FRP sheet to be used:

$$W_{FRP} := \blacksquare \cdot in$$

Calculate the number of layers needed:

Layers required = n_p

$$n_p := \frac{A_f}{W_{FRP} \cdot t_f} \qquad n := ceil(n_p)$$

$$n = \blacksquare$$

Area of FRP to be used = A_{FRP}

$$A_{FRP} := n \cdot t_f \cdot W_{FRP}$$

STEP 4: Calculate the flexural capacity with the FRP. This is the beginning of the iteration process. Start by assuming an initial C value, which is the distance from the extreme compression fiber to neutral axis. An uncracked section is assumed.

Trial & Error Method

Initial "C" can be taken as 0.15(d)

For the initial iteration let $C = C_{initial}$, adjust C for subsequent iterations.

$$C_{initial} := 0.15 \cdot d \qquad C_{initial} = \blacksquare \qquad C := \blacksquare \cdot in$$

STEP 5: Determine the failure mode by reviewing the existing state of strain in the concrete Since FRP is usually installed unstressed, and the concrete surface to which it is attached is stressed from self-weight and prestressing, the strains will be different. In order to use strain compatibility, the existing state of strain in the concrete must be calculate(This initial strain can then be added to the ultimate strain and used as shown below. As stated before, an uncracked section is assumed.

ε_{bi} = Strain in concrete substrate at time of FRP installation.

ε_{fu} = Ultimate strain of the FRP material. (given on page 1)

If $\varepsilon_{fu} + \varepsilon_{bi} < \varepsilon_{cu}(H + ts - C)/C$, Failure is controlled by concrete crushing.

If $\varepsilon_{fu} + \varepsilon_{bi} > \varepsilon_{cu}(H + ts - C)/C$, Failure is controlled by FRP rupture.

Maximum usable compressive strain in the concrete = ε_{cu}

$$\varepsilon_{cu} := 0.003$$

$$\varepsilon_{total} := \varepsilon_{cu} \cdot \frac{(H + t_s - C)}{C}$$

E_c = Approximate elastic modulus of concrete in compression (psi).

$$E_c := \frac{57 \cdot f'^{0.5}_{cbeam}}{1 \cdot psi^{0.5}} \cdot ksi$$

$$\varepsilon_{bi} := \frac{M_{initial} Y_b}{I_g \cdot E_c} - \frac{P_e}{A_c \cdot E_c} \cdot \left[1 + \frac{(Y_b - Y_s) \cdot Y_b}{\frac{I_g}{A_c}} \right]$$

$$Controlling\_Factor = if\left[\left(\varepsilon_{total} < \varepsilon_{fu} + \varepsilon_{bi}\right), \text{"Concrete crushing"}, \text{"FRP rupture"}\right]$$

Controlling_Factor= ∎

Note: It is recommended that the design be altered if concrete crushing is the failure mode. Reduce the number of FRP layers or reduce the width of the strips used. If the controlling factor cannot be changed, proceed with Step 6A; if the controlling factor is FRP rupture, proceed with Step 6B.

Step 6A: When failure is governed by<u>concrete crushing</u>, the strain in the concrete at failure will be at its maximum usable strain ε_{cu}.

$$\varepsilon_c := \varepsilon_{cu}$$

The strain in the FRP may be determined by finding the strain in the concrete substrate at ultimate and subtracting the strain in the concrete substrate at the time of FRP installation.

$$\varepsilon_f := \varepsilon_c \cdot \left(\frac{H + t_s - C}{C} \right) - \varepsilon_{bi}$$

ε_{bi} = Strain in concrete substrate at time of FRP installation.

Because the concrete is at its maximum usable strain level, the rectangular stress block specified in ACI 318 may be used to aproximate the actual non-linear stress distribution in the concrete.
The FRP sheet may be taken as linear-elastic to failure.

$$f_f := E_f \cdot \varepsilon_f$$

The estimated value of C is then checked against the value obtained, c, to satisfy equilibirum of the internal stress resultants.

$$c := \frac{A_{FRP} \cdot f_f + A_{ps} \cdot f_u}{0.85 \cdot f'_c \cdot 0.85 \cdot b}$$

c = ▮in C = ▮in

Repeat Step 4 through Step 6 by adjusting C in Step 4 until C=c, then proceed to Step 10.

Step 6B: When the failure mode is controlled by<u>FRP rupture</u>, the calculation procedure used to compute the nominal moment capacity of a section is similar to that used when there is concrete crushing. In this case, the known value of strain in the FRP may be used in conjunction with the estimated neutral axis location to determine the strain level in each of the materials.
Calculate the concrete strain, ε_c, and the strain in the FRP, ε_f.

$$\varepsilon_c := \left(\varepsilon_{fu} + \varepsilon_{bi}\right) \cdot \frac{C}{H + t_s - C}$$

$$\varepsilon_f := \varepsilon_{fu}$$

Therefore the stress in the FRP = f_f.

$$f_f := \begin{cases} f_{fu} & \text{if } \varepsilon_f \cdot E_f > f_{fu} \\ \left(\varepsilon_f \cdot E_f\right) & \text{otherwise} \end{cases}$$

f_f = ▮ksi

Step 7: Determine stress block parameters.

Because the concrete does not reach its ultimate compressive strain in Step 6B, the Whitney stress block is not applicable. The stress resultant for concrete should be determined from an appropriate non-linear stress-strain relationship or by a rectangular stress block suitable for the particular level of strain in the concrete. Parameters for the stress block are given below.

$$E_{beam} := \frac{57 \cdot f'_{cbeam}{}^{0.5}}{psi^{.0.5}} \cdot ksi \qquad E_{slab} := \frac{57 \cdot f'_{c}{}^{.5}}{1 \cdot psi^{.0.5}} \cdot ksi$$

$$n_{transformed} := \frac{E_{slab}}{E_{beam}}$$

$$\varepsilon_{pc} := \frac{1.71 \cdot f'_c}{E_{slab}} \qquad \varepsilon_n := \frac{\varepsilon_c}{\varepsilon_{pc}}$$

$$\beta_1 := \left[2 - 4 \cdot \frac{\left(\varepsilon_n - \operatorname{atan}\left(\varepsilon_n\right)\right)}{\varepsilon_n \cdot \ln\left(1 + \varepsilon_n{}^2\right)} \right]$$

$$\gamma := \frac{0.90 \cdot \ln\left(1 + \varepsilon_n{}^2\right)}{\beta_1 \cdot \varepsilon_n}$$

Step 8: Determine the strain in the prestressing strands. Total strain in the prestressing strands is due to strains at three load stages. Load stage 1 is the prestress alone, stage 2 is the decompression of the concrete, and stage 3 is the ultimate load. Total strain $=\varepsilon_1 + \varepsilon_2 + \varepsilon_3$

ε_1 = Strain in the tendons due to the initial application of the prestress force and any subsequent losses that occur.

$$\varepsilon_1 := \frac{P_e}{A_{ps} \cdot E_p}$$

ε_2 = Strain in the tendons due to decompression of the concrete at the level of the tendons.

$$\varepsilon_2 := \frac{P_e}{A_c \cdot E_c} \cdot \left[1 + \frac{\left(Y_b - Y_s\right)^2}{\frac{I_g}{A_c}} \right]$$

ε_3 = Strain in the tendons due to ultimate loading.

$$\varepsilon_3 := \begin{cases} \left[\varepsilon_f \cdot \frac{(H + t_s - Y_s - C)}{H + t_s - C}\right] & \text{if } \varepsilon_{total} > \varepsilon_{fu} + \varepsilon_{bi} \quad \text{FRP rupture} \\ \left[\varepsilon_c \cdot \left(\frac{H + t_s - Y_s - C}{C}\right)\right] & \text{otherwise} \quad \text{Concrete crushing} \end{cases}$$

$$\varepsilon_{ps} := \varepsilon_1 + \varepsilon_2 + \varepsilon_3 \qquad \varepsilon_p := \begin{cases} \varepsilon_{ps} & \text{if } \varepsilon_{ps} < 0.03 \\ 0.03 & \text{otherwise} \end{cases}$$

Step 9: Calculate the stress in prestressing strands so that c may be calculated.

$$f_{ps} := \begin{cases} \varepsilon_p \cdot E_p & \text{if } \varepsilon_p \le 0.008 \\ \text{otherwise} & \\ \quad \begin{cases} \left(\left(f_u - \frac{75 \cdot psi}{\varepsilon_p - 0.0065} - 2000 \cdot psi\right)\right) & \text{if } f_u = 270000 \cdot psi \\ \left(\left(f_u - \frac{58 \cdot psi}{\varepsilon_p - 0.006} - 2000 \cdot psi\right)\right) & \text{otherwise} \end{cases} \end{cases}$$

Force in FRP sheets

$$T_{FRP} := A_{FRP} \cdot f_f$$

Force in strands

$$T_{ps} := A_{ps} \cdot f_{ps}$$

Estimate of neutral axis location

$$c := \frac{T_{ps} + T_{FRP}}{\gamma \cdot f'_c \cdot \beta_1 \cdot b} \qquad c = \blacksquare\,in \qquad C = \blacksquare\,in$$

Re-iterate until c = C by changing C in Step 4. Then proceed to Step 10.

Step 10: Compute the nominal capacity of the beam.

Assuming $\beta_1 * C < t_s$

$\beta_1 \cdot C = \blacksquare\,in$ $\qquad t_s = \blacksquare\,in$

$$M_n := \left[T_{ps} \cdot \left(H + t_s - Y_s - \frac{\beta_1 \cdot C}{2}\right) + T_{FRP} \cdot \left(H + t_s - \frac{\beta_1 \cdot C}{2}\right)\right]$$

$\phi := 0.9$

$\phi \cdot M_n := \blacksquare$

Step 11: Check all allowable stresses that haven't been checked already.

$M_{LL\_I} := \blacksquare \cdot ft \cdot kip$ $M_{DL1} := \blacksquare \cdot ft \cdot kip$ $M_{DL2} := \blacksquare \cdot ft \cdot kip$

M_{LL_I} = live load with impact

M_{DL1} = dead load on the non composite section

M_{DL2} = superimposed dead load on the composite section

$f_{available}$ is the available stress capacity for live load.

$$f_{available} := \frac{P_e}{A_c} + \frac{P_e \cdot (Y_b - Y_s)}{S_{beam}} - \frac{M_{DL1}}{S_{beam}} - \frac{M_{DL2}}{S_{3n}}$$

$$f_{LL\_I} := \frac{M_{LL\_I}}{S_n}$$

Calculate $f_{available}$ -f_{LL_I}. If this stress is negative this is the stress to be carried by the FRP.

$$check_1 := \begin{cases} \text{"stress carried by FRP"} & \text{if } f_{available} - f_{LL\_I} < 0 \\ \text{"stress carried by tendons"} & \text{otherwise} \end{cases}$$

$check_1 = \blacksquare$

$f_{carriedbyFRP} := -(f_{available} - f_{LL\_I})$ $f_{carriedbyFRP} = \blacksquare$ ksi

Allowable stress for FRP

$f_{FRP} := 0.33 \cdot 0.95 \cdot 0.65 \cdot f_f$

$f_{FRP} = \blacksquare$ ksi

f_{FRP} must be higher than the stress to be carried by the FRP .

$$check_2 := \begin{cases} \text{"Good"} & \text{if } f_{FRP} > f_{carriedbyFRP} \\ \text{"No good"} & \text{otherwise} \end{cases}$$

$check_2 = \blacksquare$

Allowable concrete compressive stresses:

$$f_1 := \frac{-P_e}{A_c} + \frac{P_e \cdot (Y_b - Y_s)}{S_{top}} - \frac{M_{DL1}}{S_{top}} - \frac{M_{DL2}}{S_{3n\_top}} - \frac{M_{LL\_I}}{S_{n\_top}} + 0.6 \cdot f'_{cbeam}$$

$$f_2 := \frac{-P_e}{A_c} + \frac{P_e \cdot (Y_b - Y_s)}{S_{top}} - 0.5 \cdot \left(\frac{M_{DL1}}{S_{top}} + \frac{M_{DL2}}{S_{3n\_top}} \right) - \frac{M_{LL\_I}}{S_{n\_top}} + 0.4 \cdot f'_{cbeam}$$

$$f_3 := \frac{-P_e}{A_c} + \frac{P_e \cdot (Y_b - Y_s)}{S_{top}} - \frac{M_{DL1}}{S_{top}} - \frac{M_{DL2}}{S_{3n\_top}} + 0.4 \cdot f'_{cbeam}$$

If f_1, f_2, and f_3 are positive, compression in concrete is O.K.

$$check_3 := \begin{cases} \text{"Good"} & \text{if } f_1 > 0 \\ \text{"Good"} & \text{if } f_2 > 0 \\ \text{"Good"} & \text{if } f_3 > 0 \\ \text{"No good"} & \text{otherwise} \end{cases}$$

$check_3 =$ ▮

$f_1 =$ ▮ ksi $\quad f_2 =$ ▮ ksi $\quad f_3 =$ ▮ ksi

Allowable stress in prestressing steel

$$f_{allowable} := \min(0.74 \cdot f_u, 0.82 \cdot 0.85 \cdot f_u) \qquad \text{Stress Relieved Strand}$$

Final stress in strands

$$P_{final} := \frac{\frac{M_{LL\_I}}{S_n} + \frac{M_{DL1}}{S_{beam}} + \frac{M_{DL2}}{S_{3n}} - 6 \cdot f'^{0.5}_{cbeam} \cdot psi^{0.5}}{\frac{1}{A_c} + \frac{Y_b - Y_s}{S_{beam}}}$$

$$f_{final} := \frac{P_{final}}{A_{ps}} \qquad f_{final} \text{ must be less than } f_{allowable}$$

$f_{final} =$ ▮ ksi $\quad f_{allowable} =$ ▮ ksi

$$check_4 := \begin{cases} \text{"Good"} & \text{if } f_{final} < f_{allowable} \\ \text{"No good"} & \text{otherwise} \end{cases}$$

$check_4 =$ ▮

Step 12: Determine development length of the FRP according to manufacturer's recommendations

$$l_{df} := \frac{f_{fu} \cdot t_f \cdot n}{3 \cdot f'_{cbeam}{}^{0.5} \cdot psi^{0.5}}$$

$$l_{used} := \left(l_{df} + 1 \cdot in\right)$$

Find location where M = Mcr along the beam

$$Length := \blacksquare \cdot ft \qquad M_{cr} := \blacksquare \cdot ft \cdot kip$$

$$k := \frac{Mu_{original}}{\left(\frac{Length}{2}\right)^2}$$

$$x := \left(\frac{M_{cr}}{k}\right)^{0.5}$$

x = distance from centerline of beam to location where M = Mcr

Length of FRP required

$$L := 2 \cdot \left(x + l_{used}\right)$$

If more than one ply is used, extend each underlying sheet 6 inches on each end.

CFRP APPLICATION PROCEDURES

The following is a guide designed to aid in the application of CFRP. The pictures shown are from a bridge beam, but similar steps are followed for any other sort of repair/retrofit. Mbrace CFRP materials were used in this repair, thus any differences in manufacturer's materials could warrant adjustments of this procedure. The five aspects of CFRP application include: primer, putty, saturant, carbon fiber sheets/plates, and top coat.

Concrete Repair

Step 1: Repair concrete using mortar and epoxy injections according to current standards available. Forms must be used to maintain the original shape of the beam. Figures A1 and A2 show formwork and a completed patch.

Step 2: Grind off edges to a minimum of 1/2 inch for better bonding action.

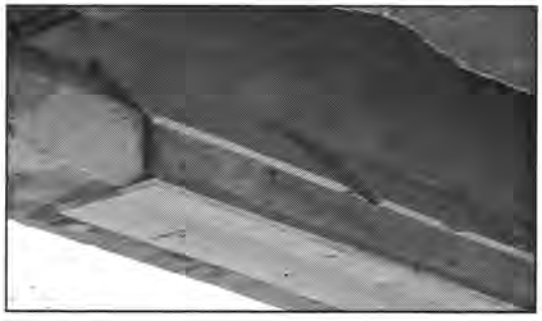

Figure A1. Formwork example.

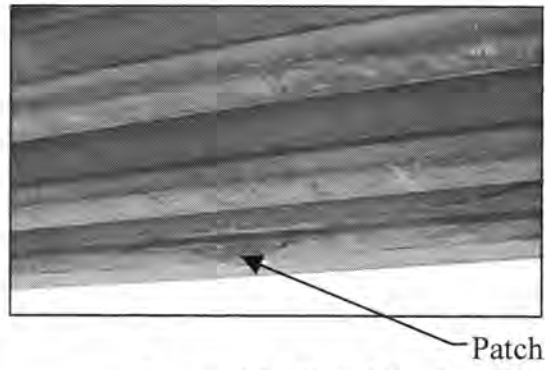

Figure A2. Cured Patch.

CFRP Installation

Application of primer:

Step 1: Clean off surface using high-pressure air or a damp cloth. Remove all dust.

Step 2: Weigh appropriate amounts of primer to be mixed, 3 parts A and 1 part B (may be different for other manufacturers). Measure only what is needed since primer has only a 35-minute pot life and will harden soon after mixing. A complete batch of primer covers 150-200 sq ft/gal. Figure A3 shows the weighing of the components.

Step 3: Mix for 3 minutes using a hammer-drill and mixing bit, shown in Figure A4.

Step 4: Pour primer into a paint tray and roll on with a medium nap roller. This can actually be completed quite quickly as long as the entire surface gets covered well. Figures A5 and A6 show the application of the primer.

Figure A3. Weighing of the primer components.

Figure A4. Mixing of the primer components with mixing drill bit.

Figure A5. Applying primer with nap roller.

Figure A6. Another view of primer application.

Application of putty:

The putty is used to plug bug holes and other small cracks for a better bond.

Step 1: Measure desired amount of both putty components with a scale.

Step 2: Premix white component for 3 minutes. Mix with other component for 3 more minutes, similar to the primer. Figures A7 and A8 show the mixing.

Step 3: Generously smear putty onto wet primer using an ordinary hand trowel. Press into any small holes that may exist. Coverage for the putty on smooth surfaces is 24 sq ft/gal and for rough surfaces about 12 sq ft/gal. Figure A9 and A10 show the putty application.

Figure A7. Putty mixture.

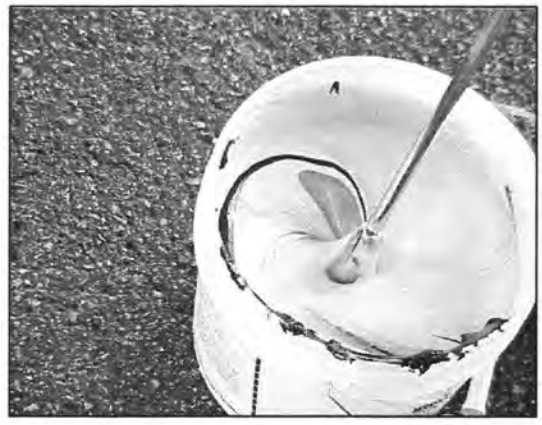

Figure A8. Mixing of the two components.

Figure A9. Applying putty with hand trowel.

Figure A10. View with putty step completed.

Application of Saturant:

The saturant impregnates the dry fibers and holds the CFRP in place while the epoxy cures.

Step 1: Weigh desired amount of saturant components. Pot life for the saturant is 30 minutes and coverage is 110-130 sq ft/gal.

Step 2: Premix the blue component for 3 minutes. Mix another 3 minutes while the colorless component is slowly added as shown in Figure A11.

Step3: Roll the saturant directly on the wet putty with a clean nap roller. The roller should be soaked with saturant, which allows for easier application. This step should go fairly quickly as long the entire surface gets covered with saturant. Figures A12 and A13 show application of the saturant.

Figure A11. Mixing the blue and color-less component of the saturant layer.

Figure A12. Beginning the application of saturant layer with nap roller.

Figure A13. Applying saturant.

Application of carbon fiber:

Step 1: Determine the size of carbon fiber sheets required and cut to length using a utility knife and a straight edge, shown in Figure A14. Ideal length is between 6 and 10 ft.

Step 2: Roll precut strips for ease in application. A rolled up strip is shown in Figure A16.

Step 3: Begin unrolling longitudinal carbon fiber onto the wet saturant. Press along the length of the material with gloved hands. Use a ribbed roller to remove air pockets and impregnate the fibers with saturant. An installed longitudinal strip is shown in Figure A15.

Step 4: Continue applying all of the longitudinal strips. A 4 in. overlap is recommended when starting the next strip. A thin strip of saturant should be applied to the last 4 in. of the previous strip so the next one will stick to it.

Step 5: One half hour after the carbon fiber strips have been applied, spread a 2nd layer of saturant over the existing carbon fiber strips.

Step 6: If applicable, apply a 2nd layer of carbon fiber strips in the new layer of saturant. If another layer is not needed, the 2nd layer of saturant should be left to dry.

Step 7: Repeat steps 5 and 6 for the desired number of layers.

Step 8: Apply transverse wrap in similar fashion. No overlap of the transverse FRP is required.

Figure A14. Cutting FRP to the predetermined size.

Figure A15. One strip of longitudinal FRP.

Figure A16. Unrolling a strip of FRP.

Figure A17. Four inch overlap splice.

Figure A18. Transverse wrap over the longitudinal FRP.

Figure A19. Transverse wrap (cut to designed length).

Figure A20. Entire beam after the longitudinal and transverse FRP are installed.

Application of topcoat:

The topcoat is similar to a final layer of paint. It is applied mainly for aesthetic purposes so the repair is not noticeable while driving past the structure.

Step 1: Weigh components of topcoat, a 4:1 ratio. Pot life of the topcoat is 3 hours. Coverage is 350 sq ft/gal.

Step 2: Mix using hammer-drill and mixing bit for 5 minutes.

Step 3: Apply over the dried saturant and FRP using rollers and brushes. Figures A21 through A23 show the painting of the topcoat and the complete repaired structure.

Figure A21. The painting of the topcoat.

Figure A22. Using a roller to paint bottom flange.

Figure A23. Final view of completely repaired bridge.

APPENDIX C

REPAIR MATERIAL PROPERTIES AND DESCRIPTIONS

EMACO S88 CI, manufactured by Master Builders Technologies, is a sprayable fiber-reinforced structural repair mortar with integral corrosion inhibitor. For this project, it was not applied using the spraying method. It is especially made for repairing vertical and overhead concrete and masonry (vertical repairs from 3/8 in. to 2 in. and overhead repairs from 3/8 in. to 1-1/2 in.). Other uses include repairs on bridges, parking ramps, repairing manholes, sewers, wet wells, and lift stations.

Some special characteristics of the EMACO S88 CI follow: it is easy to use, there is no additional bonding agent required, and it is sprayable with low waste. It also has a silica fume formulation, which contributes to a high early and ultimate compressive, flexural, and bond strengths. Some of the manufacturer's material properties are presented in Table A.1.

Table A.1. Manufacturer's properties.

Test Description	1 Day (psi)	7 Days (psi)	28 Days (psi)
Direct Tensile Bond Strength (ACI 503R, Appendix A)	100	175	300
Direct Shear Bond Strength (Michigan DOT)	350	450	700
Modulus of Elasticity (ASTM C 469)	-	-	5,000,000
Splitting Tensile Strength (ASTM C 496)	350	500	900
Flexural Strength (ASTM C 348)	650	1,000	1,300
Compressive Strength (ASTM C 109	3,500	8,000	11,000

CFRP Strengthening System

The carbon fiber strengthening system used in this project was the MBrace Composite Strengthening System, manufactured by Master Builders Inc. of Cleveland, Ohio. The MBrace system involves the use of epoxy to adhere carbon fiber sheets to concrete and/or steel surfaces. This adhesion increases the strength. The system can be used for things such as bridge repair, column wraps, shear reinforcement, and beam column connections. The Mbrace system consists of five main components. These components, in order of application, are as follows: Primer, Putty, Saturant, CFRP, and Topcoat.

Primer:

The MBrace primer is a 100% solids epoxy based primer. The primer is formulated to penetrate the pores of the concrete to provide an adequate bond between the carbon fibers and the concrete. The primer is almost colorless when applied. It is applied with a medium-sized paint roller.

Putty

The putty epoxy step is an optional step, depending on the condition of the concrete surface. The MBrace putty is a thicker epoxy than the primer. It is used to fill bug holes and small cracks in the concrete. This will create a better bond between the concrete and the carbon fibers. If needed, the putty can be used for leveling the concrete or for filling small holes. The putty is applied with a standard hand trowel and appears as a light color. It is applied directly over the wet primer.

Saturant

The MBrace Saturant is the third step in the strengthening process. The saturant is a blue color. This makes it distinguishable against either the primer or the putty so no areas are left unsaturated. The saturant is used to impregnate the dry fibers. It holds the dry fibers in place while the system cures. The saturant is also designed to protect the carbon fibers from the environment. It is also quite viscous for easy applications in overhead situations.

Carbon Fiber

Immediately after the saturant has been applied, the pre-cut carbon fiber strips are laid directly on the wet saturant. The carbon fiber is what gives the MBrace system its strength and consists of high strength unidirectional fibers together in one sheet. The carbon fiber's main feature is that it has high strength to weight and stiffness to weight ratios. This allows repairs to be made with out significantly altering the properties of the original structure.

Top Coat

The MBrace Top Coat is the final step in the repair process. The topcoat is "painted" on after all layers of carbon fiber and saturant have been applied. The topcoat can protect the epoxy and fibers from UV rays and chemical backsplash. It is mostly used for aesthetic purposes though and should come close to matching the concrete in the existing structure.

References

1. Klaiber, F.W., K.F. Dunker, T.J. Wipf, and W.W. Sanders, "Methods of Strengthening Existing Highway Bridges," NCHRP Research Report 293, Transportation Research Board, Crowthorne, United Kingdom, 1987.

2. Meier,U., and H. Kaiser, "Strengthening of Structures with CFRP Laminates," Proc., Advanced Composite Materials in Civil Engineering Structures, ASCE, New York,, 1991, 224-232.

3. Arduini, M. and Nanni, A, "Behavior of Precracked RC Beams Strenghened with Carbon FRP Sheets," Journal of Composites for Construction, May 1997, pp. 63-70.

4. Shanafelt, G.O. and W.B. Horn, "Damage Evaluation and Repair Methods for Prestressed Concrete Bridge Members," National Cooperative Highway Research Program Report 226, Washington, D.C., November 1980.

5. Teng, J.G., J.F. Chen, S.T. Smith, and L. Lam, FRP Strengthened Structures, John Wiley & Sons, Ltd, West Sussex, England, 2002.

6. Shahawy, M. and E. Beitelman, "Static and Fatigue Performance of RC Beams Strengthened with CFRP Laminates," Journal of Structural Engineering, June 1999, pp. 613-621.

7. Capozucco, R., and M. Nilde Cerri, "Static and Dynamic Behaviour of RC Beam Model Strengthened by CFRP Sheets," Construction and Building Materials, 2002, pp. 91-99.

8. Chaallal, O., M. Shahawy, and M. Hassan, "Performance of Reinforced Concrete T-Girders Strengthened in Shear with Carbon Fiber-Reinforced Polymer Fabric," ACI Structural Journal, May-June 2002, pp. 335-343.

9. Norris, T., H. Saadatmanesh, and M. R. Ehsani, "Shear and Flexural Strengthening of R/C Beams with Carbon Fiber Sheets," Journal of Structural Engineering, July 1997, pp. 903-911.

10. Chaallal, O., M.J. Nollet, and D. Perraton, "Strengthening of Reinforced Concrete Beams with Externally Bonded Fiber-Reinforced-Plastic Plates: Design Guidelines for Shear and Flexure," Canadian Journal of Civil Engineering, 1998, pp. 692-704.

11. Tann, D.B., R. Delpak, E. Andreon, "Design Aspects of Shear Strengthening of RC Beams Using Externally Bonded FRP Sheets," 9th International Conference and Exhibition, Structural Faults and Repairs, London, UK, July 2001.

12. Al-Sulaimani, G. J., A. Sharif, I.A. Basunbul, M.H. Baluch, and B.N. Ghaleb, "Shear repair for reinforced concrete by fibreglass plate bonding," ACI Structural Journal, V.91, No.3, pp. 458-464, 1994.

13. Chajes, M. J., T.F. Januszka, D.R. Mertz, T.A. Thomason, and W.W. Finch, "Shear strengthening of reinforced concrete beams using externally applied composite fabrics," ACI Structural J., V.92, No.3, pp. 295-303, 1995.

14. Sato, Y., T. Maeda, and Y. Asano, "A study on bond mechanism of carbon fibre sheet," Proceedings 3 rd International Symposium on Non-Metallic Reinforcement for Concrete Structures (FRPRCS-3), V.1, Japan Concrete Society, pp. 279-286, 1997.

15. Triantafillou, T. C., "Shear strengthening of reinforced concrete beams using epoxy-bonded FRP composites," ACI Structural J., V.95, No.2, March-April, pp107-115, 1998.

16. Swamy, R. N., P. Mukhopadhyaya, and C.J. Lynsdale, "Strengthening for shear of RC beams by external plate bonding," The Structural Engineer, V.77, No.12, pp19-30, 1999.

17. Barnes, R.A. and G.C. Mays, "Fatigue Performance of Concrete Beams Strengthened with CFRP," Journal of Composites for Construction, Vol. 3, No. 2, pp. 95-104, May 1999.

18. Stallings, J.M., J.W. Tedesco, M. El-Mihilmy, M. McCauley, "Field Performance of FRP Bridge Repairs," Journal of Bridge Engineering, May 2000, pp. 107-113.

19. Masoud, S., K. Soudki, "Serviceability of Corroded Reinforced Concrete Beams Strengthened with Carbon Fibre Reinforced Polymer Sheets," 3rd Structural Specialty Conference of the Canadian Society of Civil Engineers, London, Ontario, June 2000.

20. Watson, R.J., "Extending the Life of Bridges Using Fiber Reinforced Polymers," 9th International Conference and Exhibition, Structural Faults and Repairs, London, UK, July 2001.

21. Nanni, A., P.C. Huang, J.G. Tumialan, "Strengthening of Impact-Damaged Bridge Girder Using FRP Laminates," 9th International Conference and Exhibition, Structural Faults and Repairs, London, UK, July 2001.

22. Breña, S.F., R.M. Bramblett, S.L. Wood, M.E. Kreger, "Flexural Strengthening of Existing Reinforced Concrete Bridges Using Carbon Fiber Reinforced Polymer Composites," 9th International Conference and Exhibition, Structural Faults and Repairs, London, UK, July 2001.

23. Kachlakev, D.I., "Horsetaile Creek Bridge-Design Method Calibration and Experimental Results of Structural Strengthening with CFRP and GFRP Laminates," 9th International Conference and Exhibition, Structural Faults and Repairs, London, UK, July 2001.

24. Keble, D., G. Marshall, N. Thoday, "Strengthening of M60 Barnes Bridge, Manchester with Carbon Fibre Composites," 9th International Conference and Exhibition, Structural Faults and Repairs, London, UK, July 2001.

25. Klaiber, F.W., T.J. Wipf, F.M. Russo, R.R. Paradis, and R.E. Monteega, "Field/Laboratory Testing of Damaged Prestressed Concrete Girder Bridges," Iowa DOT Project HR-397 Final Report, Ames, Iowa, December 1999.

26. Russo, F.M., F.W. Klaiber, T.J. Wipf, "Field and Laboratory Testing of Damaged and Repaired Prestressed Concrete I-Beam Bridges," 3rd Structural Specialty Conference of the Canadian Society of Civil Engineers, London, Ontario, June, 2000.

27. Master Builders, Inc., MBrace Composite Strengthening System – Engineering Design Guidelines, Second Edition, Cleveland, OH 1998.

28. Kelley, P.L., M.L. Brainerd, and M. Vatovec, "Design Philosophy for Structural Strengthening with FRP," Concrete International, Feb. 2000, pp. 77-82.

29. Pouliot P., P. Labossiere, K.W. Neale, "Design Aids for the Flexural Strengthening of Rectangular Reinforced Concrete Beams with Composite Materials" 3rd Structural Specialty Conference of the Canadian Society of Civil Engineers, London, Ontario, June 2000.

30. Rhodes, J.D., "Repair of Impact Damaged Prestressed Concrete Girders Using Carbon Fiber Reinforced Polymers", Masters Thesis, Ames, Iowa, 2000.

ACKNOWLEDGEMENTS

The work described in this report was conducted by the Bridge Engineering Center at Iowa State University and sponsored by the Iowa Department of Transportation.

I would like to thank Dr. Terry J. Wipf, Dr. F. Wayne Klaiber and Dr. Brent Phares for all of their help and support during the preparation of this thesis. I would also like to thank Dr. Loren W. Zachary for serving on my Program of Study Committee.

I would also like to thank Master Builders, Inc. for their CFRP material donation. I would also like to thank Steve Tysl for his trip to show the application of the material to bridges. I'd like to thank Norbert Kottlers and Scott Neubauer for their help and critiques of parts of this thesis.

Thank you to Doug Wood, for all your help in the lab and in the field testing bridges. My gratitude goes out also to the undergraduate and graduate students who helped with any laboratory/field work or testing: Travis, A.J., Brett, Elizabeth, Ben, and Emily.

Finally, I would like to thank my parents for all their support and my wife for her tremendous patience.